

LabSTAF and RunSTAF

Handbook

Doc No. 2408-014-HB | Issue C

Copyright

© Chelsea Technologies Ltd 2021

The copyright of this document is the property of Chelsea Technologies Ltd. The document is supplied by Chelsea Technologies Ltd on the express terms that it is to be treated in confidence and that it may not be copied, used or disclosed to others unless authorised in writing by Chelsea Technologies Ltd.

Company Confidentiality

This document and its contents shall not be used for any purposes or disclosed to any party without the written consent of Chelsea Technologies Ltd. All recipients are required to abide by these confidentiality conditions.

Approved	Kevin Oxborough	
Checked	Nina Schuback and Mary Burkitt-Gray	
Originated	Kevin Oxborough	
Issue	ECN	Date
C	NA	08/07/2021

Contents

1	Introduction	7
1.1	The STAFES-APP project	7
1.1.1	Using STAF to monitor PhytoPP	8
1.1.2	Potential EOVs from STAF systems	8
1.1.2.1	Gross Oxygen release by PSII	9
1.1.2.2	Dark STAF parameters	9
2	STAF terminology	11
2.1	The RunSTAF screens	11
2.2	Accommodating new features	11
2.3	SI units and reported units	11
2.4	Irradiance and photon irradiance	11
2.5	Photosystem II Reaction Centre (RCII)	11
2.6	Photosystem II Light Harvesting System (LHCII)	11
2.7	Photosystem II (PSII) complex	11
2.8	PSII photochemical flux per photosystem ($J_{P_{II}}$)	12
2.9	PSII photochemical flux per unit volume ($JV_{P_{II}}$)	12
2.10	Photosynthetic Gross Oxygen release by Photosystem II ($GO_{P_{II}}$)	12
2.11	Electron Transport Rate (ETR)	12
2.12	Phytoplankton Primary Productivity (PhytoPP)	12
2.13	Units of fluorescence (F)	12
2.14	Single Turnover (ST)	12
2.15	Data averaging terminology	13
2.16	Dual ST pulse-based relaxation phase	13
2.17	Interrogated volume	14
2.18	Correcting for the package effect	14
2.19	Spectral correction	14
3	RunSTAF menus	16
3.1	File	16
3.2	Settings	16
3.3	Clipboard	17
3.4	Help	17
4	An introduction to the Auto FLC mode	18
4.1	Overview	18
4.2	Auto FLC mode	19
4.3	Starting acquisition – the pre-FLC functions	20
4.3.1	STAF setup	21
4.4	Switching between the PEP and the most recent ST curve	23
4.4.1	The data screen during Auto FLC mode	23

4.5	The relaxation phase fit	25
4.6	FLC setup	26
4.7	Archiving of data	28
5	An introduction to the Manual mode	30
6	STAF setup and STAF data	32
6.1	STAF setup section	32
6.2	Data processing	33
6.3	The automated RunSTAF functions	34
6.3.1	Auto PMT	34
6.3.2	Auto LED	34
6.3.3	Auto DWM	34
6.3.4	Auto PEP	34
7	The FLC setup	35
7.1	Elements of the FLC setup	35
7.2	The maximum step function (Step max)	35
7.3	The Pre-FLC function	36
7.4	The push up function	36
7.5	Run time	36
7.6	The Mix function	37
7.7	The Exchange function	37
7.8	Repeat FLC	37
7.9	Auto FLC	37
7.10	Wash cycle	37
8	Manual settings	38
9	Data export functions	39
9.1	The Clipboard functions	39
9.1.1	The Clipboard header	39
9.1.2	The Clipboard footer	39
9.1.3	DWM data	40
9.1.4	PEP data	41
9.1.5	SCS data	42
9.1.6	rPE data	42
9.1.7	Tau data	43
9.1.8	Saq parameters or Acq parameters	43
9.1.9	Saq traces or Acq traces	44
9.1.10	Saq trace fits or Acq trace fits (Rho)	45
9.1.11	Saq trace fits or Acq trace fits (dimer)	45
9.2	The csv functions	46
9.2.1	All file and Individual files	46
9.2.2	Auto archive report line	49

10	Data processing within RunSTAF	50
10.1	Refitting data files	50
10.2	Correcting for baseline fluorescence (F_b calculation)	50
10.3	The ST curve fitting procedures	50
10.3.1	The Rho ST curve fit	51
10.3.2	The Dimer ST curve fit	51
10.4	Fitting a dual ST pulse sequence	52
10.5	The relaxation phase (τ) fit	54
10.6	The rPE data fit	57
11	Generating values of J_{PII}, JV_{PII} and GO_{PII}	60
11.1	Absorption cross section	60
11.2	PSII photochemical flux (J_{PII} and JV_{PII})	62
11.3	Derivation of K_a	64
12	Deconstructing rho	66
12.1	Estimating the proportion of PSII complexes in the open state	67
12.2	The relationship between ρ and the yield of PSII photochemistry	68
12.3	Heterogeneity induced by dimerization of PSII	71
12.4	The impact of connectivity on quantification of $[Q_A]$	72
13	Photochemical Excitation Profile (PEP)	73
13.1	Excitation wavebands for the PEP	73
13.2	The PEP protocols	74
13.3	Checking PEP saturation	75
13.4	The impact of heterogeneity on PEP data	76
13.5	Scaling PEP data	78
13.6	Using PEP data to apply a Spectral Profile Correction (SPC)	80
13.7	Derivation of PEP values	82
13.8	Which PEP should be used for SPC?	84
14	Package Effect Correction (PEC)	84
15	Delivery pack	87
16	LabSTAF hardware setup	89
16.1	Plumbing the flow-through unit, peristaltic pump and solenoid unit	89
17	LabSTAF calibration	91
17.1	Calibration data stored within the LabSTAF unit	91
17.2	The spectral calibration spectra (scs) data file	92
17.3	Create a local backup of the calibration data stored within LabSTAF	92
17.4	Post-processing with the scs data file	92
17.5	On-site calibration of sample chamber temperature	92
17.6	Updating calibration values across existing data files	93
18	Technical information	94

18.1	The measurement LEDs and PMT	94
18.2	The actinic light source	95
18.3	Sample temperature control	96
18.4	PMT temperature coefficient	97
18.5	Events log	97
19	RunSTAF installation and setup	98
19.1	Updating an existing RunSTAF installation	98
19.2	Uninstall RunSTAF before installing the update	98
19.3	Install the new version of RunSTAF	99
19.4	First RunSTAF installation	99
19.5	Run LabSTAF on power up	99
19.5.1	Bypass the Windows 10 login	99
19.5.2	Run as a start-up program	99
19.6	Prevent the USB port going to sleep	100
19.7	Block the Serial Enumerator	101
19.8	Block serial mouse detection on Startup	101
20	Glossary of terms	103
20.1	Acronyms	103
20.1.1	CCAP	103
20.2	Term modifiers	103
20.2.1	The light-adapted state prime modifier (')	103
20.2.2	The baseline corrected modifier (c)	103
20.2.3	The second ST pulse modifier (s)	103
20.2.4	The dimer modifier (d)	103
20.3	Basic STAF terms	104
20.4	Additional STAF terms	104
20.5	Dimer-specific STAF terms	104
20.6	Basic fluorescence terms	105
20.7	Additional fluorescence terms for the second ST pulse	105
20.8	Derived fluorescence parameters	105
21	Answers to FAQs and background material	106
21.1	Deriving your own values of a_{LHII} and/or PSII concentration	106
21.2	Units for measuring LED photon irradiance (E_{ST})	106
21.3	Dark FLC step F_v/F_m and F_v'/F_m' values	106
21.4	The Stern-Volmer relationship, NPQ and NSV	106
21.5	Alternative terminology	108
21.5.1	Absorption cross sections	108
22	References	110

Changes from previous releases

Since 2408-014-HB-A

Spectral data

Spectral data (1 nm resolution) from all MLED channels and the actinic LED are used to apply a Spectral Profile Correction (SPC) to the PEP data. This allows for:

- Normalization of the F_v and σ_{PII} values at each MLED waveband to the ALED spectral output
- $J_{V_{PII}}$ and GO_{PII} values scaled to the ALED output using the F_v PEP values
- J_{PII} values scaled to the ALED output using the σ_{PII} PEP values

See: [Photochemical Excitation Profile \(PEP\)](#)

Application of SPC requires the presence of an scs file at the following location...

CT_RunSTAF → Calibration files

The required scs files have already been generated for each LabSTAF system in circulation. They can be accessed through the RunSTAF update link shown below.

See: [LabSTAF calibration](#) for installation details.

Relaxation phase

Relaxation phase parameters are now derived from the Rho fit, rather than the F_v fit, to provide a closer match to the reopening of closed RCII.

An overall relaxation phase τ value is generated as an rPE parameter

Package effect correction

The Package Effect Correction (PEC) can now be applied using the value generated from the Dual Waveband Measurement (DWM) or a user-set value.

Interface

The **Clear file details** button on the home screen has been replaced with a menu option (**File → Clear file details**)

Pre-FLC options

In FLC mode, the pre-FLC illumination function has been modified to run before the Auto LED, Auto DWM and Auto PEP functions. The function incorporates light and dark stages, either of which can be set to zero time.

Updates to this document

This document has been uploaded to oceanbestpractices.org

<http://dx.doi.org/10.25607/OBP-1029>

1 Introduction

This introductory section provides a brief overview of the development of LabSTAF and RunSTAF and future aims for the development of Single Turnover Active Fluorometry (STAF). It also includes a description of the major differences between LabSTAF and the previous generation of active fluorometers.

1.1 The STAFES-APP project

LabSTAF is the first of a new generation of research-grade active fluorometers being developed by Chelsea Technologies Ltd (CTL) in collaboration with The University of Southampton (UoS), the National Oceanographic Centre (NOC) and The University of Essex (UoE) as part of the STAFES-APP project within the NERC-funded OCEANIDS programme (NE/P020844/1).

The STAFES-APP acronym expands to Single Turnover Active Fluorometry of Enclosed Samples – for Autonomous Phytoplankton Productivity. The aim of the project is to develop highly sensitive benchtop and deployable systems that can be used to improve our understanding of the global carbon cycle and aquatic ecosystem function.

Meaningful assessment of the global carbon cycle must incorporate Phytoplankton Primary Productivity (PhytoPP) which forms the base of the marine food chain and represents approximately half of the carbon fixed by photosynthesis on a planetary scale. It follows that measurement of PhytoPP on wide spatial and temporal scales has enormous potential for developing our understanding of ocean productivity and verifying climate change models. Arguably the most important way in which this target can be achieved is through the validation and development of satellite remote sensing, which operates on the widest possible spatial scales, but which currently has large errors for the estimation of PhytoPP. Most of the current methods used to measure PhytoPP directly are laboratory-based. As a consequence, these methods can only be applied on scales that fall well short of those required. The end result is extreme undersampling of the oceanic environment for PhytoPP (e.g. Lee et al. 2015).

Global assessment of PhytoPP falls within the remit of the Global Ocean Observing System (GOOS) which defines and prioritises a range of Essential Ocean Variables (EOVs). The fundamental criteria employed for defining EOVs are impact and feasibility: to make it on to the GOOS list, an EOV must have high impact and be measurable on meaningful scales using cost effective technology. Although PhytoPP clearly satisfies the impact criterion, the limitations of existing methods means it currently scores very low on the feasibility scale. PhytoPP responds to multiple, highly dynamic environmental drivers including light, temperature and nutrients. It follows that PhytoPP needs to be assessed at spatial and temporal scales that are at least as high as for existing EOVs and that new technologies and methodologies are required achieve this.

Clearly, PhytoPP cannot be considered as a potential EOV while measurement scales are largely tied to land-based laboratories and the availability of research ships. In this context, autonomous platforms such as buoys, moorings, autonomous surface vehicles, gliders and Argo floats, provide opportunities to greatly increase both spatial and temporal scales for PhytoPP assessment. The challenge is to develop systems that can be deployed on these platforms and generate meaningful parameters with acceptably low errors. This challenge is central to the STAFES-APP project and LabSTAF is the first product. It is a highly portable benchtop system incorporating a range of options for both manual and highly automated operation.

Although LabSTAF is limited to deployment on buoys, moorings and surface vessels, a 600 m deployable version (AutoSTAF) will be available by Late 2021. A Digital Control Unit (DCU) will be released at the same time as AutoSTAF. The deployable DCU will provide control of a Sea-Bird pump for sample exchange, provide COM-based inputs for one or two Spectral Photosynthetically Active Radiation (SPAR) sensors and either fully autonomous system control using an embedded Windows

PC or remote control through an RS232 or RS422 interface. The DCU will also power the AutoSTAF unit. The DCU power input will be 9 to 36 V DC.

1.1.1 Using STAF to monitor PhytoPP

Although STAF measurements have revolutionised our understanding of phytoplankton ecophysiology in oceanic systems over more than twenty years (Kolber, Prášil and Falkowski, 1998), it is only with more recent technological and theoretical developments that STAF has become a potentially enabling technology for the assessment of PhytoPP at the resolution and accuracy required for consideration as an EOV (Oxborough et al. 2012; Boatman, Geider and Oxborough, 2019).

Rates of PhytoPP are constrained by the availability of chemical energy for carbon fixation which is almost entirely derived from the light reactions of oxygenic photosynthesis. LabSTAF provides values for the three key parameters required for quantitative assessment of oxygenic photosynthesis: the availability of photons, through use of a calibrated actinic source; the absorption of photons, using a STAF-derived absorption coefficient; and the proportion of absorbed photons used to drive oxygenic photosynthesis, using a STAF-derived efficiency parameter.

The absorption of photons by the light harvesting systems within phytoplankton is spectrally dependent, with highly variable spectral characteristics among groups (Suggett et al. 2004). To minimize spectral errors, the actinic light source used within both LabSTAF and AutoSTAF is spectrally characterised and both systems incorporate seven excitation wavebands to allow spectral assessment of photochemical activity. The deployable AutoSTAF also includes an option to incorporate spectrometer-based sensors to measure spectrally resolved photon irradiance at the point of sampling. Incorporation of a single Spectral Photosynthetically Active Radiation (SPAR) sensor allows for the monitoring of downwelling photon irradiance. Incorporation of two SPAR sensors allows for monitoring of both upwelling and downwelling photon irradiance.

The actinic light source integrated within LabSTAF and AutoSTAF allows for assessment of the photon irradiance dependence of PhytoPP through the application of Fluorescence Light Curves (FLCs). FLCs comprise an automated set of STAF measurements made at several photon irradiance levels between darkness and saturating light, providing information equivalent to the traditional carbon fixation or oxygen evolution based 'PE' curves. Depending on time of day and environmental conditions, a LabSTAF integrated within an underway system on board a research vessel can generate between two and six complete PE curves per hour. It is anticipated that AutoSTAF will achieve a similar output.

1.1.2 Potential EOVs from STAF systems

Historically, the most widely employed methods for monitoring PhytoPP have involved measurement of ^{14}C -assimilation into particulate matter or related methods that measure CO_2 or O_2 dynamics (Geider and Osborne, 1992; Sakshaug et al. 1997). These methods are not suitable for deployment on autonomous vehicles and, in addition, require long incubation times. In sharp contrast, deployed STAF systems have the potential to generate data on spatial scales from a few metres up to oceanic basin scales and temporal scales of seconds to tens of minutes, depending on the level of detail required. It follows that STAF has clear potential for the provision of meaningful EOVs for use in the assessment of PhytoPP, particularly when combined with nutrient and other EOV data.

The combination of LabSTAF hardware and RunSTAF software allows for measurement of photosystem II (PSII) photochemical flux per PSII (J_{PII}) and PSII photochemical flux per unit volume of ocean or other medium (JV_{PII}) using the so-called sigma and absorption methods respectively. The accuracy of both parameters is highly dependent on accurate calibration of the instrument, spectral correction and, in the case of JV_{PII} , correction for the so-called package effect. A great deal of work

has already gone into minimising the errors associated with these processes and this work will continue through the remainder of the STAFES-APP project and beyond. The output from this work will be made available through updates to the RunSTAF software and this document plus submissions for peer-reviewed publication.

1.1.2.1 Gross Oxygen release by PSII

On the assumption that every photon used to drive PSII photochemistry results in the transfer of an electron from the PSII Oxygen Evolving Complex (OEC) to the plastoquinone pool, JV_{PII} is proportional to Gross Oxygen release by PSII per unit volume of ocean or other medium (GO_{PII}). Because the release of each O_2 by the OEC requires the transfer of four electrons to plastoquinone, GO_{PII} is calculated as JV_{PII} divided by four. At this time, there is not enough supporting data to justify using JV_{PII} as a proxy for GO_{PII} at the EOVS level. However, the data available from past studies clearly illustrate the potential for LabSTAF and AutoSTAF to provide this parameter (Oxborough et al. 2012; Silsbe et al. 2015; Boatman, Geider and Oxborough, 2019).

1.1.2.2 Dark STAF parameters

The absorption coefficient for PSII light harvesting (a_{LHII}) is integral to the absorption method. It is generated from a STAF measurement made on a dark-adapted sample and quantifies the proportion of incident photons that are absorbed and made available for PSII photochemistry. In addition to a_{LHII} , dark STAF measurements can generate a value for the absorption cross section of PSII photochemistry (σ_{PII}), estimate PSII photochemical efficiency (ϕ_{PII}) and provide a time constant for the transfer of electrons from closed PSII to the plastoquinone pool (τ). The lack of requirement for an actinic light source means that these parameters can be generated by a STAF unit that is significantly smaller, simpler and with a lower power requirement than LabSTAF or AutoSTAF, thereby opening up the range of platforms on which STAF units can be integrated. Between now and 2024, CTL will be developing and testing STAF units of this type within the European Commission-funded HORIZON 2020 Technologies for Ocean Sensing (TechOceanS) project ([Technologies for Ocean Sensing | TechOceanS Project | H2020 | CORDIS | European Commission \(europa.eu\)](#)).

Of the dark STAF parameters, a_{LHII} arguably has the highest potential for improving the estimation of PhytoPP from satellite data, making it the best candidate for consideration as an EOVS. However, it is worth noting that σ_{PII} and ϕ_{PII} are generated by exactly the same measurement as a_{LHII} and that inclusion of τ requires minimal additional effort. Consequently, the potential exists for the inclusion of all four parameters as EOVSs.

Changes from FastOcean and Act2

LabSTAF represents a significant update to the well-established combination of FastOcean Fast Repetition Rate fluorometer (FRRf) and Act2 laboratory system. The list of advantages that LabSTAF has over FastOcean plus Act2 includes:

- More than ten times the sensitivity
- Much lower filter breakthrough
- Two fluorescence detection wavebands instead of one
- Seven fluorescence excitation LED wavebands instead of three
- DC actinic light source providing 10 to 2000 $\mu\text{mol photons m}^{-2} \text{s}^{-1}$
- A circulating water jacket that avoids intersection with all optical paths
- Increased FLC automation
- Extended data analysis

- Improved access to primary data

The increased sensitivity arises through a switch from the 1 μs FRRf 'flashlets' on a 2 μs pitch to a solid excitation pulse from the excitation LEDs plus improvements to the optical arrangement. An added advantage of the switch from FRRf to a solid pulse is that the same number of data points can be collected in half the time. Consequently, the default Single Turnover (ST) pulse has been shortened from 200 μs (FastOcean) to 100 μs (LabSTAF).

The much lower filter breakthrough is the result of the change in optical configuration and the use of better optical filters. The most obvious benefit is reduced blank values when sampling within extreme oligotrophic regions.

The incorporation of two fluorescence detection wavebands within LabSTAF, centred at 685 nm and 730 nm, allows for correction of the package effect (Boatman, Geider and Oxborough, 2019).

See: [Dual Waveband Measurement and Package Effect Correction \(DWC and PEC\)](#)

The seven measurement wavebands allow for routine spectral analysis based on variable fluorescence (F_v) and the absorption cross section of PSII photochemistry (σ_{PSII}). This analysis includes automated spectral correction of primary data by generating F_v and σ_{PSII} values for the actinic light source.

See: [Photochemical Excitation Profile \(PEP\)](#)

The blue-enhanced DC actinic source incorporated within LabSTAF improves signal to noise and avoids the potential for measurement artefacts associated with Pulse Width Modulation (PWM).

See: [The actinic light source](#)

Avoiding intersection between the water jacket and all optical paths allows underway water (for example) to be used to maintain the temperature of the sample. The LabSTAF optics and electronics are sealed to prevent condensation in situations where there is a need to maintain the sample temperature at well below ambient. The relative humidity within the LabSTAF unit is reported by RunSTAF each time it is attached.

See: [Sample temperature control](#)

The improved FLC automation allows for the inclusion of a pre-illumination and a dark step after sample exchange between successive FLCs.

See: [The actinic light source](#)

The extended data analysis includes a new ST curve fitting function that assumes connectivity among PSII complexes is entirely attributable to dimerization.

See: [Data processing within RunSTAF](#)

Although RunSTAF incorporates a range of functions for real time data analysis, straightforward transfer of primary data and derived parameters is also possible, through the Windows Clipboard and bulk generation of csv files. Access to primary data is provided to allow for analysis with user-formulated and/or third-party algorithms and integration within databases.

See: [Data export functions](#)

2 STAF terminology

This section provides an overview of the terminology used within this document and introduces some unique features of LabSTAF and RunSTAF.

2.1 The RunSTAF screens

The **home screen** is shown when RunSTAF is started and provides access to Gaq-level data when running in auto FLC mode.

The **data screen** provides access to the Saq-level ST curves and data plots for both auto FLC and manual modes.

The **calibration screen** shows the calibration data from an attached LabSTAF or open data file.

2.2 Accommodating new features

Introduction of the dual ST pulse method, the dimer fitting procedure and other new features have necessitated the introduction of new terminology. For the sake of consistency, a structured approach has been taken to generate these terms. Although this approach has led to the use of alternatives to some established terms, most are identical or very close to terms that have been in use for several decades.

See: [Glossary of parameter terms](#)

2.3 SI units and reported units

SI units and units officially accepted for use with the SI system are used throughout this document. When discussing the derivation of quantities, base SI units are used. Reported units include commonly used standard SI prefixes, where appropriate. For example, photon irradiance within an equation will have units of photons $\text{m}^{-2} \text{s}^{-1}$ or mol photons $\text{m}^{-2} \text{s}^{-1}$ (depending on context) while actinic photon irradiance is reported with units of $\mu\text{mol photons m}^{-2} \text{s}^{-1}$.

2.4 Irradiance and photon irradiance

Irradiance is the radiant flux (power) received by a surface per unit area. The SI unit of irradiance is W m^{-2} . As is generally the case for biological processes, photon flux is more useful than radiant flux when quantifying photosynthesis. Throughout this document, photon irradiance is used in preference to irradiance. The reported units are $\mu\text{mol photons m}^{-2} \text{s}^{-1}$. Photon irradiance is denoted by the symbol E.

2.5 Photosystem II Reaction Centre (RCII)

RCII is taken to include all subunits required for stable charge separation between P_{680} (the PSII primary electron donor) and Q_A (the first stable electron acceptor). An RCII can be in the open state (capable of using available photons to drive PSII photochemistry) or the closed state (where charge separation at PSII is inhibited by reduction of Q_A).

2.6 Photosystem II Light Harvesting System (LHCII)

The term LHCII is applied to any structure containing light harvesting molecules that can transfer photons to the RCII.

2.7 Photosystem II (PSII) complex

A PSII complex comprises a RCII plus a LHCII. When a PSII complex is described as being open or closed, it is referencing the status of the RCII within the complex. A PSII complex can be

photochemically active (open or closed state) or photoinactivated (requiring repair before photons can be used to drive PSII photochemistry).

2.8 PSII photochemical flux per photosystem ($J_{\text{P}_{\text{II}}}$)

This term is used to quantify the flux through the absorption cross section for PSII photochemistry provided by a single PSII complex (units of photons $\text{PSII}^{-1} \text{s}^{-1}$). The sigma method is used to generate values of $J_{\text{P}_{\text{II}}}$.

2.9 PSII photochemical flux per unit volume ($JV_{\text{P}_{\text{II}}}$)

This term is used to quantify the flux through the absorption cross section for PSII photochemistry provided by all PSII complexes within a unit volume of ocean or other medium (SI units of photons $\text{m}^{-3} \text{s}^{-1}$ or mol photons $\text{m}^{-3} \text{s}^{-1}$, reported units of $\mu\text{mol photons m}^{-3} \text{s}^{-1}$). The absorption method is used to generate values of $JV_{\text{P}_{\text{II}}}$.

See: [Generating values of \$JV_{\text{P}_{\text{II}}}\$ and \$GO_{\text{P}_{\text{II}}}\$](#)

2.10 Photosynthetic Gross Oxygen release by Photosystem II ($GO_{\text{P}_{\text{II}}}$)

This is the moles of oxygen molecules released by PSII photochemistry per unit volume per unit time (SI units of mol $\text{O}_2 \text{m}^{-3} \text{s}^{-1}$, reported units of mmol $\text{O}_2 \text{m}^{-3} \text{h}^{-1}$). Values reported by RunSTAF assume that each O_2 released requires four stabilised charge separation events at PSII.

See: [Generating values of \$JV_{\text{P}_{\text{II}}}\$ and \$GO_{\text{P}_{\text{II}}}\$](#)

2.11 Electron Transport Rate (ETR)

Although not actually reported by RunSTAF, ETR can be derived from $J_{\text{P}_{\text{II}}}$ (converting photons $\text{PSII}^{-1} \text{s}^{-1}$ to electrons $\text{PSII}^{-1} \text{s}^{-1}$) or $JV_{\text{P}_{\text{II}}}$ (converting photons $\text{m}^{-3} \text{s}^{-1}$ to electrons $\text{m}^{-3} \text{s}^{-1}$). On the assumption that each photon used to drive PSII photochemistry, the numeric value of ETR is the same as the value of $J_{\text{P}_{\text{II}}}$ or $JV_{\text{P}_{\text{II}}}$ from which it is derived. While it is generally accepted that the ultimate source of the electrons being transported is oxygen, the value of ETR is actually the rate at which electrons reach their defined destination. Clearly, the further along the electron transport chain this destination is, the more scope there is for a mismatch between $J_{\text{P}_{\text{II}}}$ or $JV_{\text{P}_{\text{II}}}$ and ETR.

2.12 Phytoplankton Primary Productivity (PhytoPP)

This term is used as a catch-all for photosynthetic carbon assimilation. No distinction is made between gross and net primary productivity and values for PhytoPP are not reported by RunSTAF.

2.13 Units of fluorescence (F)

Although the reported fluorescence values are unitless, the LabSTAF calibration procedure places the fluorescence output on a defined STAF Unit (**SU**) scale. Importantly, this allows for derivation of the absorption coefficient for PSII light harvesting (a_{LHII}) which is used in the calculation of $JV_{\text{P}_{\text{II}}}$ and $GO_{\text{P}_{\text{II}}}$.

See: [LabSTAF calibration](#)

2.14 Single Turnover (ST)

This term implies that each PSII reaction centre undergoes one charge separation event during each Single Turnover (ST) pulse. A more reasonable assumption is that approximately 12% of centres undergo a second charge separation event when the default 100 μs ST pulse is used. This figure more than doubles with a 200 μs ST pulse, to approximately 27%.

2.15 Data averaging terminology

At very low biomass, averaging of ST data is required to generate reliable curve fits. The base level of ST data is termed the **Seq** (sequence). Several Seqs can be averaged to generate the next level of ST data, the **Acq** (acquisition) and several Acqs averaged to generate the next level of ST data, the **Saq** (super acquisition). These relationships are illustrated by the example in Figure 2.1.

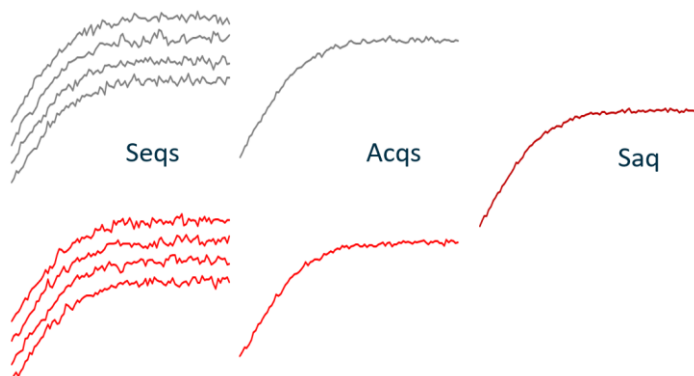


Figure 2.1: Sample ST data acquired at 4 Seqs per Acq and 2 Acqs per Saq.

Seqs are not stored within a RunSTAF data file. Acqs are stored, but not processed in real time. Saqs are processed in real time and displayed. This data structure provides a high degree of control over data acquisition. For example, one Seq per Acq and eight Acqs per Saq could be set for a low biomass sample to provide the highest level of temporal resolution (since every Acq stored will represent a single Seq) while generating a high enough S:N to allow real time fitting of the Saq level data. At the other end of the scale, setting eight Seqs per Acq and one Acq per Saq minimises the size of the data file at a set temporal resolution.

When the dual ST pulse method is used, the programmed level of data averaging is applied to each gap length within the Set. The product of Seqs per Acq, Acqs per Saq and gaps per Set is defined as a **Group**. When running in the Auto FLC mode, all first ST pulses from the Saqs within a Group are averaged to generate a Group acquisition (**Gaq**). With this example, the six gaps and eight Seq per Acq make each Gaq an average of 48 Seqs.

Gaq ST curves are not displayed by RunSTAF but are accessible through data export functions.

See: [The rPE data fit](#) and [Data export functions](#)

2.16 Dual ST pulse-based relaxation phase

The established FRRf method (Kolber, Prášil and Falkowski, 1998) uses a series of very short, very intense 'flashlets' to form a ST pulse. Typically, each flashlet is 1 μ s and the interval between successive flashlets is also 1 μ s. As an example, the default FastOcean ST pulse comprises 100 flashlets over 200 μ s. At the end of this ST pulse, most PSII reaction centres (RCIIs) are in the closed state.

With the FRRf method, the reopening of closed RCIIs can be tracked by applying a relaxation phase measurement that typically comprises tens of widely spaced flashlets. Analysis of the relaxation phase is complicated because a proportion of the reopened RCIIs are reclosed by each relaxation phase flashlet.

LabSTAF uses a dual ST pulse-based relaxation phase method. This incorporates a repeating 'Set' comprising pairs of ST pulses (Figure 2.2). The paired pulses are normally the same duration, with a variable gap between them. The default Set incorporates six gaps of 200, 400, 800, 1600, 3200 and 6400 μ s between the end of the first ST pulse and the start of the second ST pulse. The interval between the end of the second ST pulse in one pair and the start of the first ST pulse in the next pair is constant, with a default value of 120 ms. Although this approach usually generates fewer relaxation phase points than a typical FRRf relaxation phase measurement, these points have much

higher precision and require fewer assumptions to be made when deriving relaxation phase parameters.

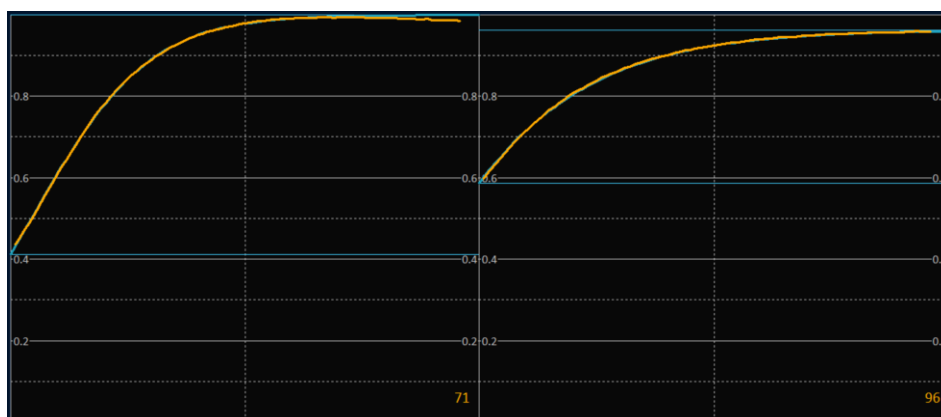


Figure 2.2: The gap between the two ST pulse in this example cropped from the data screen is 800 μ s.

See: [The relaxation phase fit](#)

2.17 Interrogated volume

The LabSTAF sample chamber can hold up to 20 mL of sample. ST data are acquired from a sub-volume of approximately 0.5 mL (the interrogated volume). The measurement LEDs (MLEDs) are focussed on a slightly larger volume to ensure that the interrogated volume is evenly illuminated by the MLEDs. The entire sample is evenly illuminated by the actinic light source.

The default Seq interval set by RunSTAF is 120 ms. Although RCIIIs closed by a single ST pulse normally reopen on a much shorter timescale than this, a long sequence of ST pulses applied to a static dark sample can result in the accumulation of closed RCIIIs. This occurs over several seconds to tens of seconds and is due to the reduction of electron carriers downstream of PSII. This downstream reduction of electron carriers feeds back to PSII and increases the time required for RCIIIs that have been closed by an ST pulse to reopen.

Exchange of cells between the interrogated volume and the rest of the sample within the LabSTAF sample chamber greatly decreases the accumulation of closed RCIIIs. If the supplied stirrer unit is used, the cells within the interrogated volume are actually exchanged several times during a Group acquisition of a few seconds which further decreases the accumulation of closed RCIIIs.

See: [LabSTAF hardware setup](#)

2.18 Correcting for the package effect

The absorption method for assessing $J_{V_{PII}}$ and GO_{PII} is sensitive to the so-called package effect (Boatman, Geider and Oxborough, 2019). Within RunSTAF, a Package Effect Correction (PEC) is applied to correct for this phenomenon. A value for the PEC parameter can be set manually by the user or generated by the Automated Dual Waveband Measurement (Auto DWM) function.

See: [Auto DWM](#) and [Package Effect Correction \(PEC\)](#)

2.19 Spectral correction

The Measurement LEDs (MLEDs) within LabSTAF emit within narrow spectral bands while the Actinic LED (ALED) within LabSTAF provides a broad spectral output. It follows that derivation of J_{PII} , $J_{V_{PII}}$ and GO_{PII} values must include a spectral correction for the difference between the overall output from the combination of MLEDs used to generate the primary ST data and the output of the ALED.

The spectral correction protocol incorporated within RunSTAF generates values of F_v and σ_{PII} for each of the MLED wavebands through the Photochemical Excitation Profile (PEP) function. The PEP data are then used to generate values of F_v and σ_{PII} that are spectrally matched to the ALED.

See: [The Photochemical Excitation Profile \(PEP\) and Spectral Correction \(SC\)](#)

In Figures 2.3 and 2.4, the F_v and σ_{PII} values shown next to the key lines are for the selected MLED waveband (447 nm). The numbers in brackets are ratios of the selected MLED parameter values to the ALED values. In this case, the photon yield of F_v for the 447 nm waveband is 1.618 x greater than it would be for the ALED and the σ_{PII} value for the 447 nm waveband is 1.77 x greater than it would be for the ALED.

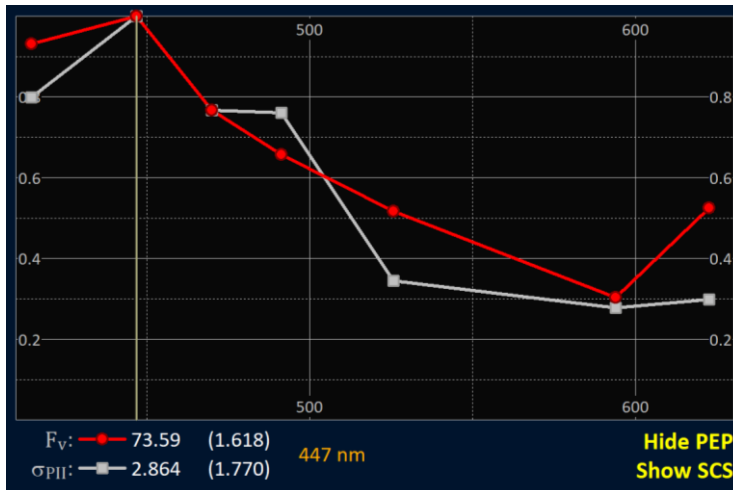


Figure 2.3: This PEP example, cropped from the home screen, plots the F_v and σ_{PII} values for each MLED waveband. The sample was cultured cells of the diatom, *Conticribra weissflogii* (CCAP 1085/18). The differences observed between F_v and σ_{PII} values were consistent over a series of reps.

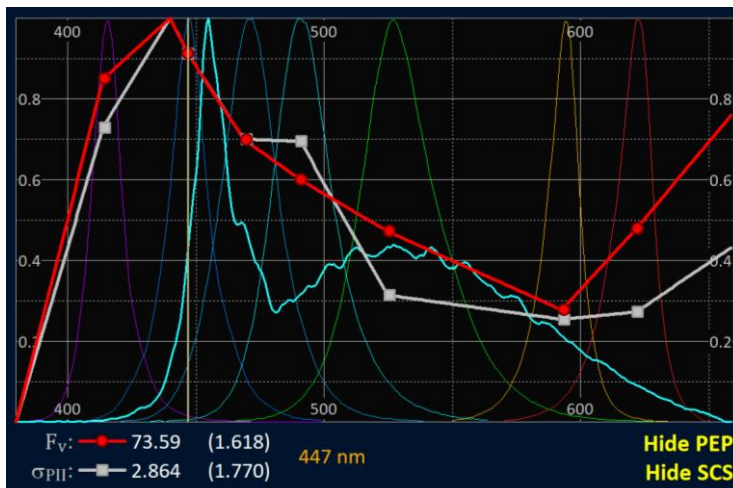
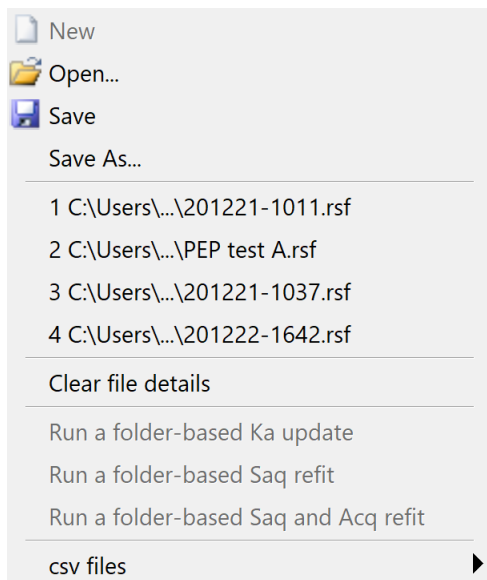


Figure 2.4: The Spectral Correction Spectra (SCS) from the MLEDs and ALED are recorded at 1 nm resolution as part of the LabSTAF calibration procedure. These data are used by RunSTAF within the spectral correction protocol.

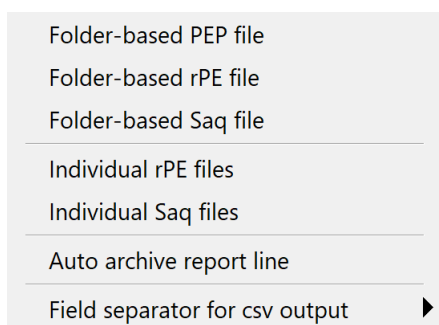
3 RunSTAF menus

3.1 File



In addition to the standard file menu options, the **File** menu includes functions to update the K_a value applied across all files within a folder and refit all RunSTAF files within a folder.

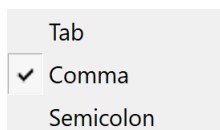
Only one file at a time can have access to an attached LabSTAF. Consequently, the **New** command is only active when the current file contains data (and is, by definition, no longer new) and acquisition has been stopped to release the LabSTAF unit.



The **csv files** option opens a sub-menu of functions for generating character separated value (csv) files. The **Folder-based file** and **Individual files** options are only available when RunSTAF is first started.

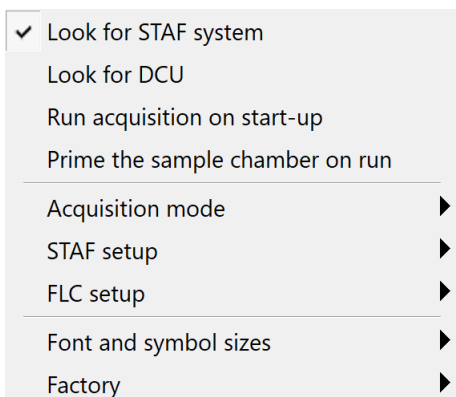
If the **Auto archive report line** option is checked, a csv summary file is created to match with each data file generated by RunSTAF.

See: [Data export functions](#)



The **Field separator for csv output** option opens a sub-menu that allows the default **Comma** field separator to be replaced with a **Tab** or a **Semicolon**. The selection is applied across all csv files generated by RunSTAF.

3.2 Settings

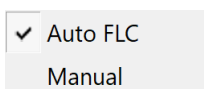


Look for STAF system must be active for data acquisition.

Look for DCU should be set as active if RunSTAF is installed on a DCU.

When **Run acquisition on start-up** is active, acquisition starts as soon as the connected LabSTAF is attached to RunSTAF.

If **Prime the sample chamber on run** is active, RunSTAF will implement the **Exchange** settings from **FLC Setup** before starting acquisition.



The **Acquisition mode** sub-menu can be used to switch between the **Auto FLC** mode and **Manual** mode.

- Save to file...
- Load from file...
- Load defaults

The **STAF setup** and **FLC setup** menus both provide options to save and load settings to a named file and to reset to the default values.

- ✓ Font A
- Font B
- Font C
- Font D (largest)

- Symbol A
- Symbol B
- ✓ Symbol C
- Symbol D (largest)

The **Font** and **Symbol** sizes sub-menu provides options that can be used to improve the screen layout. These are primarily for use on computers other than the supplied Surface Go 2.

RunSTAF must be restarted to implement a change in font size. Symbol size changes are implemented immediately.

- View calibration data
- Save calibration data
- Load calibration data
- Update across files

- Import calibration text
- Import US-SQS/L values
- US-SQS/L MLED correction

- Make SPC file

- Calibration and test modes ▶

The **Factory** sub-menu provides access to functions for factory use.

See: [LabSTAF calibration](#)

3.3 Clipboard

- DWM data
- PEP data
- SCS data
- rPE data
- Tau data

- Saq parameters
- Saq traces
- Saq trace fits (rho)
- Saq trace fits (dimer)


- Acq parameters
- Acq traces
- Acq trace fits (rho)
- Acq trace fits (dimer)

The **Clipboard** menu incorporates options for copying data from an open file to the Windows Clipboard.

Options not available from a specific file are greyed out. In the example shown here, the file includes valid **DWM data**, **PEP data**, **rPE data** and **Tau data**. The **Acq** options are greyed out because the number of Acqs per Saq was set to one. Consequently, these functions would generate the same output as the equivalent **Saq** functions.

3.4 Help

The Help menu has only one member...

-  About RunSTAF...

This provides the current version of RunSTAF through **About RunSTAF...**

4 An introduction to the Auto FLC mode

4.1 Overview

The **Auto FLC** mode within RunSTAF incorporates a wide range of features for protocol design. The LabSTAF system includes a range of accessories which can be combined with these features to provide different levels of automation. Figure 4.1 shows the physical setup used for this introduction to the FLC mode. It incorporates the peristaltic pump unit, solenoid unit and flow-through stirrer unit included within the supplied accessory kit.

For sample exchange, solenoid valve A is switched from the default position of Normally Open (**NO**) to Normally Closed (**NC**) state. This allows the peristaltic pump to pull a fresh sample into the sample chamber (in this case, from the sample bottle located within the water bath). This displaces the previous sample which passes through the peristaltic pump head (in this case, into a waste bottle located behind the unit).

Once sample exchange has completed, solenoid valve A is switched back to the NO state and all tubing between the solenoid valve and the waste bottle are flushed with air. The peristaltic pump is then turned off. While the FLC is running, the **Mix** function is used to refresh the air space above the sample between **Steps**.

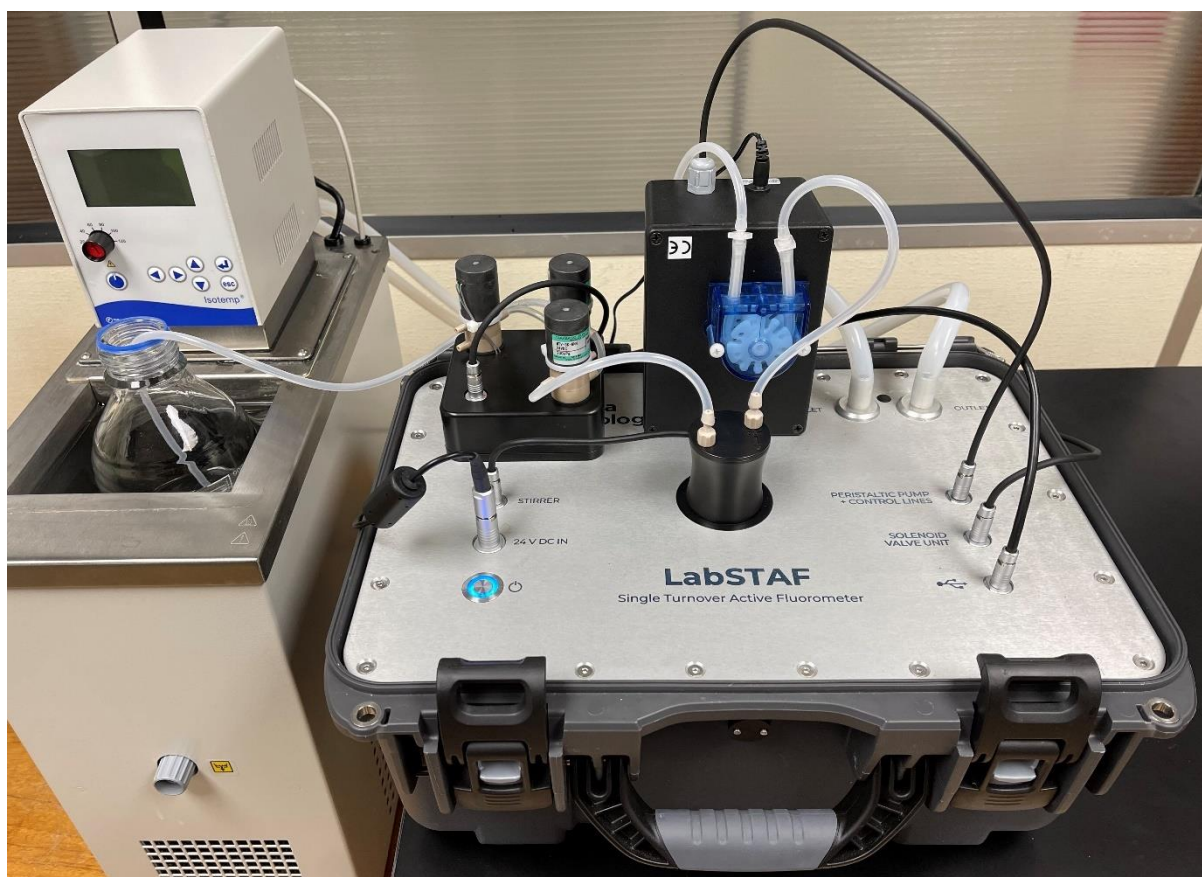
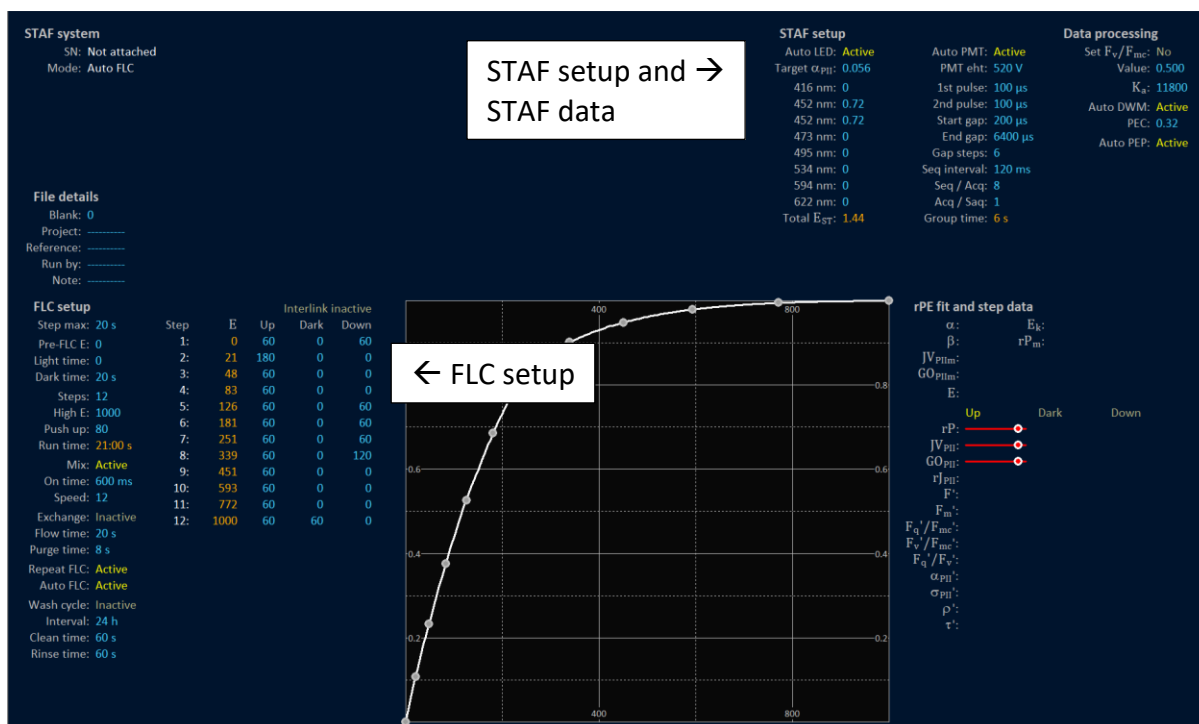


Figure 4.1: The system used to generate the examples within this section. The sample exchange process displaces the cells within the sample chamber with cells from the bottle sat in the water bath. The displaced cells are transferred to a waste bottle located out of view. The only section of tubing that isn't emptied by the **Exchange (purge)** phase of sample exchange (see below) is the short length between the sample bottle and the solenoid valve unit.

4.2 Auto FLC mode

The screenshot below provides an example of the RunSTAF home screen when the **Auto FLC** acquisition mode is selected and before a RunSTAF unit has been attached. The values shown in teal are editable. The orange values are set by RunSTAF. Yellow text fields are buttons. An editable field can be selected by touching the screen or use of the keyboard touchpad. Buttons can be pressed in the same way.



A LabSTAF unit takes around 30 s to boot up and attach to RunSTAF. This is a fully automated process which includes the uploading of stored calibration data from the LabSTAF unit.

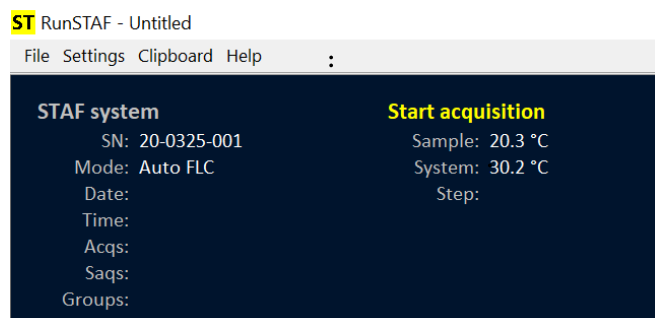
FLC setup	FLC setup
Step max: 20 s	Step max: 20 s
Pre-FLC E: 20	Pre-FLC E: 20
Light time: 0	Light time: 0
Dark time: 0	Dark time: 0
Steps: 12	Steps: 12
High E: 800	High E: 800
Push up: 72	Push up: 72
Run time: 23:00 s	Run time: 23:00 s
Mix: Inactive	Mix: Inactive
On time: 600 ms	On time: 600 ms
Speed: 12	Speed: 12
Exchange: Inactive	Exchange: Active
Flow time: 20 s	Flow time: 20 s
Purge time: 8 s	Purge time: 8 s
Repeat FLC: Active	Repeat FLC: Active
Auto FLC: Active	Auto FLC: Active
Wash cycle: Inactive	Wash cycle: Inactive
Interval: 24 h	Interval: 24 h
Clean time: 60 s	Clean time: 60 s
Rinse time: 60 s	Rinse time: 60 s

For this demonstration, sample exchange between successive FLCs has been activated by pressing the button next to **Exchange**.

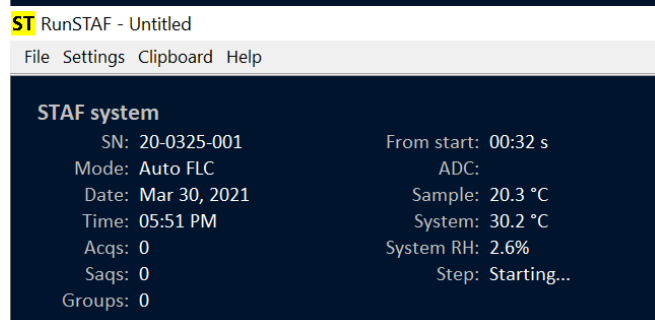
In addition, the sample prime function has been activated through the menu bar...

Settings → Prime the sample chamber on run

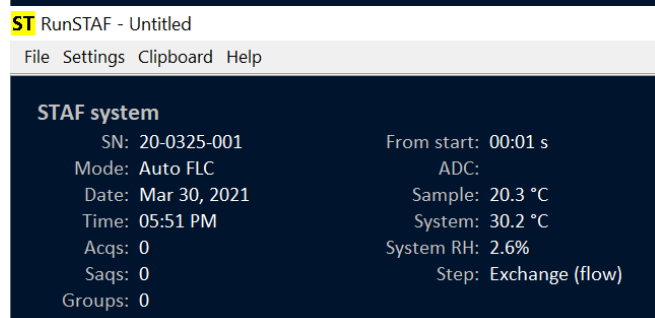
4.3 Starting acquisition – the pre-FLC functions



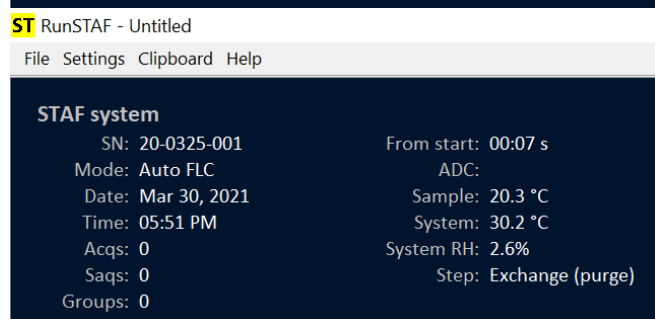
The **Start acquisition** button appears once the boot up sequence has completed. The **Sample** and **System** temperatures are updated every second or so.



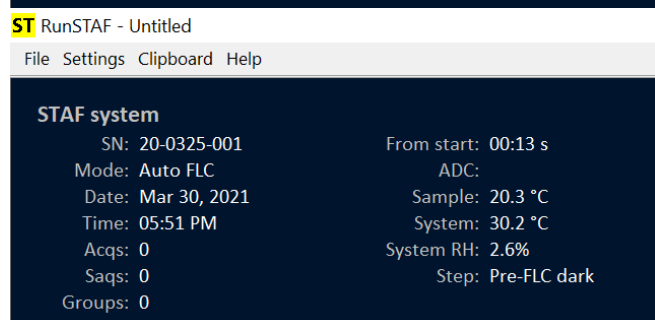
Pressing the **Start acquisition** button starts the LabSTAF programming sequence. Because the sample prime function is active, the **Auto LED** step is interrupted by the sample exchange sequence.



The first step is **Exchange (flow)**. Solenoid A is switched from the default condition of Normally Open (**NO**) to Normally Closed (**NC**) immediately before the peristaltic pump starts. The **From start** value is reset to zero at each step.



Once the flow phase has completed, the peristaltic pump is stopped. The next step is **Exchange (purge)**. Solenoid A is switched back to the NO state immediately before the pump restarts.



Once the purge step has completed, the peristaltic pump is stopped, and the **Pre-FLC light and/or dark** phases are run (if active). In this case, the light step has been set to zero and the dark step has been set to 20 s.

```

ST RunSTAF - Untitled
File Settings Clipboard Help

STAF system
  SN: 20-0325-001           From start: 00:33 s
  Mode: Auto FLC           ADC: 42.1
  Date: Mar 30, 2021       Sample: 20.3 °C
  Time: 05:51 PM          System: 30.2 °C
  Acqs: 0                  System RH: 2.6%
  Saqs: 0                  Step: Auto LED
  Groups: 0

```

The next step is **Auto LED** which incorporates the **Auto PMT** function

```

ST RunSTAF - Untitled
File Settings Clipboard Help

STAF system
  SN: 20-0325-001           From start: 00:37 s
  Mode: Auto FLC           ADC: 40.4
  Date: Mar 30, 2021       Sample: 20.3 °C
  Time: 05:51 PM          System: 30.2 °C
  Acqs: 0                  System RH: 2.6%
  Saqs: 0                  Step: DWM 1 of 3
  Groups: 0

```

In this example, the **Auto DWC** option is active. Three DWC reps are run after the Auto LED step.

See: [Package Effect Correction \(PEC\)](#)

```

ST RunSTAF - Untitled
File Settings Clipboard Help

STAF system
  SN: 20-0325-001           From start: 00:40 s
  Mode: Auto FLC           ADC: 41.5
  Date: Mar 30, 2021       Sample: 20.3 °C
  Time: 05:51 PM          System: 30.2 °C
  Acqs: 0                  System RH: 2.6%
  Saqs: 0                  Step: PEP 1 of 3
  Groups: 0

```

The **Auto PEP** option is also active. Three PEP reps are run after the Auto LED and DWC step.

See: [Photochemical Excitation Profile \(PEP\)](#)

4.3.1 STAF setup

```

STAF setup
  Auto LED: Active           Auto PMT: Active
  Target  $\alpha_{PII}$ : 0.056   PMT eht: 520 V
  416 nm: 0                   1st pulse: 100  $\mu$ s
  452 nm: 0.9242             2nd pulse: 100  $\mu$ s
  452 nm: 0.9688             Start gap: 200  $\mu$ s
  473 nm: 0                   End gap: 6400  $\mu$ s
  495 nm: 0                   Gap steps: 6
  534 nm: 0                   Seq interval: 120 ms
  594 nm: 0                   Seq / Acq: 16
  622 nm: 0                   Acq / Saq: 1
  Total  $E_{ST}$ : 1.893         Group time: 12 s

```

The protocol set for these measurements includes the dual ST pulse function with the default option of 100 μ s pulses and six gap steps between 200 and 6400 μ s.

```

STAF setup
  Auto LED: Active           Auto PMT: Active
  Target  $\alpha_{PII}$ : 0.056   PMT eht: 520 V
  416 nm: 0                   1st pulse: 100  $\mu$ s
  452 nm: 0.9242             2nd pulse: ----
  452 nm: 0.9688             Start gap: ----
  473 nm: 0                   End gap: ----
  495 nm: 0                   Gap steps: 6
  534 nm: 0                   Seq interval: 120 ms
  594 nm: 0                   Seq / Acq: 16
  622 nm: 0                   Acq / Saq: 1
  Total  $E_{ST}$ : 1.893         Group time: 12 s

```

The second ST pulse (**2nd pulse**) is automatically set to zero while the **Auto LED**, **Auto DWC** and **Auto PEP** functions are running.

STAF setup

Auto LED: Active	Auto PMT: Active
Target α_{PII} : 0.056	PMT eht: 360 V
416 nm: 0	1st pulse: 100 μ s
452 nm: 0.5237	2nd pulse: ----
452 nm: 0.5511	Start gap: ----
473 nm: 0	End gap: ----
495 nm: 0	Gap steps: 6
534 nm: 0	Seq interval: 120 ms
594 nm: 0	Seq / Acq: 16
622 nm: 0	Acq / Saq: 1
Total E_{ST} : 1.075	Group time: 12 s

STAF setup

Auto LED: Active	Auto PMT: Active
Target α_{PII} : 0.056	PMT eht: 340 V
416 nm: 0.5235	1st pulse: 100 μ s
452 nm: 0.5237	2nd pulse: ----
452 nm: 0.3768	Start gap: ----
473 nm: 0.5236	End gap: ----
495 nm: 0.6587	Gap steps: 1
534 nm: 0.6577	Seq interval: 120 ms
594 nm: 0.1731	Seq / Acq: 16
622 nm: 0.4729	Acq / Saq: 1
Total E_{ST} : 3.91	Group time: 2 s

STAF setup

Auto LED: Active	Auto PMT: Active
Target α_{PII} : 0.056	PMT eht: 360 V
416 nm: 0	1st pulse: 100 μ s
452 nm: 0.5237	2nd pulse: 100 μ s
452 nm: 0.5511	Start gap: 200 μ s
473 nm: 0	End gap: 6400 μ s
495 nm: 0	Gap steps: 6
534 nm: 0	Seq interval: 120 ms
594 nm: 0	Seq / Acq: 16
622 nm: 0	Acq / Saq: 1
Total E_{ST} : 1.075	Group time: 12 s

The **Auto LED** function runs first. This adjusts the E_{ST} values for non-zero channels to aim at the **Target α_{PII}** value. In this example, the E_{ST} values for the two 452 nm channels have been decreased. These values are used for the DWC function.

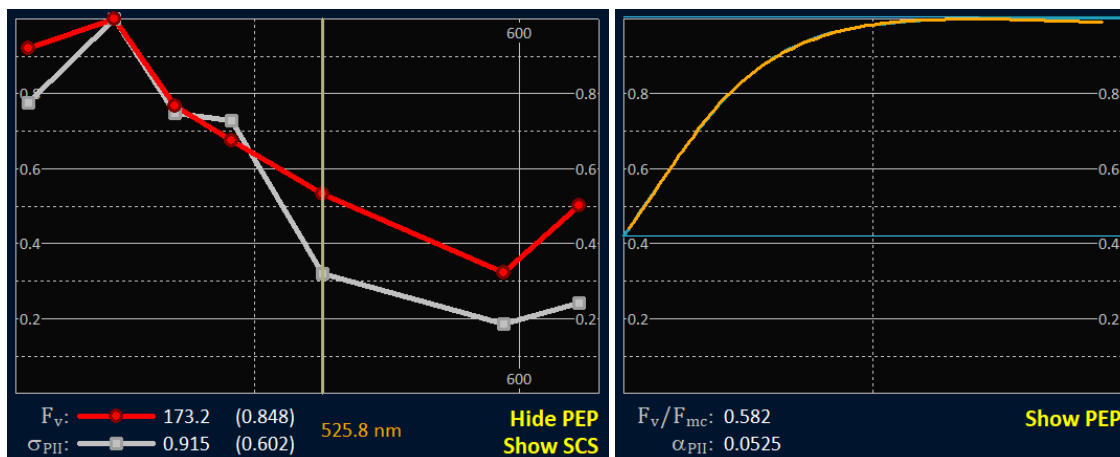
The **Auto PEP** function sets appropriate E_{ST} values for all eight channels.

See: [Photochemical Excitation Profile \(PEP\)](#)

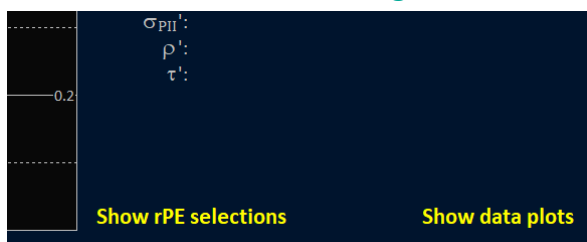
Once the **Auto PEP** function has completed, the second ST pulse is set back to its original value and the E_{ST} values previously set by the **Auto LED** function are implemented.

4.4 Switching between the PEP and the most recent ST curve

If the **Auto PEP** function is run, the PEP generated is shown on the home screen by default. Once the FLC starts, the most recent ST curve can be shown in place of the PEP by pressing the **Show ST curve** button. Pressing the **Show PEP** button returns to the PEP.

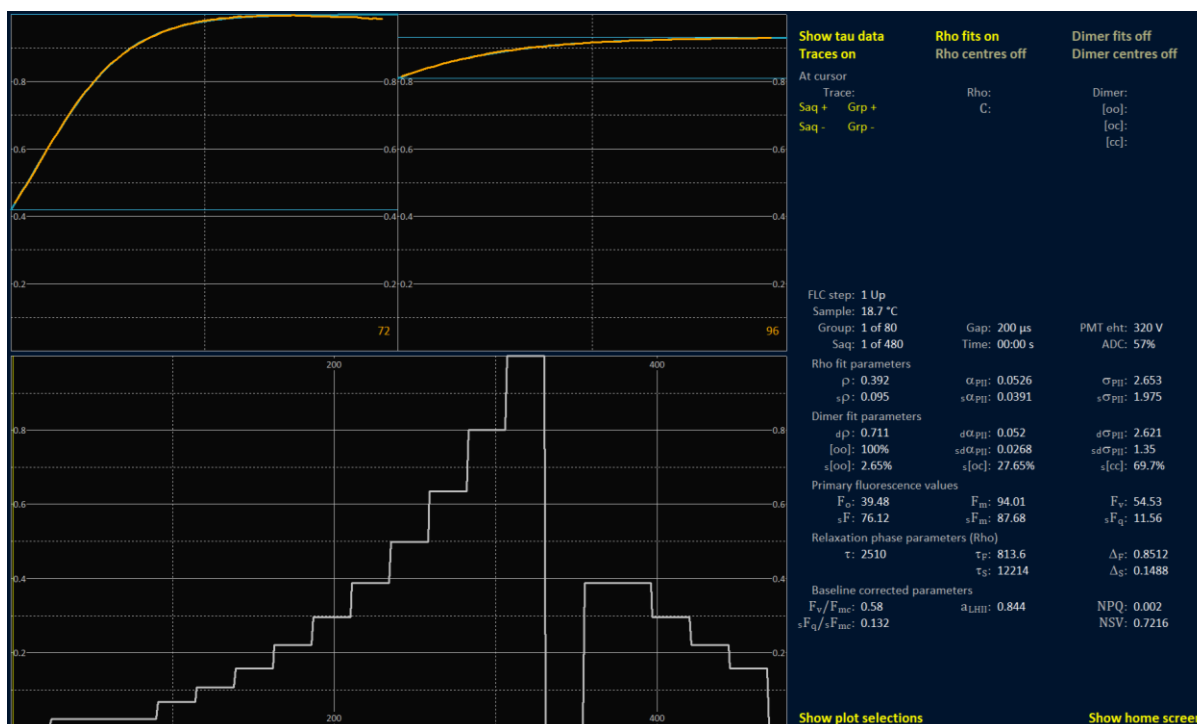


4.4.1 The data screen during Auto FLC mode

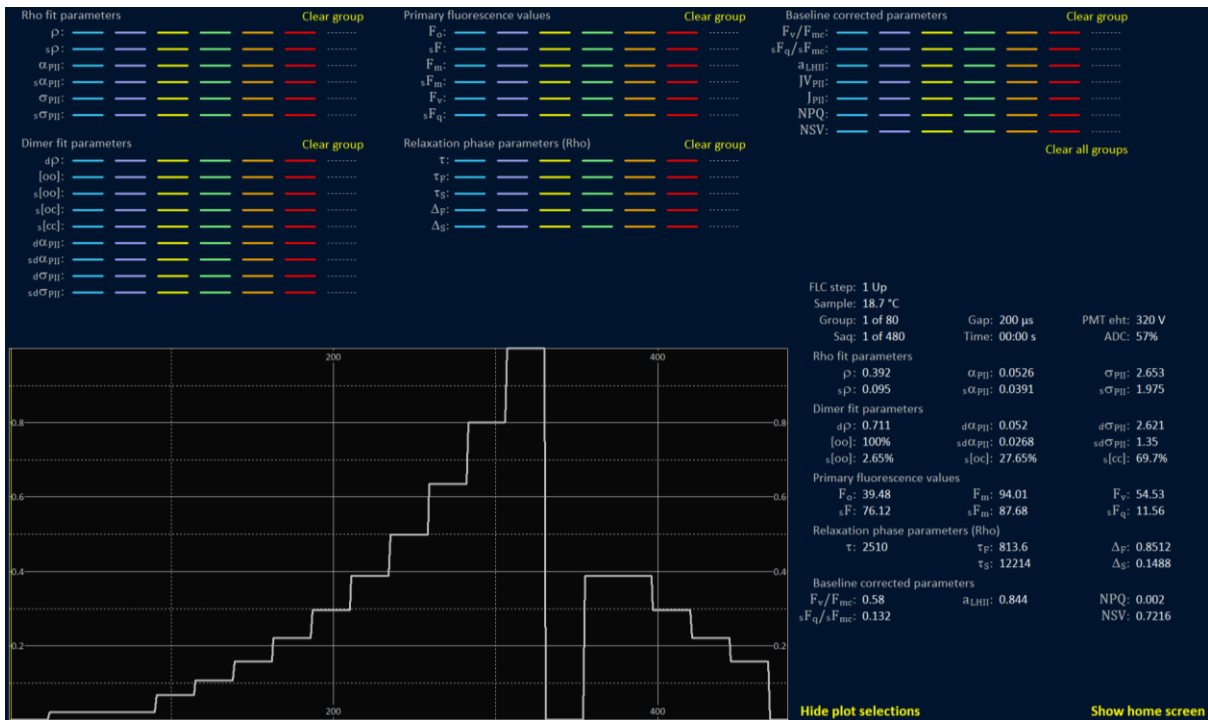


The **Show data plots** button appears at the bottom right of the home screen once the FLC has started. Pressing this button switches the view to the **data screen**.

The screenshot below shows the data screen with the default selections active (**Show tau data**, **Traces on** and **Rho fits on**). The two plots on top show a dual pulse ST acquisition, while the lower plot window shows the actinic LED protocol implemented during this FLC as a white line.

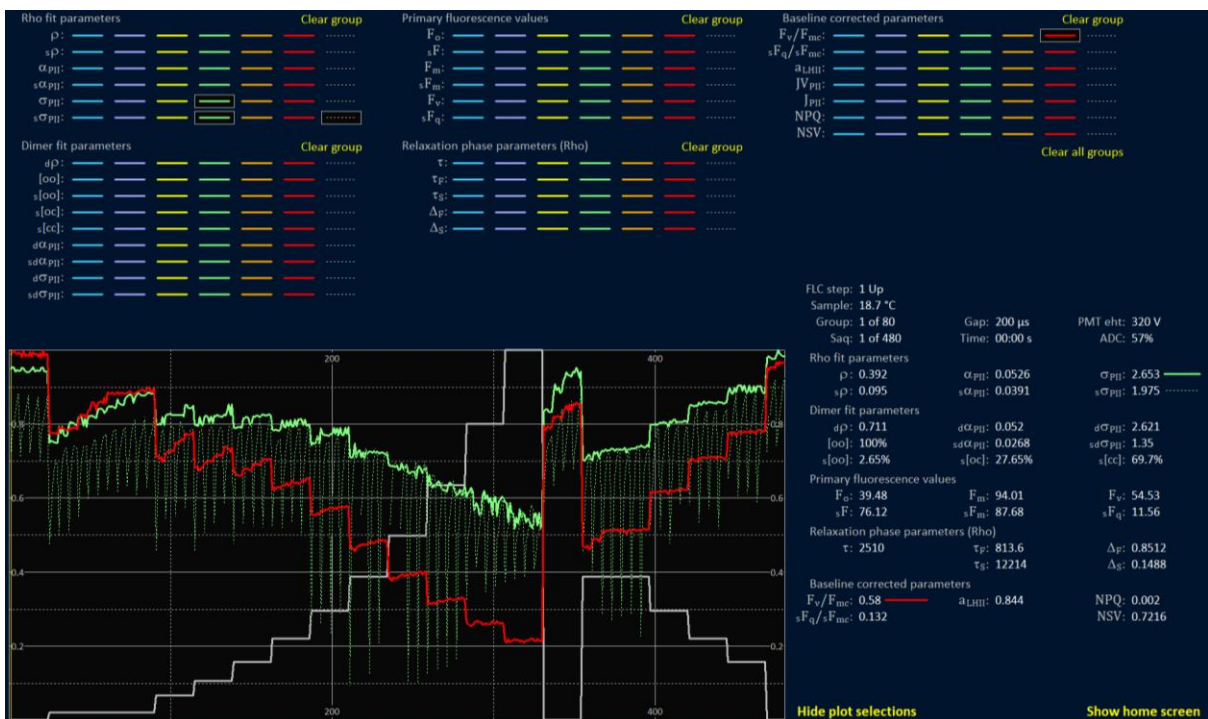


Pressing the **Show plot selections** button reveals the range of plot options.



Most plot selection labels are appropriate for a dark-adapted sample. In the example below, σ_{PII} and $s\sigma_{PII}$ are selected as green plots with the latter as a dashed line. F_v/F_{mc} is plotted in solid red. For light measurements, σ_{PII}' and $s\sigma_{PII}'$ and F_q'/F_{mc}' are plotted with the same pens.

See: [Glossary of parameter terms](#)

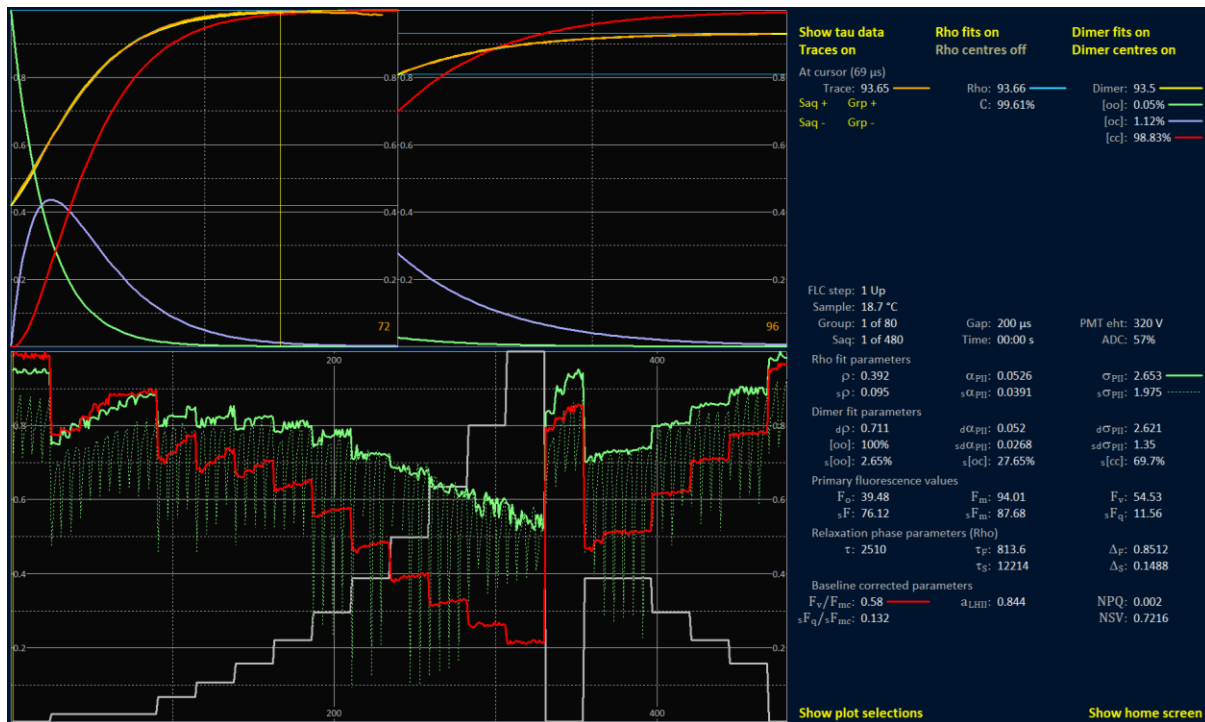


Pressing the Hide plot selections returns the top half of the view to the ST pulse or pulse pair.

In the next example, the **Dimer fits on** and **Dimer centres on** options have been activated. The Dimer fits are shown as yellow traces. The green, purple and red traces track the proportions of dimers in the open-open (oo), open-closed (oc) and closed-closed (cc) states, respectively. For a

homogeneous population of cells, the Rho and Dimer fits generate very similar curves. The data shown were recorded from culture cells of the marine diatom, *Phaeodactylum tricornutum*.

See: [The Rho ST curve fit](#) and [the Dimer ST curve fit](#)



4.5 The relaxation phase fit

Pressing the **Show tau data** button switches the top panel to show a plot of the relaxation phase data. The first screenshot below shows the default tau data fit (**Rho** selection).



The next screenshot shows the **Fv**, **Rho** and **Dimer** tau fits. The **Fv** plot tracks the recovery back towards F_v or F_v' with the increasing gap between the first and second ST pulses in a dual pulse

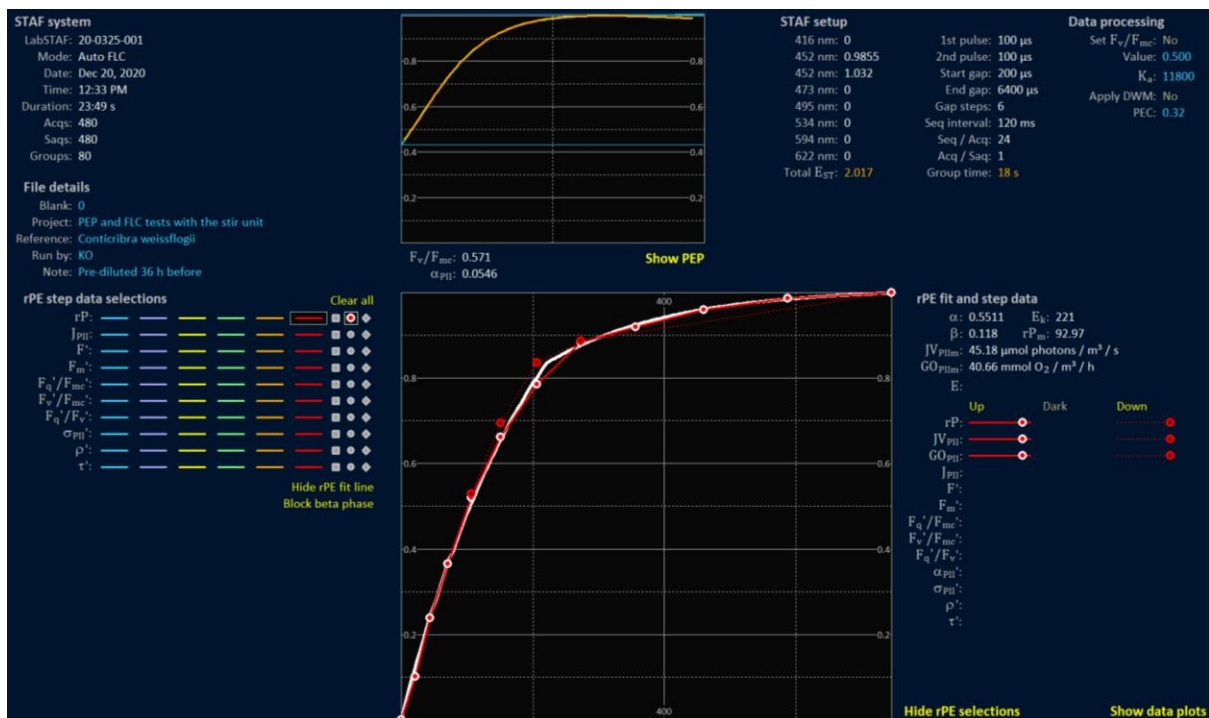
sequence. Rho and Dimer fits track the reopening of PSII reaction centres between the first and second ST pulses. Each plot value is the proportion of centres closed by the first ST pulse that are still in the closed state at the start of the second ST pulse.



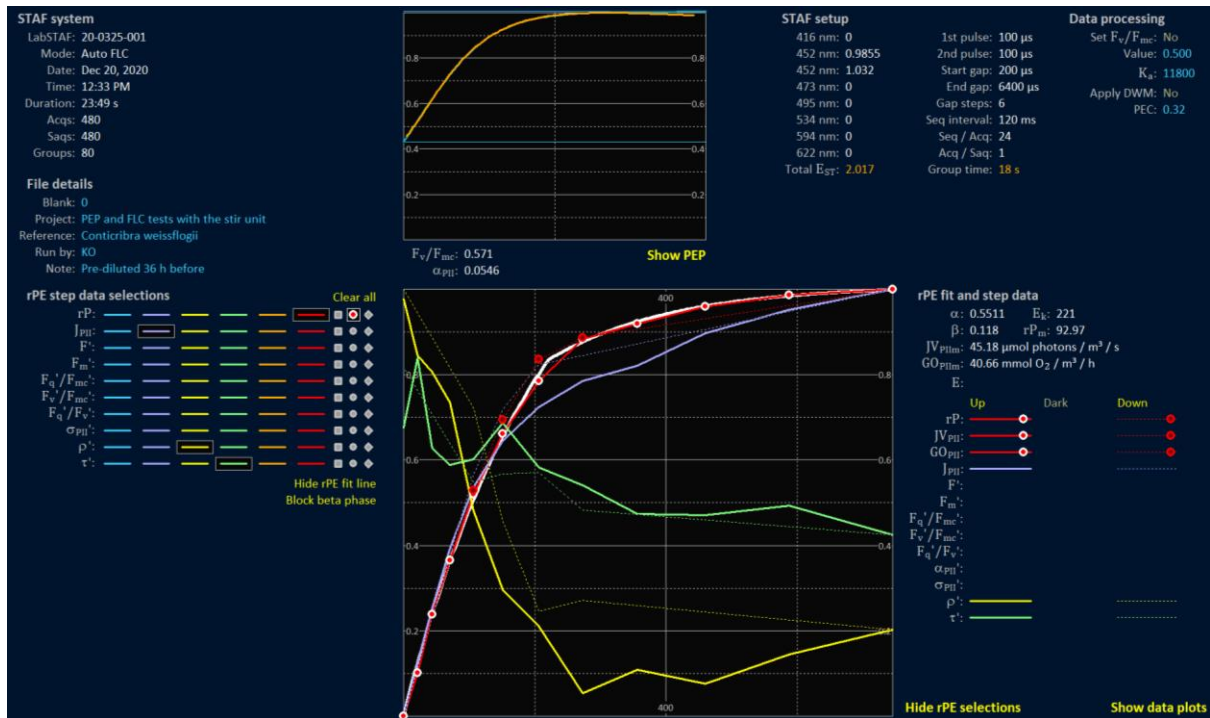
See: [Analysis of dual ST pulse data](#)

4.6 FLC setup

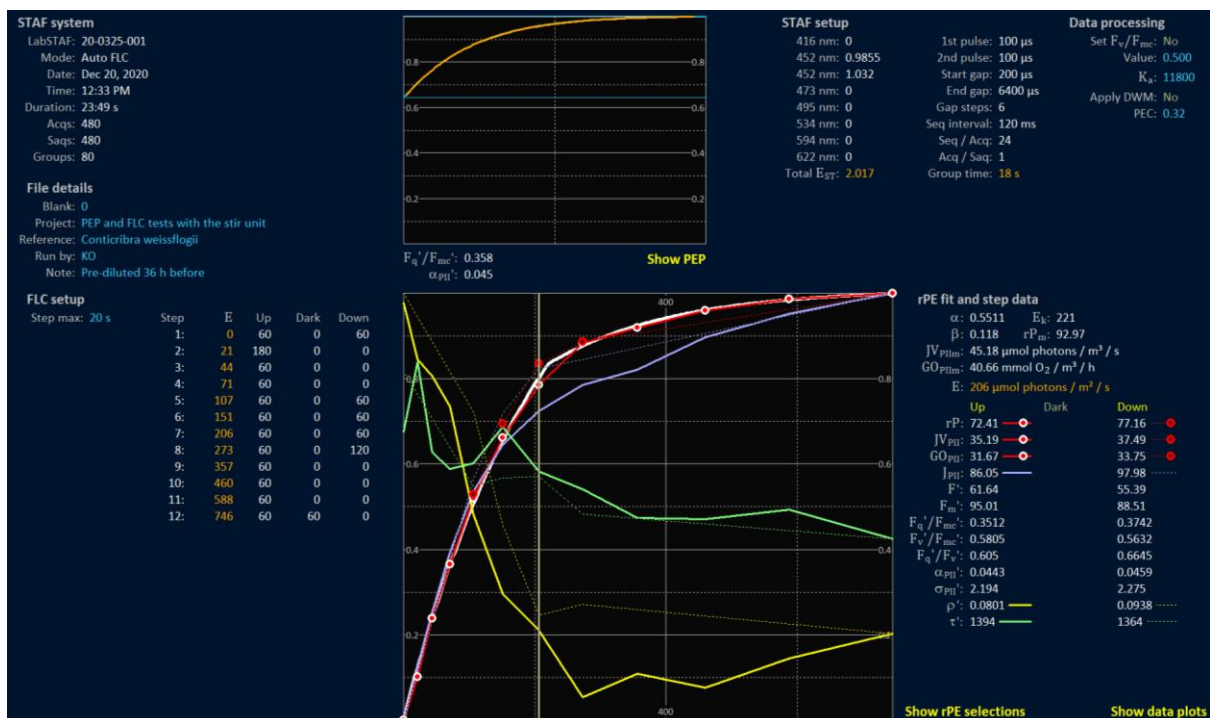
The **Auto FLC** option under **FLC setup** is active in this example. The next screenshots show how this option operates during a sequence of FLCs. The first screenshot shows a completed FLC with the **Show rPE selections** button pressed. The red line and symbols show the actual data values while the white line shows the curve fit used to generate the reported values of α , E_k , β and rP_m .



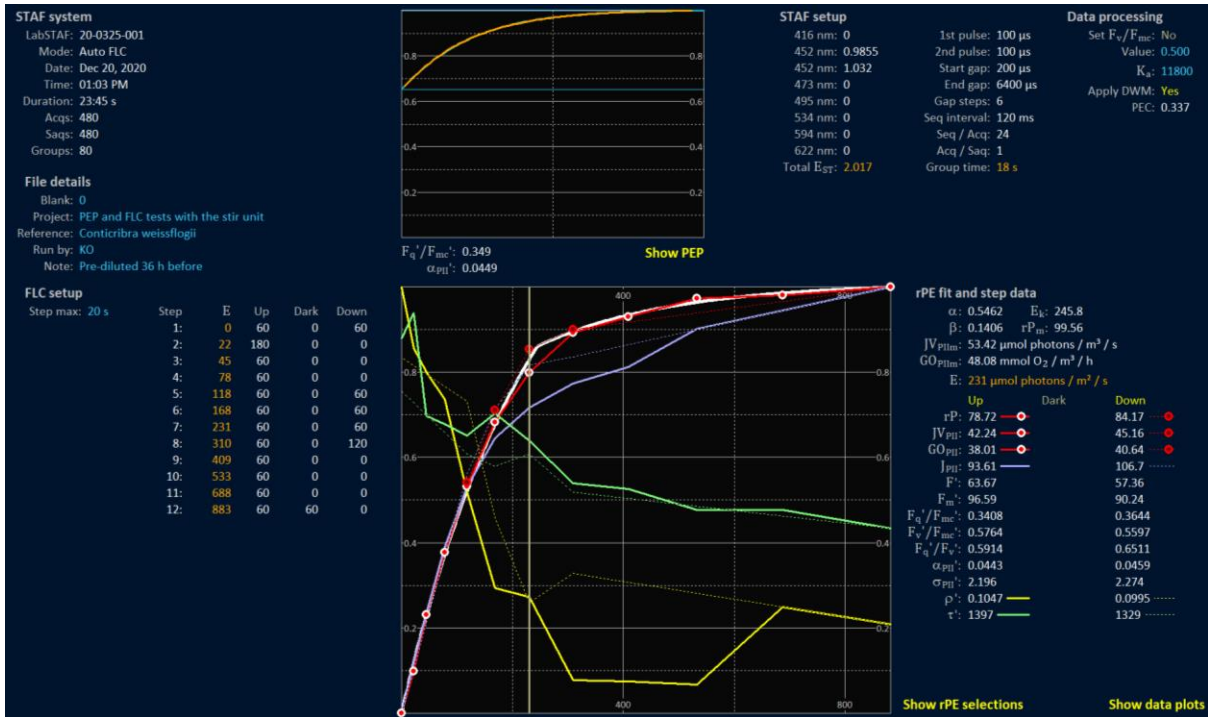
In the screenshot below, the plot options for J_{PII} , ρ' and τ' have been selected for display as lines without symbols.



In the next screenshot, the Hide rPE selections button has been pressed, hiding the plot options on the left hand side of the plot. Within the plot, the closest point to E_k has been selected, indicated by the vertical line. Values corresponding to this photon irradiance are now displayed on the right.



If the Auto FLC option is active, the High E value is automatically adjusted to four times the E_k value from the previous FLC. In this example, the previous FLC (above) has an E_k of 220.7 μ mol photons $m^{-2} s^{-1}$ which has been rounded up to 221 μ mol photons $m^{-2} s^{-1}$ on the screen. Consequently, the High E value for the next FLC (at Step 12 in the screenshot below) is set to 883 μ mol photons $m^{-2} s^{-1}$. The next two completed FLCs in the sequences are shown below.



4.7 Archiving of data

Completed data files are automatically archived with a timestamp as the filename (YYMMDD followed by the time in 24 h format). Within the example in Figure 4.2, the first file generated is named 201220-1233 indicating that the FLC started on 20th December 2020 at 12:33 pm.

...\Documents\CT-RunSTAF\Data files\

<input checked="" type="checkbox"/>	Run STAT	201220-1233	✔	08/01/2021 12:34	RSF File	1,170 KB
	Run STAT	201220-1303	✔	19/02/2021 19:07	RSF File	1,156 KB
	Run STAT	201220-1332	✔	08/01/2021 12:34	RSF File	1,184 KB
	Run STAT	201220-1402	✔	08/01/2021 12:34	RSF File	1,288 KB
	Run STAT	201220-1435	✔	08/01/2021 12:34	RSF File	1,288 KB

Figure 4.2: Screenshot from the Auto-saved sub-folder showing consecutive files.

5 An introduction to the Manual mode

The manual mode is set by selecting...

Settings → Acquisition mode → Manual

Switching the mode from **Auto FLC** to **Manual** allows for more settings to be changed during an experiment. The screenshot below shows the RunSTAF home screen with the manual mode selected and the RunSTAF unit attached.

STAF system
 SN: 20-0325-001
 Mode: Manual
 Date:
 Time:
 Acqs:
 Saqs:
 Groups:

Start acquisition
 Sample: 21.8 °C
 System: 25.7 °C

STAF setup
 Auto LED: **Active**
 Target α_{PII} : 0.056
 416 nm: 0
 452 nm: 0.9708
 452 nm: 1.016
 473 nm: 0
 495 nm: 0
 534 nm: 0
 594 nm: 0
 622 nm: 0
 Total E_{ST} : 1.987

Data processing
 Auto PMT: **Active**
 PMT eht: 440 V
 1st pulse: 100 μ s
 2nd pulse: 100 μ s
 Start gap: 200 μ s
 End gap: 6400 μ s
 Gap steps: 6
 Seq interval: 120 ms
 Seq / Acq: 16
 Acq / Saq: 1
 Group time: 12 s

Data processing
 Set F_v/F_{mc} : No
 Value: 0.500
 K_a : 11800
 Auto DWM: Inactive
 PEC: 0.32
 Auto PEP: Inactive

File details
 Blank: 0
 Project: _____
 Reference: _____
 Run by: _____
 Note: _____

Manual settings
 Pause acquisition: Off
 PMT waveband: HC685 \pm 10 nm
 Actinic: 0
 Solenoid A: NO to COM
 Solenoid B: NO to COM
 Solenoid C: NO to COM
 Pump: Off
 Speed: 12
 Mix: Inactive
 On time: 600 ms
 Speed: 12
 Interval: 60 s
 Auto archive: **Active**
 New file every: 60 minutes

Auto FLC and → Manual modes

← Manual mode only

The **STAF setup** and **Data processing** sections are identical for both the Auto FLC and Manual modes. The **Manual settings** section provides real time control of LabSTAF functions.

STAF setup		Data processing
Auto LED: Active	Auto PMT: Active	Set F_v/F_{mc} : No
Target α_{PII} : 0.056	PMT eht: 440 V	Value: 0.500
416 nm: 0	1st pulse: 100 μ s	K_a : 11800
452 nm: 0.9708	2nd pulse: 100 μ s	Auto DWM: Inactive
452 nm: 1.016	Start gap: 200 μ s	PEC: 0.32
473 nm: 0	End gap: 6400 μ s	Auto PEP: Inactive
495 nm: 0	Gap steps: 6	
534 nm: 0	Seq interval: 120 ms	
594 nm: 0	Seq / Acq: 16	
622 nm: 0	Acq / Saq: 1	
Total E_{ST} : 1.987	Group time: 12 s	

In this first step, data were acquired for a basic check with the **Auto DWM** and **Auto PEP** both set as **Inactive**.

The **Auto LED** and **Auto PMT** were left as **Active**.

Halt acquisition
 From start: 00:28 s
 ADC: 69.9
 Sample: 21.9 °C
 System: 25.6 °C
 System RH: 23.4%
 Step: Manual

F_v/F_{mc} : 0.454
 α_{PII} : 0.0594

After the **Start acquisition** button was pressed, the system ran through the **Auto LED** function and started acquiring data. Here, the most recent Saq is shown on the home screen.

STAF setup

Auto LED: **Active**
 Target α_{PII} : **0.056**
 416 nm: 0.9705
 452 nm: 0.9708
 452 nm: 0.6986
 473 nm: 0.9703
 495 nm: 0.6587
 534 nm: 0.6577
 594 nm: 0.1731
 622 nm: 0.4729
 Total E_{ST} : **5.572**

Auto PMT: **Active**
 PMT eht: **380 V**
 1st pulse: **100 μ s**
 2nd pulse: ----
 Start gap: ----
 End gap: ----
 Gap steps: **1**
 Seq interval: **120 ms**
 Seq / Acq: **16**
 Acq / Saq: **1**
 Group time: **2 s**

Data processing

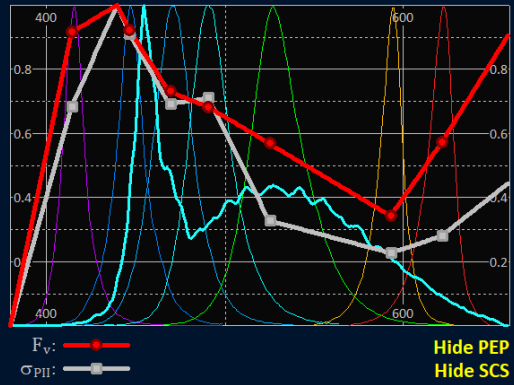
Set F_v/F_{mc} : No
 Value: **0.500**
 K_a : **11800**
 Auto DWM: **Active**
 Apply DWM: **Yes**
 PEC: **0.451**
 Auto PEP: **Active**

The next step was to restart acquisition with the **Auto DWM** and **Auto PEP** both set as **Active**.

This crop from the home screen was acquired while the PEP was running (after the DWM had completed).

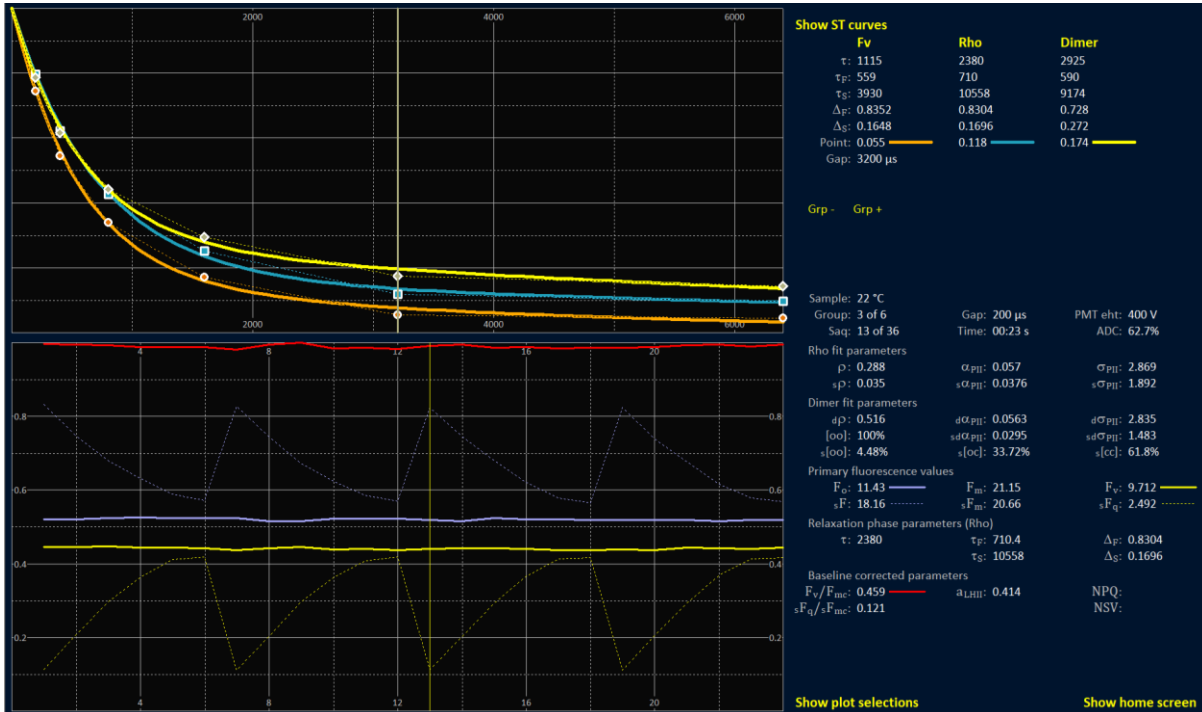
Halt acquisition

From start: 00:40 s
 ADC: 64.3
 Sample: 22 °C
 System: 26.8 °C
 System RH: 23.1%
 Step: Manual



This crop from the home screen shows the completed PEP with **Show SCS** active.

On the data screen, the only difference between the two acquisition modes is the absence of the **FLC step** field when in Manual mode.



Manual settings

Pause acquisition: Off
 PMT waveband: **HC685 \pm 10 nm**
 Actinic: **0**
 Solenoid A: NO to COM
 Solenoid B: NO to COM
 Solenoid C: NO to COM

Manual settings

Pause acquisition: Off
 PMT waveband: **HC730 \pm 10 nm**
 Actinic: **0**
 Solenoid A: NO to COM
 Solenoid B: NO to COM
 Solenoid C: NO to COM

All Manual settings are available during data acquisition. In this example, the **PMT waveband** has been switched from **HC685 \pm 10 nm** to **730 \pm 10 nm**.

6 STAF setup and STAF data

STAF setup		Data processing
Auto LED: Active	Auto PMT: Active	Set F_v/F_{mc} : No
Target α_{PII} : 0.056	PMT eht: 440 V	Value: 0.500
416 nm: 0	1st pulse: 100 μs	K_a : 11800
452 nm: 0.72	2nd pulse: 100 μs	Auto DWM: Active
452 nm: 0.72	Start gap: 200 μs	PEC: 0.32
473 nm: 0	End gap: 6400 μs	Auto PEP: Active
495 nm: 0	Gap steps: 6	
534 nm: 0	Seq interval: 120 ms	
594 nm: 0	Seq / Acq: 8	
622 nm: 0	Acq / Saq: 1	
Total E_{ST} : 1.44	Group time: 6 s	

The **STAF setup** and **Data processing** options are available within both acquisition modes.

This crop from the home screen shows the options available before acquisition has started.

STAF setup		Data processing
416 nm: 0	1st pulse: 100 μs	Set F_v/F_{mc} : No
452 nm: 0.9953	2nd pulse: 100 μs	Value: 0.500
452 nm: 1.044	Start gap: 200 μs	K_a : 11800
473 nm: 0	End gap: 6400 μs	Apply DWM: No
495 nm: 0	Gap steps: 6	PEC: 0.32
534 nm: 0	Seq interval: 120 ms	
594 nm: 0	Seq / Acq: 8	
622 nm: 0	Acq / Saq: 1	
Total E_{ST} : 2.039	Group time: 6 s	

This crop from the home screen shows the **STAF setup** and **Data processing** sections for a completed file with the **Set F_v/F_{mc}** and **Apply DWM** options both set to **No**.

STAF setup		Data processing
416 nm: 0	1st pulse: 100 μs	Set F_v/F_{mc} : Yes
452 nm: 0.9953	2nd pulse: 100 μs	Value: 0.500
452 nm: 1.044	Start gap: 200 μs	K_a : 11800
473 nm: 0	End gap: 6400 μs	Apply DWM: Yes
495 nm: 0	Gap steps: 6	PEC: 0.354
534 nm: 0	Seq interval: 120 ms	
594 nm: 0	Seq / Acq: 8	
622 nm: 0	Acq / Saq: 1	
Total E_{ST} : 2.039	Group time: 6 s	

Here, the **Set F_v/F_{mc}** and **Apply DWM** options both set to **Yes**.

With the **Apply DWM** option set to **No**, the **PEC** value can be edited. With the **Apply DWM** option set to **Yes**, the **PEC** value is generated by the DWM function and cannot be edited.

6.1 STAF setup section

All settings in the left column of **STAF setup** are for the MLEDs. If **Auto LED** is active, the **Set α_{PII}** value provides the target initial slope of RCII closure during the first ST pulse. The value of **0.056** in the above example is equivalent to 5.6% of the RCII population in the open state at $t = 0$ being closed by $t = 1 \mu$ s. The **Auto LED** function adjusts the photon flux from the MLEDs to try and achieve the requested α_{PII} value. LED channels set to zero by the user are left unchanged.

The editable value for each of the eight MLED channels is the photon flux delivered to the interrogated volume by each LED channel with units of photons $\text{nm}^{-2} (100 \mu\text{s})^{-1}$. The **Total E_{ST}** field provides the sum of values from all active channels. $1.0 \text{ photons nm}^{-2} (100 \mu\text{s})^{-1}$ is equivalent to $16,603 \mu\text{mol photons m}^{-2} \text{ s}^{-1}$.

See: [Auto LED](#)

The top two settings in the right column of **STAF setup** set the **Auto PMT** function and the starting **PMT eht**. The Auto PMT function is set to **Active** every time RunSTAF is started.

See: [Auto PMT](#)

Below the PMT settings are the **1st Pulse**, **2nd Pulse**, **Start gap**, **End gap** and **Gap Steps** fields for the dual ST pulse relaxation phase. The default ST pulse duration is 100 μs for both pulses. The start gap, end gap and gap steps values collectively define the sequence of gaps between the end of the first pulse and the start of the second pulse. The first and last gaps are always as set. RunSTAF fills in the intermediate values such that the increase between successive gap lengths is always by the same factor. For example, the default gap sequence (as shown in the above example) is 200, 400, 800, 1600, 3200 and 6400 μs . The relaxation phase analysis is based on the recovery of variable fluorescence between the first and second ST pulses.

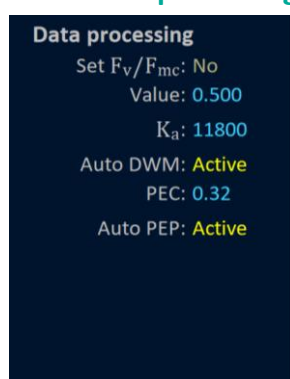
See: [The relaxation phase fit](#)

The **Sequence interval** value sets the interval between the end of one sequence and the start of the next. When the dual pulse method is being used, this is between the end of the second ST pulse for one sequence and the start of the first ST pulse for the next sequence.

The **Seq / Acq** and **Acq / Saq** values define the level of signal averaging.

See: [Data averaging terminology](#)

6.2 Data processing



The **Data processing** section of the home screen facilitates correction for baseline fluorescence (F_b), setting the value of K_a and correction for the package effect.

The first elements (**Set F_v/F_{mc}** and **Value**) control baseline correction by setting an assumed intrinsic value of F_v/F_{mc} for PSII complexes that incorporate photochemically active RCIIIs.

See: [Setting baseline fluorescence \(\$F_b\$ calculation\)](#)

The next element in the **Data processing** column is K_a . Calculated values of JV_{PII} and GO_{PII} are in direct proportion to the set value of K_a . If the value is changed by the user, the new value is immediately applied to values of JV_{PII} and GO_{PII} . All Clipboard and csv functions that incorporate calculated values of JV_{PII} and GO_{PII} include the applied value of K_a .

See: [Generating values of \$JV_{PII}\$ and \$GO_{PII}\$](#)

The **Auto DWM** function runs the Dual Waveband Measurement function when active.

See: [Dual Waveband Measurement \(DWM\)](#)

The **PEC** field sets the value for Package Effect Correction. As shown above, the PEC value is only editable when **Apply DWM** is set to **No**. The calculated values of JV_{PII} and GO_{PII} are inversely proportional to the PEC value.

See: [Package Effect Correction \(PEC\)](#)

6.3 The automated RunSTAF functions

STAF setup		Data processing
Auto LED: Active	Auto PMT: Active	Set F_v/F_{mc} : No
Target α_{PII} : 0.056	PMT eht: 440 V	Value: 0.500
416 nm: 0	1st pulse: 100 μs	K_a : 11800
452 nm: 0.72	2nd pulse: 100 μs	Auto DWM: Active
452 nm: 0.72	Start gap: 200 μs	PEC: 0.32
473 nm: 0	End gap: 6400 μs	Auto PEP: Active
495 nm: 0	Gap steps: 6	
534 nm: 0	Seq interval: 120 ms	
594 nm: 0	Seq / Acq: 8	
622 nm: 0	Acq / Saq: 1	
Total E_{ST} : 1.44	Group time: 6 s	

When data acquisition is started, the active automated functions are run in the order shown below.

6.3.1 Auto PMT

Auto PMT is always active when RunSTAF is started. There is generally no reason to deactivate this function, which optimises the dynamic range of signal detection by adjusting the PMT eht (V). Throughout the experiment, the function continuously monitors the fluorescence signal and ensures that it is kept within dynamic range of the PMT. The value set within the **PMT eht** field is the first value tried when the **Run acquisition** button is pressed. The upper and lower limits for the PMT eht are 800 V and 280 V, respectively. The change in sensitivity of the PMT approximates to a doubling for every 40 V increase in the PMT eht (a factor of 8192:1 between 280 V and 800 V).

6.3.2 Auto LED

This function adjusts the output of all MLED wavebands that are set to non-zero values. In the above example, both **452 nm** channels are set as **0.72**. RunSTAF adjusts the output of both wavebands in proportion to the value set by the user to achieve the **Target α_{PII}** value. These settings are used during the **Auto DWM** function (if active) and while running the FLC. The **Auto LED** function will always run if the **Auto DWM** or **Auto PEP** is active.

6.3.3 Auto DWM

This function measures F_v three times with each of the 685 nm or 730 nm bandpass filters (both ± 10 nm FWHM) located in front of the PMT. Primary DWM data can be accessed through a Clipboard function:

Clipboard → DWM data

See: [Package Effect Correction \(PEC\)](#)

6.3.4 Auto PEP

If this function is active, RunSTAF will work through a set protocol to generate the PEP as relative photon yield values of F_v and values of σ_{PII} for all seven wavebands. The primary PEP data can be accessed through a Clipboard function:

Clipboard → PEP data

The emission spectra for the seven MLED wavebands and the ALED can also be accessed through a Clipboard function:

Clipboard → SCS data

See: [Photochemical Excitation Profile \(PEP\)](#)

7 The FLC setup

FLC setup	Step	E	Up	Dark	Down
Step max: 20 s	1:	0	90	0	60
Pre-FLC E: 20	2:	18	180	0	0
Light time: 0	3:	41	60	60	0
Dark time: 0	4:	70	60	0	0
Steps: 12	5:	106	60	30	60
High E: 800	6:	152	60	0	60
Push up: 72	7:	209	60	0	60
Run time: 23:00 s	8:	280	60	0	120
Mix: Inactive	9:	370	60	0	0
On time: 600 ms	10:	482	60	0	0
Speed: 12	11:	623	60	0	0
Exchange: Inactive	12:	800	60	60	0
Flow time: 20 s					
Purge time: 8 s					
Repeat FLC: Active					
Auto FLC: Active					
Wash cycle: Inactive					
Interval: 24 h					
Clean time: 60 s					
Rinse time: 60 s					

This screenshot shows the **FLC setup** section of the home screen. The left column provides a range of options for setting up the FLC, sample mixing, sample exchange and running a wash cycle. The right side of the FLC setup shows the **E** values ($\mu\text{mol photons m}^{-2} \text{s}^{-1}$) generated by the **Steps**, **High E** and **Push up** values entered in the left column and the set time for each of the steps.

The sequence starts by running through the **Up** column. A non-zero **Dark** period is implemented after the **Up** value at the same **Step**. The **Down** column is run in reverse order after the **Up** column and non-zero **Dark** values have all been implemented.

7.1 Elements of the FLC setup

- Step max:** defines how many Gaqs are used to define each **rPE fit and step data** value
- Pre-FLC E:** photon irradiance for a pre-illumination step ($\mu\text{mol photons m}^{-2} \text{s}^{-1}$)
- Light time:** time at the Pre-FLC E (s)
- Dark time:** time in the dark after the Pre-FLC E step (s)
 - Steps:** number of steps for the FLC
 - High E:** highest actinic photon irradiance for the FLC ($\mu\text{mol photons m}^{-2} \text{s}^{-1}$)
 - Push up:** rate at which the photon irradiance increases through the **Up** steps
- Run time:** minimum time that the FLC will take to run
 - Mix:** injects air between FLC steps when active
- Exchange:** runs a sample exchange cycle when active
- Repeat FLC:** starts a new FLC after each FLC completes when active
 - Auto FLC:** optimises the **High E** value between successive FLCs when active
- Wash cycle:** runs the programmed wash cycle when active
 - Interval:** time between successive wash cycles (h)
- Clean time:** using the cleaning fluid connected to the NO port of solenoid valve C (s)
- Rinse time:** using the cleaning fluid connected to the NC port of solenoid valve C (s)

7.2 The maximum step function (Step max)

The **rPE fit and step data** values are averages from the last Gaqs at each **FLC Step**. The **Step max** defines how many Gaqs are included within the average. For example, if the **Group time** (shown under **STAF setup** on the home screen) is 6 s and the step max value is 20 s, the last three Gaqs at each step will be processed. Increasing the **Step max** value to 24 s would result in the last four Gaqs being included.

By excluding the first Gaqs at each step, the parameter values can be pushed towards steady-state. When the **Step max** value is changed, all rPE step data are recalculated immediately.

7.3 The Pre-FLC function

The **Pre-FLC E**, **Light time** and **Dark time** fields can be used to implement pre-illumination and dark acclimation steps before the FLC starts. Either step can be skipped by setting the time to zero. Data are not logged during these steps, which are run before the **Auto LED**, **Auto DWM** and **Auto PEP** functions. The Pre-FLC function has primarily been incorporated to facilitate low light-induced relaxation of non-photochemical quenching which is widely observed in diatoms and cyanobacteria (e.g. Lavaud and Goss, 2014; Lacour et al. 2018).

When the Pre-FLC E value is set to a low value (below 20 $\mu\text{mol photons m}^{-2} \text{s}^{-1}$) the relationship between drive current and photon output becomes temperature dependent. To ensure that the actual output from the ALED is as close as possible to the requested value, a photodiode-monitored feedback loop has been incorporated. The same feedback loop is used to set low **Step E** values within Auto FLC protocols.

ST RunSTAF - Untitled

File Settings Clipboard Help

STAF system

SN: 20-0325-001	From start: 00:02 s
Mode: Auto FLC	ADC:
Date: Jun 07, 2021	Sample: 21.9 °C
Time: 04:55 PM	System: 27.3 °C
Acqs: 0	System RH: 5.2%
Saqs: 0	Step: Pre-FLC light
Groups: 0	Set E: 29.4

In this example, the requested **Pre-FLC E** value was set to 10 $\mu\text{mol photons m}^{-2} \text{s}^{-1}$. This was low enough to trigger the photodiode-monitored feedback loop to set the closest **Set E** value possible. The starting value was 29.4 $\mu\text{mol photons m}^{-2} \text{s}^{-1}$.

ST RunSTAF - Untitled

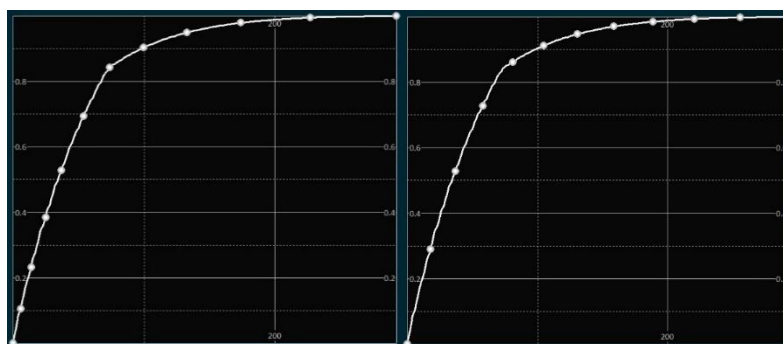
File Settings Clipboard Help

STAF system

SN: 20-0325-001	From start: 00:05 s
Mode: Auto FLC	ADC:
Date: Jun 07, 2021	Sample: 21.9 °C
Time: 04:55 PM	System: 27.3 °C
Acqs: 0	System RH: 5.2%
Saqs: 0	Step: Pre-FLC light
Groups: 0	Set E: 12.2

After automated adjustment, the **Set E** value was set at 12.2 $\mu\text{mol photons m}^{-2} \text{s}^{-1}$.

7.4 The push up function



The **Push up** function determines the distribution of **E** values within the FLC. Increasing the value pushes the distribution towards **High E**. The examples below show the extremes of **24** (left) and **240** (right).

7.5 Run time

Once the set step time has been reached, RunSTAF will complete the existing Saq group before switching to the next step. If the Group time is long (to compensate for very low biomass, for example), the actual run time can be significantly longer than the value shown under **Run time**.

7.6 The Mix function

When active, the peristaltic pump runs for the **On time** at the set **Speed**. The **Mix** function can be implemented with or without the solenoid unit being plumbed in. This function can be run with the flow-through unit or the flow-through stirrer unit.

7.7 The Exchange function

When active, this function is triggered at the end of an FLC. The solenoid unit and peristaltic pump must both be plumbed in. There are two stages to the **Exchange** cycle. During the first stage, the peristaltic pump runs for the set **Flow time** with **Solenoid A** set to NC. This displaces the existing sample with a new sample. For the second stage, **Solenoid A** returns to NO and the peristaltic pump runs for the set **Purge time**. This clears all plumbing after the solenoid valve.

7.8 Repeat FLC

If this function is active, FLCs are run continuously. If the exchange function is also active, the sample is exchanged between the end of one FLC and the start of the next. The FLC that has just finished is archived and a new data file is generated for the next FLC.

7.9 Auto FLC

When active, the **High E** value is set to four times the E_k from the previous FLC, to a maximum of $2000 \mu\text{mol photons m}^{-2} \text{s}^{-1}$.

7.10 Wash cycle

When active, this function is triggered at the end of the first FLC to complete after the set **Interval** is reached. During the first stage of the cleaning cycle, set by the **Clean time**, Solenoids A and B are both set to the NC position. During the second stage of the cleaning cycle, set by the **Rinse time**, all three solenoids are set to the NC position. If the **Wash cycle** and **Exchange** functions are both active, the Wash cycle runs first.

8 Manual settings

Manual settings	Manual settings
Pause acquisition: Off	Pause acquisition: Off
PMT waveband: HC685 ± 10 nm	PMT waveband: HC730 ± 10 nm
Actinic: 0	Actinic: 40
Solenoid A: NO to COM	Solenoid A: NC to COM
Solenoid B: NO to COM	Solenoid B: NO to COM
Solenoid C: NO to COM	Solenoid C: NO to COM
Pump: Off	Pump: On
Speed: 12	Speed: 12
Mix: Inactive	Mix: Active
On time: 600 ms	On time: 600 ms
Speed: 12	Speed: 12
Interval: 60 s	Interval: 60 s
Auto archive: Inactive	Auto archive: Active
New file every: 60 minutes	New file every: 60 minutes

Manual settings provides real time control over a range of LabSTAF system functions when the Manual acquisition mode is active.

Pause acquisition halts data input when turned **On** and resumes acquisition when turned off.

PMT waveband manually exchanges the bandpass filter in front of the PMT. If the default of **HC685 ± 10 nm** is clicked, it changes to **HC730 ± 10 nm**.

The **Actinic** field can be edited to set the required incident photon irradiance provided by the ALED.

Solenoid A, B or C: The **NO to COM** values are **Normally Open to Common**. This is the default (unpowered) state. The powered state is **NC to COM (Normally Closed to Common)**.

Pump turns the peristaltic pump **On** and **Off**. The pump runs at the set **Speed** (1 – 16).

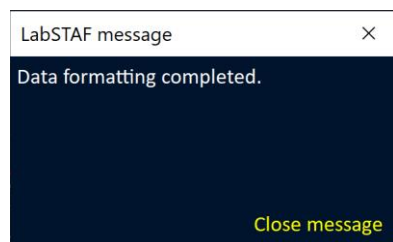
Mix Runs the peristaltic pump when active. The pump runs for **On time** at the set **Speed** (1 – 16) and **Interval**.

Auto archive automatically archives data to a timestamped file when **Active**. The interval between files is set by the **New file every** value.

9 Data export functions

9.1 The Clipboard functions

The **Clipboard** menu provides options for accessing primary and processed data in a range of different formats.



When a Clipboard function is run, the dialog shown below will open once the data array has been constructed. When this message is closed, the data are written to the Clipboard in a tab-delimited text format. This format is suitable for pasting directly into Excel and many other spreadsheet-based applications.

9.1.1 The Clipboard header

A header with the format shown below is incorporated within all Clipboard functions.

	A	B	C	D	E	F	G	H	I	J	K
1	File path: C:\Projects\STAFES\Data\201220-210104 PEP stir unit and cultures B\C Conticribra weissflogii\201221-1037.rsf										
2											
3	LabSTAF: 20-0325-001		416 nm:	0		1st pulse:	100 µs	Sample:	18 °C		
4	Mode: Auto FLC		452 nm:	0.9953		2nd pulse:	100 µs	System:	22.3 °C		
5	Date: Dec 21, 2020		452 nm:	1.044		Start gap:	200 µs				
6	Time: 10:37		473 nm:	0		End gap:	6400 µs				
7	Duration: 23:07 s		495 nm:	0		Gap steps:	6				
8	Acqs: 1374		534 nm:	0		Seq interval:	120 ms				
9	Saqs: 1374		594 nm:	0		Seq / Acq:	8				
10	Groups: 229		622 nm:	0		Acq / Saq:	1				
11						Group time:	6 s				
12											
13	Blank:	0									
14	Project:	Test with the stir unit									
15	Reference:	Conticribra weissflogii									
16	Run by:	KO									
17	Note:	Pre-diluted 36 h before the test									

9.1.2 The Clipboard footer

The same footer format is used by all Clipboard functions. It provides a record of the calibration values used at the time the data within the file were acquired.

	A	B	C	D	E	F	G	H	I	J	K	L	M	N	O	P
129	Calibration date: Dec 19, 2020															
130																
131	PMT dynamic range				CPN-680 dilution				PMT wavebands							
132	System °C:	28			Slope	ADC			Filter A: HC685 ± 10							
133	LED mA:	160	0.48:	8.964	3553			Filter B: HC730 ± 10								
134	PMT eht:	560	2.4:	8.961	16010			DW slope: 1.59								
135	PMT slope:	8.907	6.0:	8.89	39060											
136	Signal slope:	6166	12.0:	8.811	73997											
137																
138	LEDs				ALED calibration				MLED calibration							
139	MLED library:	LabSTAF A	DAC	uA	EST			416 nm	452 nm	452 nm	473 nm	495 nm	534 nm	594 nm	622 nm	
140	ALED type:	CXB1304 4000 K	143	0.063	26.7			80 mA:	0.1806	0.1849	0.1973	0.213	0.1489	0.1196	0.0227	0.0713
141	ALED window:	BG38/635 nm A	147	0.104	44.1			160 mA:	0.4042	0.4172	0.4407	0.4464	0.2875	0.2579	0.053	0.1579
142	ALED PADC slope:	0.2351	158	0.141	59.7			240 mA:	0.6116	0.625	0.6561	0.6456	0.4042	0.3772	0.0848	0.2434
143	US_SQS/L constant:	2.36	172	0.169	71.6			320 mA:	0.7989	0.8261	0.8684	0.8337	0.5009	0.4971	0.1168	0.3284
144			184	0.19	80.5			400 mA:	0.9819	1.022	1.069	1.013	0.5842	0.5842	0.1489	0.4116
145			200	0.216	91.5			460 mA:	1.119	1.155	1.211	1.138	0.6587	0.6577	0.1731	0.4729
146		Thermocouple	400	0.515	218.2											
147	TC slope:	0.038	600	0.816	345.8											
148	TC offset:	0	1000	1.423	603											
149			1400	2.027	858.9											
150		System response	2000	2.916	1236											
151	Decrease per °C:	0.38 %	4095	5.84	2475											

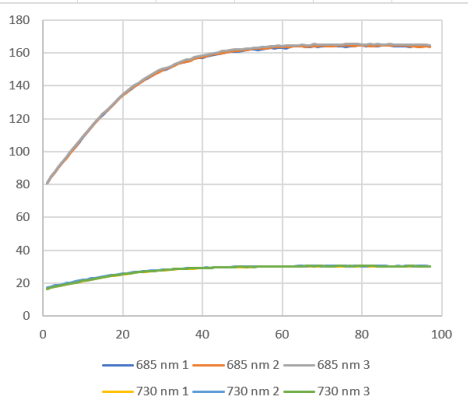
See: [LabSTAF calibration](#)

9.1.3 DWM data

Accessed through **Clipboard** → **DWM data**

The dataset copied to the Clipboard includes the trace data used to generate the DWM value. Either this value or a user-set value is used for Package Effect Correction (PEC). In the example shown below, the data have been pasted into Excel and a plot has been generated by the user.

1	File path: C:\Users\PEP and SCS files\Chlorella vulgaris\201220-1632.rsrf													
2														
3	LabSTAF:	20-0325-001	416 nm:	0	1st pulse:	100 µs	Sample:	21 °C						
4	Mode:	Auto FLC	452 nm:	0.8135	2nd pulse:	100 µs	System:	25.8 °C						
5	Date:	Dec 20, 2020	452 nm:	0.8525	Start gap:	200 µs								
6	Time:	16:32	473 nm:	0	End gap:	6400 µs								
7	Duration:	23:13 s	495 nm:	0	Gap steps:	6								
8	Acqs:	1392	534 nm:	0	Seq interval:	120 ms								
9	Saqs:	1392	594 nm:	0	Seq / Acq:	8								
10	Groups:	232	622 nm:	0	Acq / Saq:	1								
11						Group time:	6 s							
12														
13	Blank:	0												
14	Project:	Test with the stir unit												
15	Reference:	Chlorella vulgaris												
16	Run by:	KO												
17	Note:													
18														
19	W685				W730				W730/W685					
20		Fo	Fm	Fv	Fv/Fm	Fo	Fm	Fv	Fv/Fm	Fo	Fm	Fv	Fv/Fm	DWM
21	Rep 1:	80.19	164.5	84.35	0.5126	16.65	30.24	13.59	0.4494	0.2076	0.1838	0.1611	0.8766	0.2561
22	Rep 2:	80.73	164.7	84.01	0.51	17.51	30.5	12.99	0.426	0.2168	0.1851	0.1546	0.8353	0.2459
23	Rep 3:	81.8	165.5	83.66	0.5056	16.47	30.34	13.86	0.4569	0.2014	0.1833	0.1657	0.9037	0.2635
24	Mean:	80.91	164.9	84.01	0.5094	16.88	30.36	13.48	0.4441	0.2086	0.1841	0.1605	0.8717	0.2551
25	SE:	0.4722	0.2776	0.2003	0.00205	0.3186	0.07563	0.2568	0.00931	0.00449	0.00054	0.00321	0.01988	0.0051
26														
27	Traces													
28	µs	685 nm 1	685 nm 2	685 nm 3	730 nm 1	730 nm 2	730 nm 3							
29	1	80.95	80.77	80.94	16.58	17.49	16.54							
30	2	84.81	84.48	84.94	17.15	17.95	17.23							
31	3	87.58	87.34	87.92	17.73	18.57	17.69							
32	4	90.66	90.51	91.07	18.21	18.96	18.17							
33	5	93.48	93.42	94.08	18.8	19.41	18.8							
34	6	96.34	96.16	97.05	19.27	19.95	19.27							
35	7	99.62	99.4	100.1	19.63	20.38	19.68							
36	8	102.7	102.6	103.3	20.2	20.95	20.15							
37	9	105.3	105.7	106.3	20.68	21.44	20.81							
38	10	108.5	109	109.2	21.06	21.84	21.46							
39	11	111.5	111.8	112.2	21.65	22.14	21.6							
40	12	114.4	114.4	114.7	22.22	22.83	22.25							
41	13	117.1	117.2	117.8	22.53	23.16	22.68							
42	14	120.2	119.7	120.2	22.98	23.64	23.09							
43	15	122.2	122.7	123.1	23.44	24.01	23.53							
44	16	124.7	124.9	125.5	23.86	24.31	23.97							
45	17	127.2	127.4	127.8	24.25	24.78	24.21							
46	18	130.5	130.5	130.1	24.63	25.03	24.83							



See: **Package Effect Correction (PEC)**

9.1.4 PEP data

Accessed through **Clipboard** → PEP data

The dataset copied to the Clipboard includes the trace data used to generate the **Fv** and **SigmaPII** values for each of the seven MLED wavebands. In the example shown below, the plots have been generated by the user within Excel.

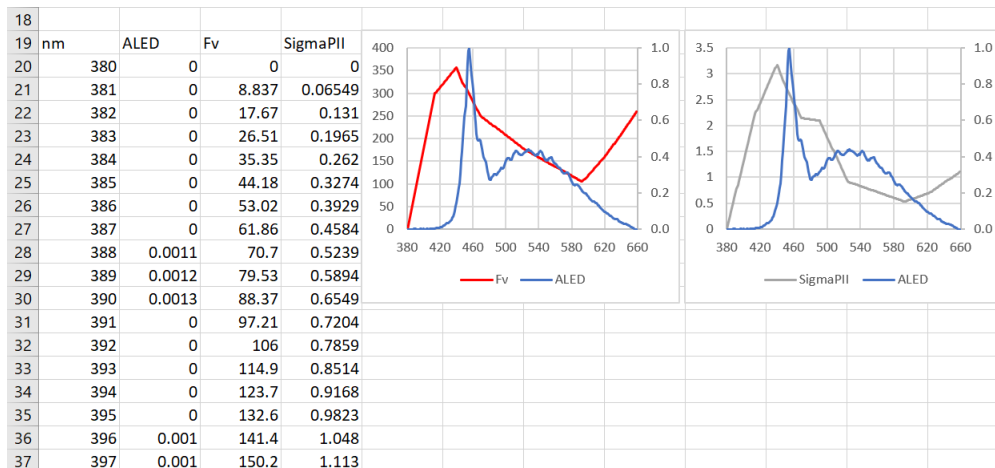
	A	B	C	D	E	F	G	H	I	J	K	L	M	N	O	P	Q
1	File path:	C:\Users\Projects\STAFES\Data\201220-210104 PEP stir unit and cultures B\K Chlorella vulgaris\201222-1215.rsf															
2																	
3	LabSTAF:	20-0325-001	416 nm:	0	1st pulse:	100	µs	Sample:	18.7 °C								
4	Mode:	Auto FLC	452 nm:	0.8923	2nd pulse:	100	µs	System:	22.6 °C								
5	Date:	Dec 22, 2020	473 nm:	0.9362	Start gap:	200	µs										
6	Time:	12:15	495 nm:	0	End gap:	6400	µs										
7	Duration:	23:15 s	534 nm:	0	Gap steps:	6											
8	Acqs:	1386	594 nm:	0	Seq interv:	120	ms										
9	Saqs:	1386	622 nm:	0	Seq / Acq:	8											
10	Groups:	231			Acq / Saq:	1											
11					Group tim	6	s										
12																	
13	Blank:	0															
14	Project:	Test with the stir unit															
15	Reference:	Chlorella sp.															
16	Run by:	KO															
17	Note:																
18																	
19	Corrected values																
20			Mean	Mean													
21	Total EST	Peak nm	Fv	SigmaPII	Fv 1	Fv 2	Fv 3	SE	SigmaPII 1	SigmaPII 2	SigmaPII 3	SE					
22	416 nm:	1.783	414.8	81.07	2.877	80.08	82.32	80.8	0.6601	2.875	2.886	2.87	0.0049				
23	452 nm:	1.532	447	81.46	3.141	81.3	81.28	81.8	0.1704	3.135	3.136	3.151	0.00545				
24	473 nm:	1.784	469.9	62.47	2.425	62.6	61.44	63.36	0.5596	2.414	2.439	2.422	0.00727				
25	495 nm:	1.551	491.3	47.54	1.832	48.05	47.53	47.05	0.288	1.809	1.868	1.818	0.01842				
26	534 nm:	1.55	525.8	11.64	0.3697	13.38	10.11	11.44	0.9491	0.3315	0.4842	0.2935	0.05829				
27	594 nm:	1.705	593.9	24.41	0.6444	27.31	22.78	23.14	1.453	0.3513	0.8215	0.7604	0.1476				
28	622 nm:	2.005	622.5	41.46	1.358	42.06	42.16	40.15	0.6555	1.353	1.411	1.31	0.02924				
29	Optimisation:	chlorophyll b/c															
30																	
31	Normalized values																
32	Total EST	Peak nm	Fv 1	Fv 2	Fv 3	SE	SigmaPII 1	SigmaPII 2	SigmaPII 3	SE							
33	416 nm:	1.783	414.8	80.08	82.34	80.3	0.7175	2.875	2.885	2.854	0.00907						
34	452 nm:	1.532	447	81.3	81.3	81.3	0	3.135	3.135	3.135	0						
35	473 nm:	1.784	469.9	62.6	61.45	62.97	0.4587	2.414	2.438	2.409	0.00897						
36	495 nm:	1.551	491.3	48.05	47.53	46.76	0.374	1.809	1.867	1.808	0.01962						
37	534 nm:	1.55	525.8	13.38	10.11	11.36	0.9515	0.3315	0.484	0.2919	0.05857						
38	594 nm:	1.705	593.9	27.31	22.78	23	1.474	0.3513	0.8211	0.7563	0.147						
39	622 nm:	2.005	622.5	42.06	42.17	39.9	0.7392	1.353	1.41	1.303	0.03104						
40																	
41	Uncorrected values																
42	Fo	Fm	Fv	AlphaPII													
43	452A + 416 nm:	112.4	256.3	143.8	0.05357												
44		112.2	258	145.8	0.05368												
45		113.2	258.1	144.9	0.05367												
46	452A + 452B nm:	95.73	220.3	124.6	0.04803												
47		96.67	221.2	124.5	0.04805												
48		96.47	221.8	125.3	0.04829												
49	452A + 473 nm:	99.97	228.4	128.4	0.0495												
50		101.8	229.1	127.3	0.04973												
51		100.7	230.2	129.5	0.04972												
52	452A + 495 nm:	79.67	183.9	104.2	0.03988												
53		80.32	184.2	103.8	0.04029												
54		80.7	184.7	104	0.0401												
55	452A + 452B + 534 nm:	103.6	237	133.4	0.05021												
56		105.9	237.1	131.2	0.05123												
57		105.6	238.5	132.9	0.05022												
58	452A + 452B + 594 nm:	99.33	228.6	129.3	0.04864												
59		100.5	229	128.5	0.04947												
60		100.4	229.8	129.3	0.0496												
61	452A + 452B + 622 nm:	112.7	257.1	144.5	0.05443												
62		113.5	258	144.5	0.05472												
63		114.4	258.7	144.3	0.05448												
64																	
65	Traces																
66	µs	416 nm 1	416 nm 2	416 nm 3	452 nm 1	452 nm 2	452 nm 3	473 nm 1	473 nm 2	473 nm 3	495 nm 1	495 nm 2	495 nm 3	534 nm 1	534 nm 2	534 nm 3	
67	1	111.7	112.8	113.4	96.14	96.51	96.74	100	100.8	101.3	79.29	79.89	80.23	103.5	104.5	105	
68	2	117.3	118.7	118.9	100.3	101.3	101.6	104.6	105.2	106.1	82.84	82.98	83.57	108.7	109.6	110.3	
69	3	121.8	123.1	123.5	103.6	104.5	104.7	108.2	108.9	109.5	84.78	85.39	85.73	112.8	113.5	113.9	
70	4	126.2	127.4	127.8	107.1	107.8	108.6	112	112.3	113.3	87.03	88.02	88.12	116.5	117.5	117.6	
71	5	130.9	131.7	132.7	110.7	111.6	112.2	115.8	116.4	116.7	89.38	90.15	90.52	120.5	121.6	122.1	

See: **Photochemical Excitation Profile (PEP)**

9.1.5 SCS data

Accessed through **Clipboard** → **SCS data**

This function copies the Actinic LED (**ALED**) emission spectrum plus the **Fv** and **SigmaPII** absorption spectra at 1 nm resolution. In the example shown below, the plots have been generated by the user within Excel.

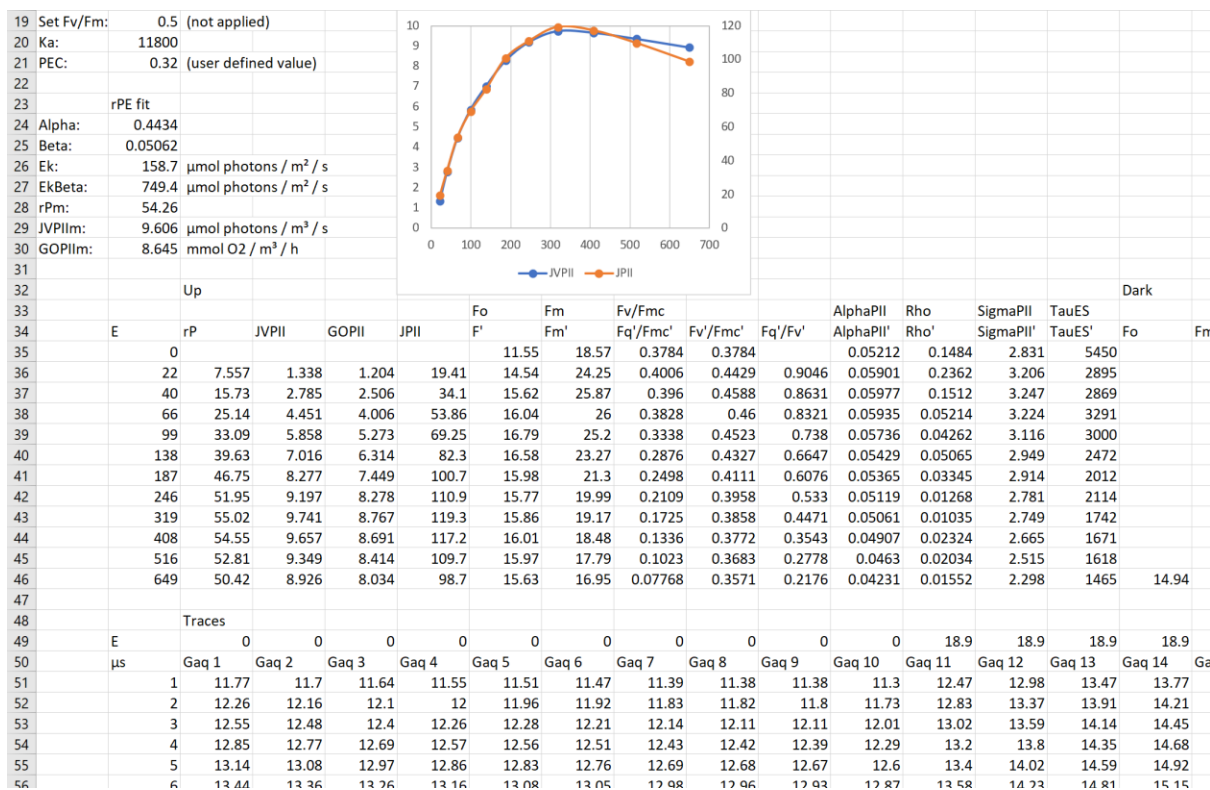


See: **Photochemical Excitation Profile (PEP)**

9.1.6 rPE data

Accessed through **Clipboard** → **rPE data**

The dataset copied to the Clipboard includes $J_{V_{PII}}$ and GO_{PII} values generated using the Absorbance method plus J_{PII} values generated using the Sigma method. In the example shown below, the data have been pasted into Excel and a data plot has been generated within Excel. The G_{aq} traces used to generate the rPE values are also included within the output.



9.1.9 Saq traces or Acq traces

Accessed through **Clipboard** → **Saq traces** or **Clipboard** → **Acq traces**

The main purpose of this function is to copy the primary Saq or Acq trace data to the Clipboard. Above the trace data, a range of calculated parameters are provided in a vertical format, as shown in the left screenshot below. The trace data include the baseline. The timescale (the μs column in the right screenshot below) shows the baseline values as negative. The 0 value in the μs column is $t = 0$ for the first ST pulse.

18					
19	Set Fv/Fm:	0.5	(not applied)		
20	Ka:	11800			
21	PEC:	0.32	(user defined value)		
22					
23		Saq	1	2	3
24		E	0	0	0
25	Gap Index:	1	2	3	4
26	Gap (μs):	200	400	800	1600
27	Reps:	1	1	1	1
28		From linear regression			
29	Base:	18.12	18.12	18.12	18.12
30	F', Fo:	14.78	14.72	14.68	14.73
31	Fm', Fm:	32.17	31.68	31.98	31.87
32	sF', sF:	27.26	23.53	20.62	18.36
33	sFm', sFm:	30.74	30.89	31.73	32.66
34		From rho fit			
35	F', Fo:	14.39	14.33	14.35	14.45
36	Fm', Fm:	32.87	32.51	32.68	32.57
37	Fq', Fv:	18.48	18.19	18.33	18.12
38	Rho', Rho:	0.3328	0.35	0.3434	0.3538
39	AlphaPII', AlphaPII:	0.05501	0.05612	0.0556	0.05505
40	SigmaPII', SigmaPII:	2.697	2.752	2.726	2.699
41	SE:	0.007819	0.007247	0.007646	0.007772
42	sF', sF:	27.12	23.23	20.25	18.01
43	sFm', sFm:	30.74	30.75	31.59	32.3
44	sFq', sFq:	3.626	7.518	11.34	14.28
45	sRho', sRho:	0.07926	0.01493	0.1026	0.2376
46	sAlphaPII', sAlphaPII:	0.04126	0.0436	0.04586	0.0492
47	sSigmaPII', sSigmaPII:	2.023	2.138	2.249	2.413
48	sSE:	0.004675	0.00586	0.007718	0.0104
49		From dimer fit			
50	dRhoPII:	0.6041	0.6275	0.6275	0.636
51	AlphaPII', AlphaPII:	0.05435	0.05545	0.05504	0.05439
52	SigmaPII', SigmaPII:	2.665	2.719	2.699	2.667
53	[oo]:	1	1	1	1
54	SE:	0.01039	0.01342	0.01122	0.01069
55	sAlphaPII', sAlphaPII:	0.03044	0.03433	0.03822	0.04273
56	sSigmaPII', sSigmaPII:	1.492	1.684	1.874	2.095
57	s[oo]:	0.02651	0.1258	0.295	0.4941
58	s[oc]:	0.2765	0.4603	0.4978	0.4184
59	s[cc]:	0.697	0.4139	0.2072	0.0875
60	sSE:	0.004787	0.007817	0.009056	0.008927
61		Derived			
62	Fq'/Fmc', Fv/Fmc:	0.5622	0.5594	0.561	0.5563
63	sFq'/Fmc', sFq'/Fmc:	0.1179	0.2445	0.3589	0.4423
64	sFq'/Fv', sFq'/Fv:	0.1962	0.4133	0.6184	0.7884
65	JVPll:				
66	JPII:				
67	NPQ:	0.001024	0.01202	0.006853	0.01033
68	NSV:	0.7971	0.8058	0.8017	0.8045
69					
70	μs	Saq 1	Saq 2	Saq 3	
71		-22	18.12	18.12	18.12
72		-21	18.12	18.12	18.12
73		-20	18.12	18.12	18.12

67	NPQ:	0.001024	0.01202	0.006853	0.01033
68	NSV:	0.7971	0.8058	0.8017	0.8045
69					
70	μs	Saq 1	Saq 2	Saq 3	
71		-22	18.12	18.12	18.12
72		-21	18.12	18.12	18.12
73		-20	18.12	18.12	18.12
74		-19	18.12	18.12	18.12
75		-18	18.12	18.12	18.12
76		-17	18.12	18.12	18.12
77		-16	18.11	18.12	18.12
78		-15	18.12	18.12	18.12
79		-14	18.12	18.12	18.12
80		-13	18.12	18.11	18.12
81		-12	18.12	18.12	18.12
82		-11	18.12	18.11	18.12
83		-10	18.11	18.12	18.12
84		-9	18.12	18.11	18.12
85		-8	18.11	18.12	18.11
86		-7	18.12	18.11	18.11
87		-6	18.12	18.11	18.12
88		-5	18.11	18.11	18.11
89		-4	18.11	18.11	18.11
90		-3	18.11	18.11	18.12
91		-2	18.11	18.12	18.11
92		-1	19.49	19.51	19.49
93		0	30.04	30.11	30.03
94		1	32.51	32.51	32.46
95		2	33.28	33.24	33.2
96		3	33.94	33.85	33.86
97		4	34.55	34.46	34.44
98		5	35.27	35.17	35.08
99		6	35.87	35.79	35.73
100		7	36.46	36.46	36.44
101		8	37.14	37.14	37.12
102		9	37.8	37.77	37.79
103		10	38.46	38.42	38.42
104		11	39.19	38.99	39.09
105		12	39.77	39.64	39.73
106		13	40.42	40.29	40.35
107		14	41.02	40.88	40.93
108		15	41.56	41.48	41.55
109		16	42.06	41.97	42.06
110		17	42.7	42.57	42.64
111		18	43.16	43.09	43.16
112		19	43.57	43.5	43.54
113		20	44.08	43.97	44.05
114		21	44.54	44.41	44.43
115		22	44.96	44.81	44.88
116		23	45.4	45.18	45.27
117		24	45.62	45.57	45.69
118		25	46.06	45.91	45.99
119		26	46.41	46.15	46.31
120		27	46.66	46.5	46.68
121		28	47.01	46.9	46.96

↓...

9.2 The csv functions

Accessed through **File** → **csv files**

9.2.1 All file and Individual files

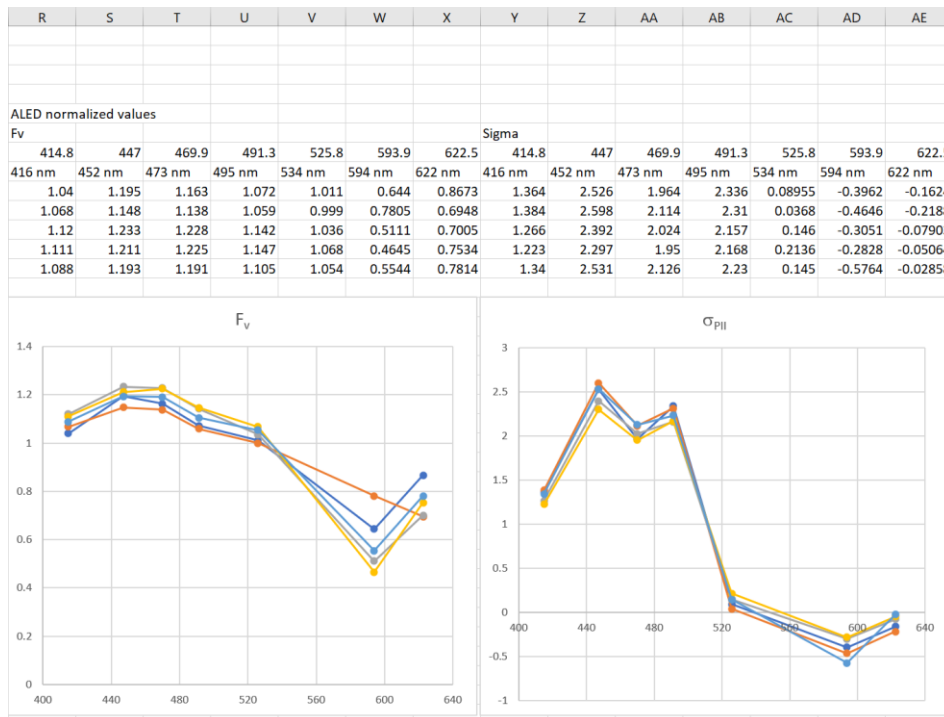
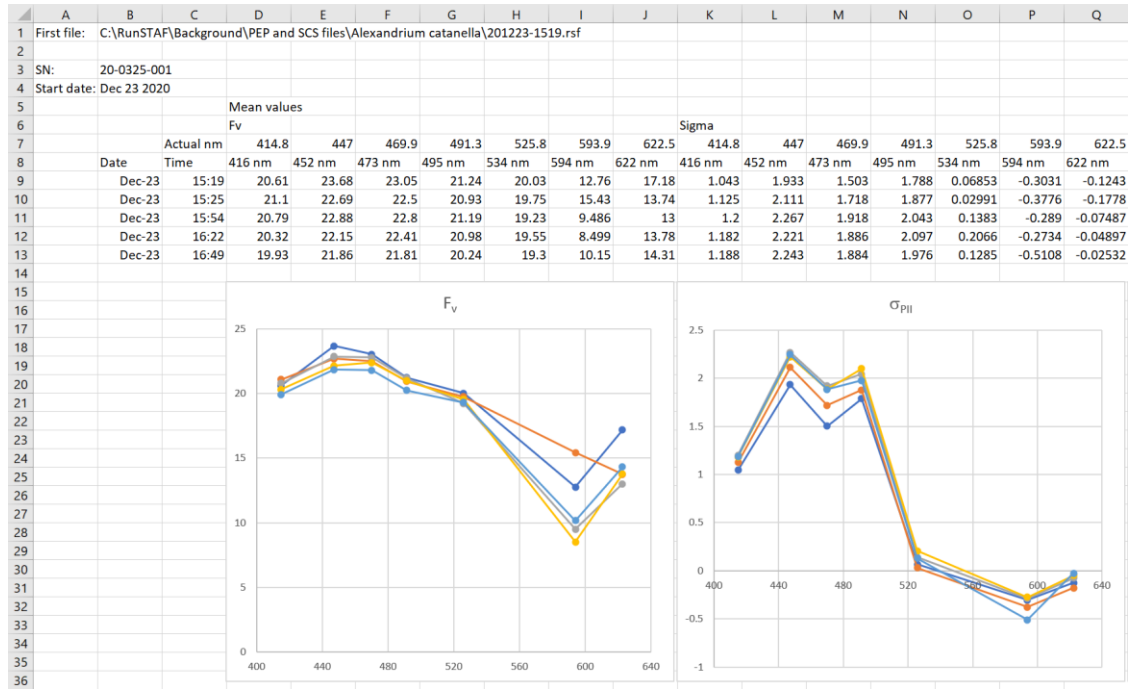
The **Folder-based PEP file**, **Folder-based rPE file** and **Folder-based Saq file** options create a single csv file generated by extracting data across all files within the selected folder. The **Individual rPE files** and **Individual Saq files** options generate a csv file for each RunSTAF data file.

Selecting any of the csv files by folder options opens a file dialog. Double-clicking on any file within the folder triggers the selected function.

The screenshot below shows a folder containing six RunSTAF data files. All csv functions have been run on this folder to generate the csv files. The naming for these files is automatic. The **Folder-based PEPs**, **Folder-based rPEs** and **Folder-based Saqs** file names comprise the timestamp for the most recent file in the folder plus **All PEPs**, **All rPEs** or **All Saqs**.

<input type="checkbox"/>	Name	Status	Date modified	Type	Size
	200607-0014 rPE	✓	02/07/2020 11:30	Microsoft Excel Comma Separated Values File	115 KB
	200607-0014 Saq	✓	02/07/2020 11:30	Microsoft Excel Comma Separated Values File	331 KB
<input checked="" type="checkbox"/>	ST 200607-0014	✓	07/06/2020 00:36	RSF File	2,710 KB
	200607-0036 rPE	✓	02/07/2020 11:30	Microsoft Excel Comma Separated Values File	115 KB
	200607-0036 Saq	✓	02/07/2020 11:30	Microsoft Excel Comma Separated Values File	331 KB
<input checked="" type="checkbox"/>	ST 200607-0036	✓	07/06/2020 00:58	RSF File	2,710 KB
	200607-0058 rPE	✓	02/07/2020 11:30	Microsoft Excel Comma Separated Values File	115 KB
	200607-0058 Saq	✓	02/07/2020 11:30	Microsoft Excel Comma Separated Values File	330 KB
<input checked="" type="checkbox"/>	ST 200607-0058	✓	07/06/2020 01:20	RSF File	2,710 KB
	200607-0120 rPE	✓	02/07/2020 11:30	Microsoft Excel Comma Separated Values File	114 KB
	200607-0120 Saq	✓	02/07/2020 11:30	Microsoft Excel Comma Separated Values File	329 KB
<input checked="" type="checkbox"/>	ST 200607-0120	✓	07/06/2020 01:41	RSF File	2,696 KB
	200607-0141 rPE	✓	02/07/2020 11:30	Microsoft Excel Comma Separated Values File	115 KB
	200607-0141 Saq	✓	02/07/2020 11:30	Microsoft Excel Comma Separated Values File	329 KB
<input checked="" type="checkbox"/>	ST 200607-0141	✓	07/06/2020 02:03	RSF File	2,710 KB
	200607-0203 All PEPs	✓	02/07/2020 11:10	Microsoft Excel Comma Separated Values File	1 KB
	200607-0203 All rPEs	✓	02/07/2020 11:30	Microsoft Excel Comma Separated Values File	1 KB
	200607-0203 All Saqs	✓	02/07/2020 11:30	Microsoft Excel Comma Separated Values File	1,974 KB
	200607-0203 rPE	✓	02/07/2020 11:30	Microsoft Excel Comma Separated Values File	114 KB
	200607-0203 Saq	✓	02/07/2020 11:30	Microsoft Excel Comma Separated Values File	329 KB
<input checked="" type="checkbox"/>	ST 200607-0203	✓	07/06/2020 02:25	RSF File	2,696 KB

Example **Folder-based PEP file**. The plots were generated within Excel. The **ALED normalized values** are the MLED waveband values of F_V and σ_{PII} normalized to the ALED values for each parameter.



Example Folder-based rPE file...

	A	B	C	D	E	F	G	H	I	J	K	L	M	N
1	First file: C:\Projects\STAFES\Data\201220-210104 PEP stir unit and cultures B\B Chlorella sp\201220-1632.rsf													
2														
3	SN: 20-0325-001													
4	Start date: Dec 20 2020													
5														
6		Date	Time	Seconds	Minutes	PEC	Fo	Fm	Fv/Fmc	Alpha	Ek	Beta	EkBeta	rPm
7		Dec-20	16:32	0	0	0.2551	12.29	25.47	0.5174	0.5312	123.3	0.03586	985.2	54.44
8		Dec-20	16:59	1613	26.88	0.2699	11.48	18.55	0.381	0.442	162.3	0.05046	588.9	55.82
9		Dec-20	17:25	3152	52.53	0.264	11.55	18.57	0.3784	0.4434	158.7	0.05062	749.4	54.26
10		Dec-20	17:50	4694	78.23	0.268	12.25	19.9	0.3843	0.4393	156.8	0.04664	796.4	53.73
11		Dec-20	18:16	6239	104	0.2633	12.8	21.16	0.3952	0.4337	165.6	0.06051	640.2	53.58
12														

Example Folder-based Saqs file...

	A	B	C	D	E	F	G	H	I	J	K	L	M	N	
1	First file: C:\Users\kmo\OneDrive - snetad\Documents\csv test\200607-0014.rsf														
2															
3	SN: 19-0105-008														
4	Start date: Jun 07 2020														
5	Start time: 00:14														
6															
7															
8	Step max: 20 s														
9															
10	FLC protocol														
11		Step	E	Up	Dark	Down									
12		1	0	60	0	60									
13		2	25	120	0	0									
14		3	57	60	0	0									
15		4	99	60	0	0									
16		5	154	60	0	60									
17		6	226	60	0	60									
18		7	321	60	0	120									
19		8	444	60	0	0									
20		9	605	60	0	0									
21		10	817	60	0	0									
22		11	1093	60	0	0									
23		12	1454	60	60	0									
24															
25		x-axis				Derived parameters									
26						Fq'/Fmc'	sFq'/sFmc'	Fq'/Fv'	Fv'/Fmc'	sFq'/Fv'	sFmc'/Fmc'				
27		Gap (µs)	Time (s)	Saq	E	Fv/Fmc	sFq/sFmc			sFq/Fv	sFmc/Fmc	s[oo]	s[oc]	s[cc]	
28		Jun 07 2020	200	0	1	0	0.4177	0.1114	1.003	0.4177	0.2639	0.9898	0.04646	0.3417	0
29		Time: 00:14	400	0	2	0	0.4104	0.1976	0.9906	0.4104	0.4813	0.9996	0.1515	0.4778	0
30		Sample: 28.9°C	800	0	3	0	0.4326	0.2808	1.039	0.4326	0.6575	1.013	0.3393	0.4877	0
31		System: 27.6°C	1600	0	4	0	0.4253	0.3392	1.022	0.4253	0.8164	1.024	0.5227	0.4012	0
32			3200	0	5	0	0.4207	0.3663	1.011	0.4207	0.8952	1.028	0.6185	0.3363	0

9.2.2 Auto archive report line

Activated through **File** → **csv files** → **Auto archive report line**

This function generates a simple summary csv file each time a RunSTAF data file is completed. The default comma used to separate adjacent values can be switched to a tab or semicolon.

Accessed through **File** → **csv files** → **Field separator for csv output**

The report line csv has the same filename as the associated RunSTAF data file.

<input type="checkbox"/>	Name	Date modified	Type	Size
	200807-1743	07/08/2020 19:20	RSF File	2,316 KB
<input checked="" type="checkbox"/>	200807-1743	07/08/2020 19:20	Microsoft Excel Com...	1 KB
	200807-1705	07/08/2020 18:43	RSF File	2,302 KB
<input checked="" type="checkbox"/>	200807-1705	07/08/2020 18:43	Microsoft Excel Com...	1 KB
	200807-1628	07/08/2020 18:06	RSF File	2,316 KB
<input checked="" type="checkbox"/>	200807-1628	07/08/2020 18:06	Microsoft Excel Com...	1 KB

Example Auto archive report line file...

	A	B	C	D	E	F	G	H	I	J	K	L	M	N	O	P	Q
1	SN	Year	Month	Day	Hour	Minute	Second	Sample °C	System °C	PEC	Fv416	Fv542	Fv473	Fv495	Fv534	Fv594	Fv622
2	20-0325-001	20	8	7	17	43	3	28.4	37.8	0.2279	14.94	15.37	11.75	9.073	6.923	4.479	6.468
	R	S	T	U	V	W	X	Y	Z	AA	AB	AC	AD	AE	AF	AG	AH
→	S416	S542	S473	S495	S534	S594	S622	Fo	Fm	Fv/Fmc	Alpha	Ek	Beta	rPm	JVPllm	GOPIIm	High E
	3.366	4.125	2.946	2.411	1.203	0.5536	0.9087	4.243	9.228	0.5402	0.5293	278.7	0.07878	113.4	10.5	9.454	1099

10 Data processing within RunSTAF

10.1 Refitting data files

The curve fitting functions incorporated within RunSTAF are sometimes updated. Where appropriate, the updated fits are applied to older RunSTAF data files as they are opened. In some cases, refitting a single file can take tens of seconds. RunSTAF includes two functions to run a bulk refit on all files within a folder to avoid any delay as individual files are opened.

The refit functions can be accessed through **File → Run a folder-based Saq refit** and **File → Run a folder-based Acq refit**. When either function is run, the home screen reports progress on the refitting process (Figure 10.1).

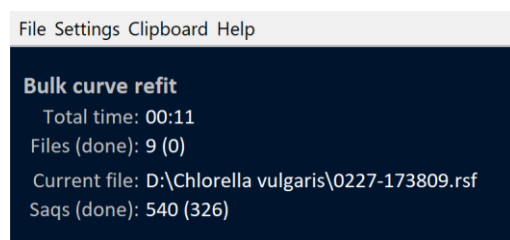


Figure 10.1: Crop from a screenshot of the home screen taken while a folder-based Acq refit is running.

RunSTAF does not report Acq parameters derived from curve fits. Consequently, it only makes sense to run the Acq level refit if you need access to primary data at the Acq level (through the Clipboard functions).

If you move away from the RunSTAF window while refitting is running, you are likely to get a 'RunSTAF not responding' message. This message can be ignored as data processing will continue in the background.

10.2 Correcting for baseline fluorescence (F_b calculation)

The fraction of F_o that does not originate from photochemically active PSII complexes is termed baseline fluorescence (F_b) and the fraction that does is termed baseline corrected F_o (F_{oc}). An estimated value for F_b can be calculated using Equation 10.1.

$$F_b = F_m - \frac{F_v}{(F_v/F_{mc})} \quad \text{Equation 10.1}$$

Where F_v/F_{mc} is the assumed 'intrinsic' value of F_v/F_m for photochemically active PSII complexes within the sample.

Within a study conducted by Boatman, Geider and Oxborough (2019), an F_v/F_{mc} of 0.518 generated a good match between STAF-generated estimates of GO_{PII} and more direct estimation of GO_{PII} using a Clark-type O_2 electrode. Although a value of 0.518 is unlikely to be appropriate in every circumstance, these data do indicate that it may be possible to extrapolate from a relatively small number of direct measurements of GO_{PII} across a much wider dataset of STAF-derived values.

10.3 The ST curve fitting procedures

The default RunSTAF ST pulse is 100 μ s. Data are acquired at 1 MHz starting 20 μ s before the ST pulse is triggered and running through to the end of the pulse. If a second ST pulse is included within a Seq (dual ST pulse mode), data are also acquired for the entire duration of this pulse. No data are acquired during the gap between the first and second ST pulses.

Although the first ST pulse is always triggered 20 μ s into the sequence, it takes approximately 3 μ s after this trigger for the MLEDs to get to full output. Table 10.1 shows typical MLED output data for the first 4 μ s after the ST pulse is triggered.

t (μs)	ST fit t (μs)	delivery	sum
1	-1	<< 1%	<< 1%
2	0	30%	30%
3	1	80%	110%
4+	2+	100%	-

Table 10.1: All curve fitting functions within RunSTAF use an offset of 2 μs . Working from the values presented here, this means that at $t = 1 \mu\text{s}$ for the ST fit, the sample will have received 110% of the photons normally delivered in 1 μs . This 110% value is the sum of 80% delivered between $t = 0$ and $t = 1$ and 30% between $t = -1$ and $t = 0$ on the ST fit scale.

10.3.1 The Rho ST curve fit

The ST curve fitting procedure within RunSTAF is centred around Equations 10.2 and 10.3 (Kolber, Prášil and Falkowski, 1998).

$$C_t = C_{t-1} + C_{t=1} \cdot (1 - C_{t-1}) / (1 - C_{t-1} \cdot \rho) \quad \text{Equation 10.2}$$

$$F_t = F_o + F_v \cdot C_t \cdot (1 - \rho) / (1 - C_t \cdot \rho) \quad \text{Equation 10.3}$$

Where F_t is the fluorescence intensity at time t , C_t is the fraction of closed reaction centres at time t , ρ (Rho) accounts for connectivity between RCIIIs, and $F_v = F_m - F_o$. It is assumed that $C = 0$ at $t = 0$. During the fit, $C_{t=1}$, ρ , F_o and F_m are all allowed to float. Adjacent values of t are always 1 μs apart (1 MHz acquisition). The connectivity parameter ρ accounts for the transfer of photons from closed RCIIIs to open RCIIIs.

The value of $C_{t=1}$ provides the initial rate at which photons are used to drive PSII photochemistry during a ST pulse (α_{PII}). For the LabSTAF system, $C_{t=1}$ defines the proportion of PSII complexes at which a photon was absorbed and used to drive PSII photochemistry during the first microsecond of the ST pulse. It follows that α_{PII} has units of photons PSII⁻¹ μs^{-1} .

The value of σ_{PII} can then be generated using Equation 10.4.

$$\sigma_{\text{PII}} = \alpha_{\text{PII}} \cdot 100 / E_{\text{ST}} \quad \text{Equation 10.4}$$

This provides a value for σ_{PII} with units of $\text{nm}^2 \text{PSII}^{-1}$.

Although Equations 10.2 and 10.3 use terminology appropriate to a dark-adapted sample, these equations can also be applied to a light-adapted sample. This is because the term C within these equations is always set to zero at $t = 0$ under ambient light, even though a proportion of PSII reaction centres within the sample are closed at $t = 0$. The reason for this is that Equations 10.2 and 10.3 only track the closure of PSII reaction centres that are open at $t = 0$ and implicitly assume that the proportion of PSII centres held in the closed state by the actinic light remains constant throughout the ST pulse. Equations 10.5 and 10.6 provide the light-adapted versions of Equations 10.2 and 10.3.

$$C_t = C_{t-1} + C_{t=1} \cdot (1 - C_{t-1}) / (1 - C_{t-1} \cdot \rho') \quad \text{Equation 10.5}$$

$$F_t' = F' + F_q' \cdot C_t \cdot (1 - \rho') / (1 - C_t \cdot \rho') \quad \text{Equation 10.6}$$

10.3.2 The Dimer ST curve fit

It is now widely accepted that photochemically active PSII complexes form structural dimers within thylakoid membranes (e.g. Nield and Barber, 2006; Watanabe et al. 2009; Umena et al. 2011) and it seems likely that this dimerization can at least partially account for the connectivity defined by ρ in

Equations 10.5 and 10.6. The dimer curve fit incorporated within RunSTAF makes the following basic assumptions:

- All functional PSII reaction centres are incorporated within dimeric complexes and the two reaction centres within each dimer effectively share a single light harvesting system
- PSII dimer complexes are completely isolated from each other, preventing the transfer of photons from one dimer to another

With these assumptions in place, the following Equations can be used to fit the first ST curve in a dual ST measurement from dark-adapted samples:

$$[oo]_t = [oo]_{t-1} - [oo]_{t-1} \cdot C_{t=1} \quad \text{Equation 10.7A}$$

$$[oc]_t = [oc]_{t-1} + [oo]_{t-1} \cdot C_{t=1} \quad \text{Equation 10.7B}$$

$$[oc]_t = [oc]_{t-1} - [oc]_{t-1} \cdot C_{t=1} \cdot 0.5 / (1 - 0.5 \cdot \rho) \quad \text{Equation 10.7C}$$

$$[cc]_t = [cc]_{t-1} + [oc]_{t-1} \cdot C_{t=1} \cdot 0.5 / (1 - 0.5 \cdot \rho) \quad \text{Equation 10.7D}$$

$$ooF = [oo] \cdot F_o \quad \text{Equation 10.8A}$$

$$ocF = [oc] \cdot (F_o + F_v \cdot 0.5 \cdot [1 - \rho] / [1 - 0.5 \cdot \rho]) \quad \text{Equation 10.8B}$$

$$ccF = [cc] \cdot F_m \quad \text{Equation 10.8C}$$

Within Equations 10.8A-C, ooF, ocF, and ccF are the relative fluorescence intensities from [oo], [oc], and [cc] dimers, respectively. Because the two reaction centres within each dimer are assumed to share a single light harvesting system, ρ is theoretically equal to ϕ_{PII} .

See: [Deconstructing Rho](#)

For the second ST curve in a dual ST sequence and measurements from light-adapted samples, the Dimer fit requires initial ($t=0$) values for [oo], [oc] and [cc]. These values are estimated by assuming that [cc] equals unity at the asymptote of the ST fit (F_m or F_m').

It is worth noting that heterogeneity has a larger impact on the Dimer fit than the Rho fit. This is particularly true when a sample contains significant proportions of cells with very different values of $C_{t=1}$ in the above equations. Mainly for this reason, the Dimer fit is only used to generate parameters that directly relate to this fitting process (within the **Dimer fit parameters** section of the data screen). All other parameters that have dependence on a ST curve fit (within the **Rho fit parameters**, **Primary fluorescence values**, **Relaxation phase parameters (Rho)** and **Baseline corrected parameters** sections) are generated using the Rho fit.

10.4 Fitting a dual ST pulse sequence

The screenshot below shows a dual ST pulse sequence from a dark-adapted sample. The gap applied between the first and second ST pulses in this example was 200 μ s. The small orange numbers in the bottom right corner of each ST plot is the number of points incorporated within the Rho and Dimer fits. The first ST pulse fit was to the first 68 points. Over the last part of the curve, there is a clear decrease in fluorescence which was excluded from the fit. The second ST pulse was fit to all 96 available points.

The observed decrease in fluorescence towards the end of the first ST pulse tends to be most evident when the ratio of variable fluorescence to total fluorescence is relatively high (above approximately 0.5). The decrease in fluorescence towards the end of the first ST pulse is correlated with an absorption change centred at 515 nm (Witt, 1971) which tracks the rapid formation of an electric field across the thylakoid membrane ($\Delta\psi$) as most of the RCII within the interrogated volume undergo charge separation within the timeframe of the ST pulse. To minimise the impact of

this electric field-dependent quenching on the Rho curve fit, the part of the algorithm that determines the number of points to be fit incorporates F_v/F_m or F_q'/F_m' for the first ST pulse and sF_q/sF_m or sF_q'/sF_m' for the second ST pulse.

Within the example provided by Figure 10.2, the first ST pulse is fit to 68 points because the value of F_v/F_m is high (0.572). The second ST pulse is fit to all 96 points because sF_q/sF_m is much lower (0.203). The overall result is consistent with the amplitude of the electric field-dependent quenching evident at the end of the first ST pulse being increased by charge separation during the second ST pulse. As a result, sF_m is significantly lower than F_m .

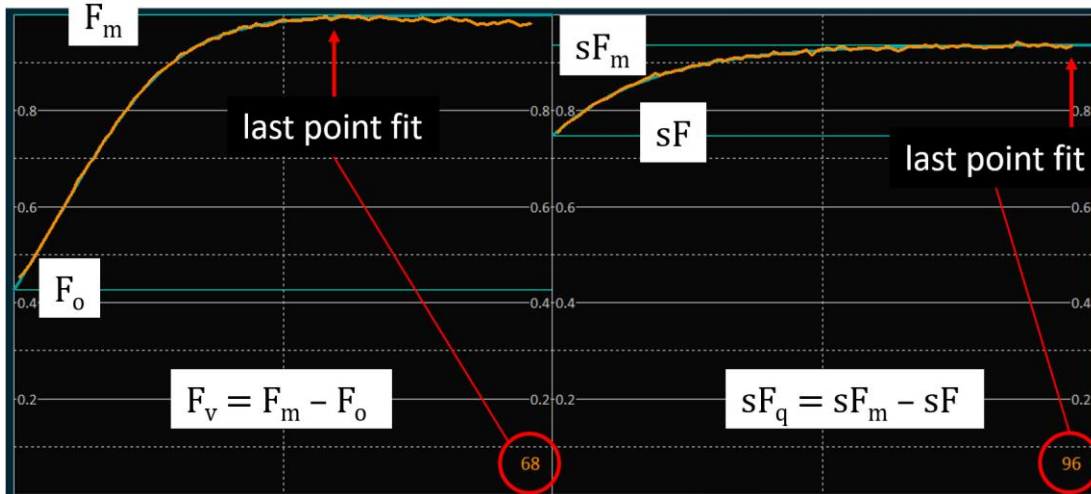


Figure 10.2: Crop from a screenshot of the data screen showing a dual ST pulse. The gap interval was 200 μ s.

Figure 10.3 shows an entire dark group from which the example in Figure 10.2 was extracted.

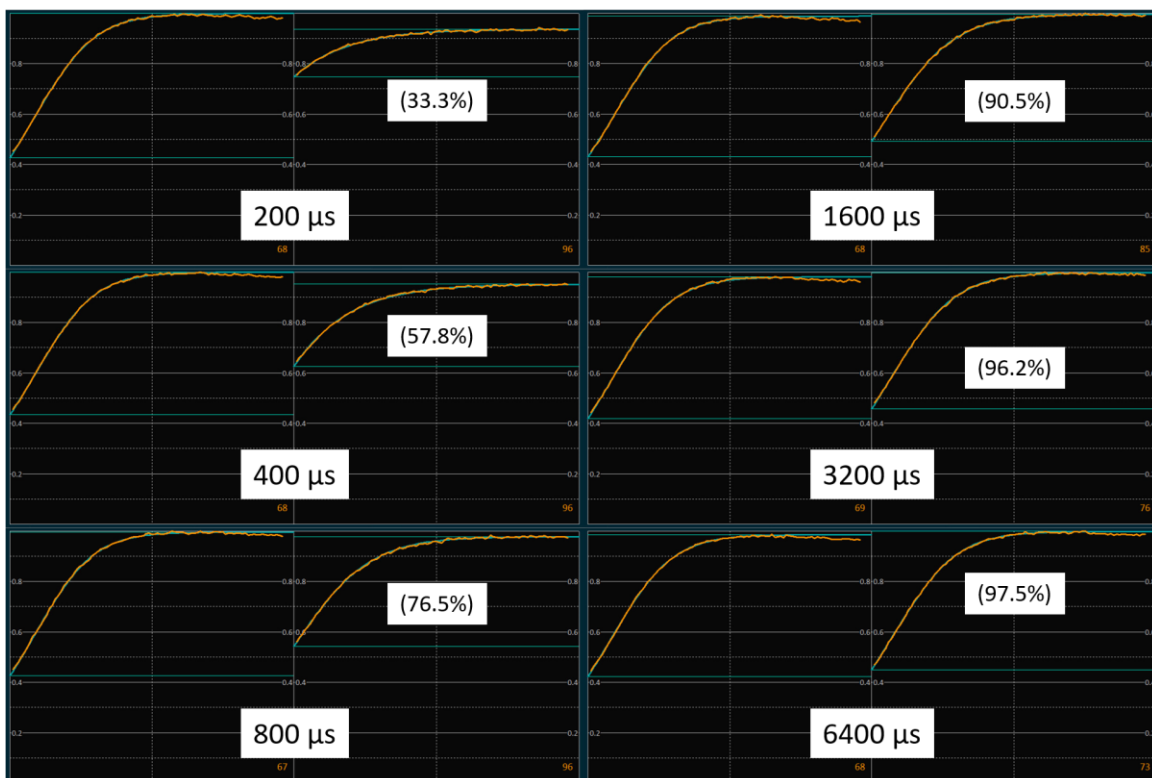


Figure 10.3: Composite of crops from screenshots of the data screen showing curves from a complete dual ST pulse Set. The target sample was dark adapted. The times shown are the gap intervals. The numbers within brackets are % recovery of variable fluorescence between the first and second ST pulse.

Working through the gap intervals from shortest to longest, there is a consistent increase in sF_m , relative to F_m . At 200 μs , sF_m is noticeably lower than F_m . By 1600 μs , sF_m is slightly higher than F_m and by 6400 μs sF_m is very noticeably higher than F_m . The relative increase in sF_m is consistent with neutralisation of the electric field-dependent quenching between the end of the first ST pulse and the start of the second ST pulse with a time constant of around 1 ms (Witt, 1971; Johnson and Ruban, 2014). In addition, the increase in sF_m to a point that is higher than F_m can be at least partly attributed to transient reduction of plastoquinone to semi-plastoquinone and semi-plastoquinone to plastoquinol as closed RCIIIs are reopened through the transfer of electrons from reduced Q_A (Verotte, Etienne and Briantais, 1979).

For comparison, Figure 10.4 shows a group from the same sample under actinic illumination of 1000 $\mu mol photons m^{-2} s^{-1}$. Recovery of variable fluorescence is broadly in line with the dark group shown above. One important difference is that the electric field-dependent quenching evident in the dark group is not evident within this group. This can be attributed to the much smaller number of RCIIIs undergoing charge separation during the first ST pulse. In contrast, sF_m is very slightly higher than F_m between 1600 and 6400 μs . This is consistent with short-lived formation of plastoquinol as this relatively small pool of RCIIIs reopen.

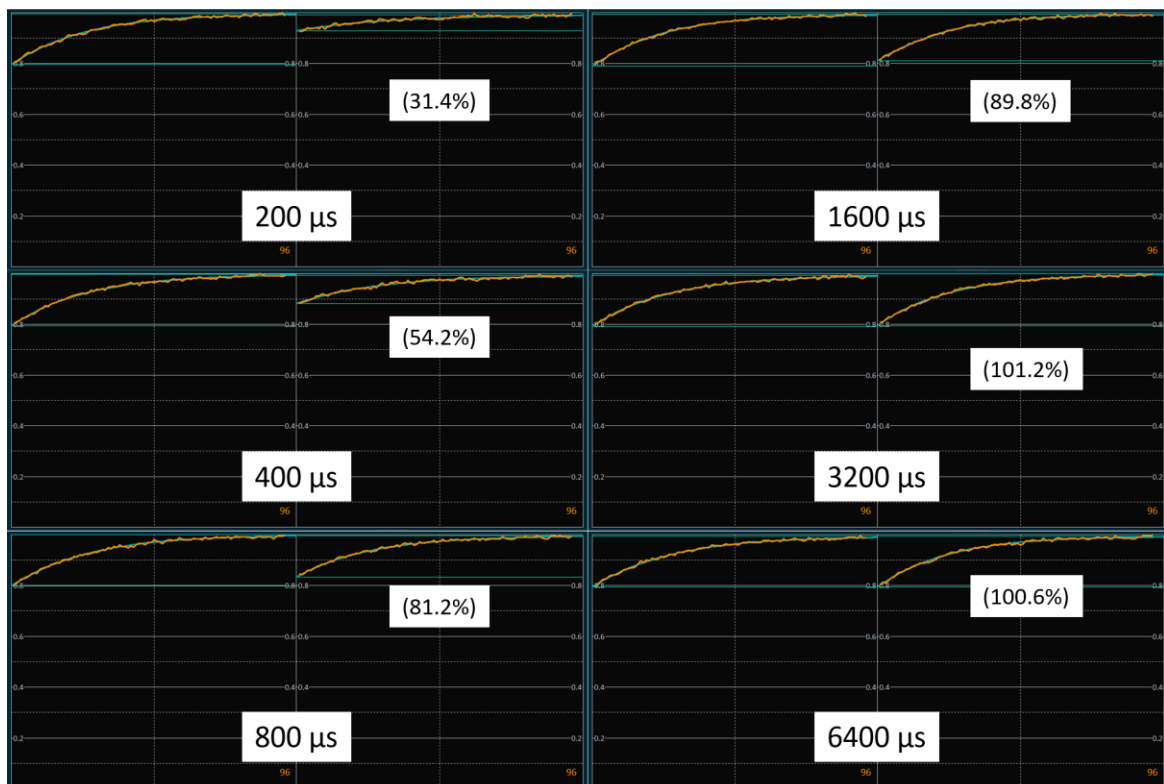


Figure 10.4: Composite of crops from screenshots of the data screen showing curves from a complete dual ST pulse Set. The target sample was under actinic illumination of 1000 $\mu mol photons m^{-2} s^{-1}$.

10.5 The relaxation phase (tau) fit

Three relaxation phase fits are generated by RunSTAF: **Fv**, **Rho** and **Dimer**. The **Fv** fit tracks the recovery of variable fluorescence during the gap between the first and second ST pulses as $1 - sF_q/F_v$ for a dark measurement or $1 - sF_q'/F_q'$ under actinic light. The **Rho** and **Dimer** relaxation phase fits track the reopening of RCIIIs during the gap between the first and second ST pulses using the Rho and Dimer models. All three fits use Equation 10.9 to generate values for comparison with the **Fv**, **Rho** and **Dimer** values. The fitting process minimises the sum of squares between values of F_t and actual data values at the same timepoint.

$$F_t = \Delta_F \cdot e^{-\frac{t}{\tau_F}} + \Delta_S \cdot e^{-\frac{t}{\tau_S}} \quad \text{Equation 10.9}$$

Where the subscripts F and S refer to the fast and slow phases of the relaxation phase. It is assumed that the fast phase is tracking the reopening of RCIIIs with plastoquinone or semi-plastoquinone bound at the Q_B site at the end of the ST pulse while the slow phase tracks the reopening of RCIIIs with an empty Q_B site at the end of the ST pulse. Δ_F and Δ_S are the proportions of the total amplitude of the relaxation phase attributable to the fast and slow phases, respectively, while τ_F and τ_S are the time constants for these phases.

The relaxation phase shown within the upper panel of the screenshot in Figure 10.5 is selected by moving the cursor in the lower panel. RunSTAF finds the group for the selected Saq and plots the curves for that Group. In the example below, the selected Saq was logged while the sample was in the dark. In the dark-adapted state, the separation of curves is usually as shown here: the **Rho** fit curve is above the **Fv** fit curve all the way through while the **Dimer** fit curve starts out with the **Rho** curve fit and then runs above it.

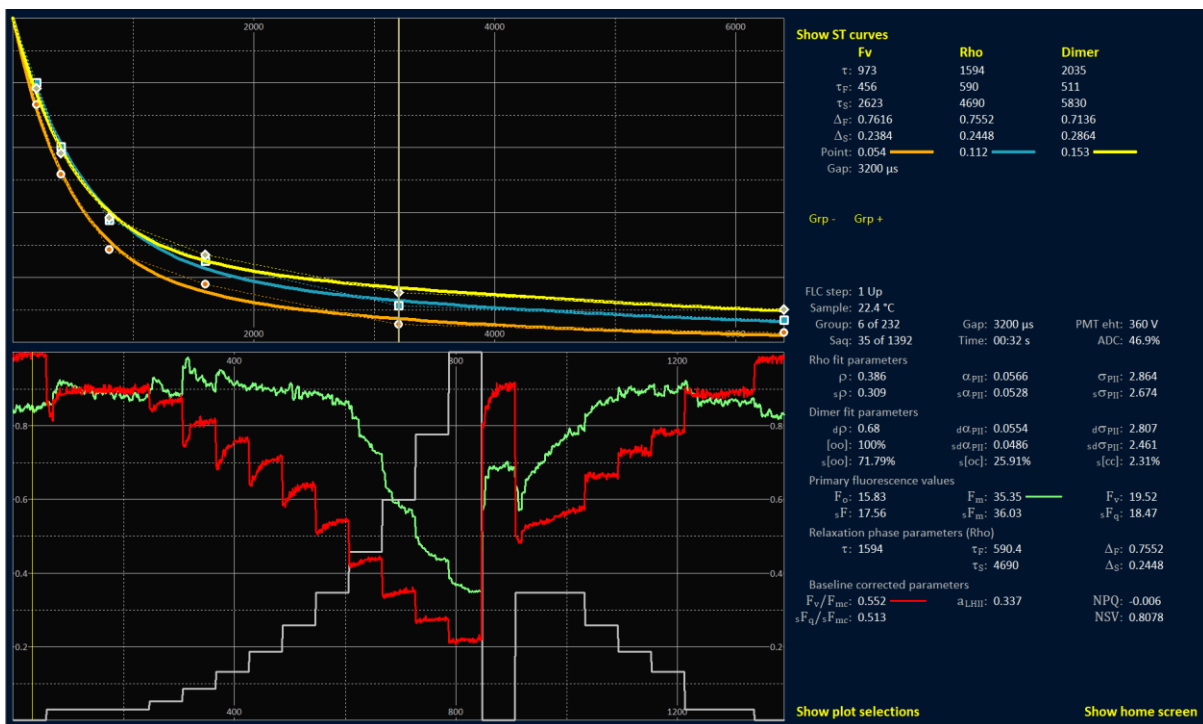


Figure 10.5: Screenshot of the data screen with the **Show tau data** option active.

With increasing actinic illumination, the **Rho** and **Dimer** fit curves both move closer to the **Fv** curve, as illustrated in Figure 10.6. This phenomenon can be attributed to connectivity between and among PSII complexes, as explained below.

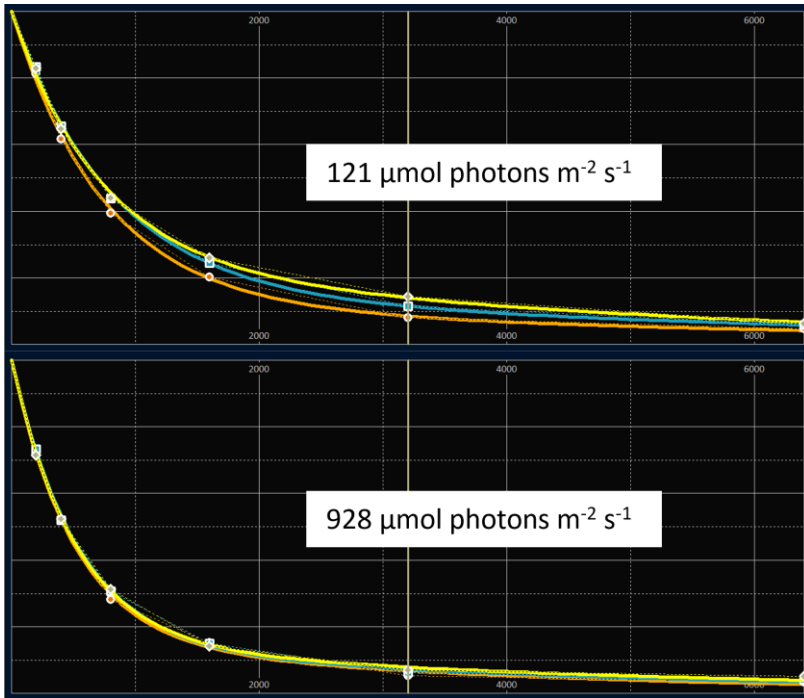


Figure 10.6: Crops from screenshots of the data screen showing relaxation phase curve fits generated from dual ST pulse data acquired at the photon irradiances shown.

The orange lines are the **Fv** fits, the teal lines are the **Rho** fits and the yellow lines are the **Dimer** fits.

In the absence of connectivity ($\rho = 0$), the **Fv** and **Rho** fits should match perfectly from the dark-adapted state through to saturating actinic photon irradiance. The observation that the **Fv**, **Rho** and **Dimer** fit curves converge under increasing actinic photon irradiance is consistent with a decrease in the value of ρ (Rho model) and an increase in $[oc]$ (Dimer model) as the proportion of RCIs in the closed state increases.

See: [Deconstructing Rho](#)

The bottom panel of the screenshot in Figure 10.7 shows plots of all five relaxation phase parameters from the **Rho** fit.

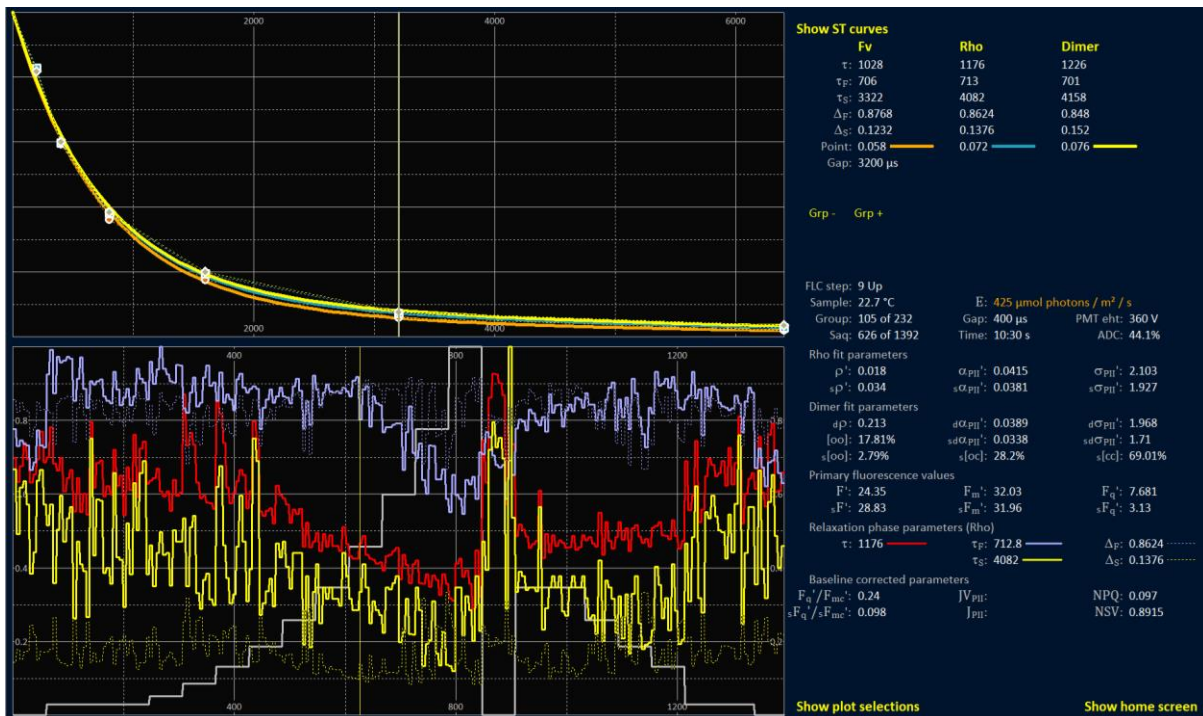


Figure 10.7: Screenshot from the data screen showing all five relaxation phase parameters derived from the Rho fit.

With the fitting algorithm incorporated within RunSTAF, the total amplitude of the recovery phase ($\Delta_F + \Delta_S$) is always unity. The complete relaxation phase dataset for all three fits can be accessed through the Clipboard function...

Clipboard → Tau data

In addition to the parameter plots on the data screen, τ from the **Rho** fit can be plotted within the rPE window on the home screen, as shown within Figure 10.8.

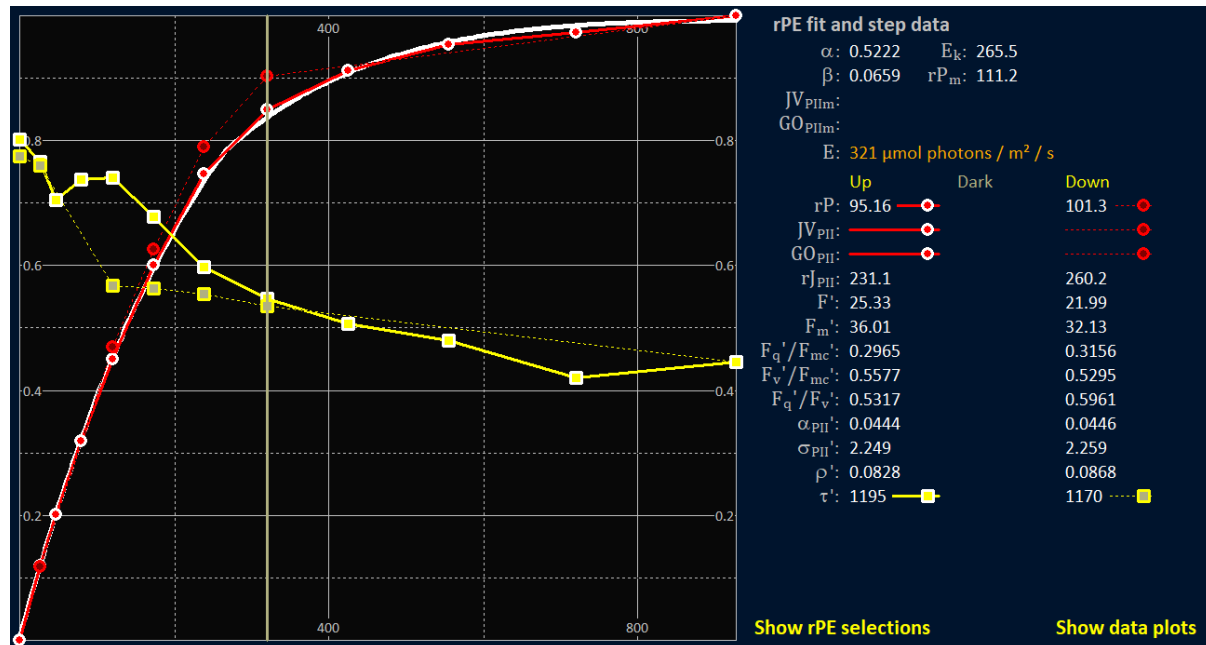


Figure 10.8: Crop from a screenshot of the home screen showing the $\tau^{(i)}$ parameter within the rPE data plot. The $\tau^{(i)}$ values were generated from the Rho fit to ST data.

10.6 The rPE data fit

The rPE curve is a variant of the widely used photosynthesis – photon irradiance (PE) response curve. The 'P' in PE is generally taken to represent mass-specific photosynthesis (normalised to chlorophyll *a* or carbon, for example). In contrast, the rPE curve plots relative photosynthesis (rP) against photon irradiance. Although values of rP are reported on a unitless scale within RunSTAF, they are actually calculated as the product of E and F'_q / F'_{mc} . This generates units of $\mu\text{mol photons m}^{-2} \text{s}^{-1}$ which translates as $\mu\text{mol photons s}^{-1}$ through a population of PSII complexes with a combined absorption cross section for PSII photochemistry (σ_{PII}) of 1 m^2 .

There are three basic parameters derived from all PE curve fits: α , E_k , and P_m . The value of α provides the initial slope of the relationship between P and E. E_k is an inflection point along the PE curve which is often described as the light saturation parameter (Platt and Gallegos, 1980). P_m is the maximum rate of photosynthesis.

A range of models have been used to generate a fit to rPE and other PE curves (see Silsbe and Kromkamp, 2012 and references therein). The fitting method used within RunSTAF takes advantage of the fact that data points on the rPE curve up to E_k invariably have a higher signal to noise ratio than points after E_k . This is the opposite of the situation with ^{14}C or O_2 -based PE curve datasets where the signal to noise tends to increase with photon irradiance up to P_m . Importantly, the reliance of the RunSTAF fitting procedure on a high signal to noise up to E_k makes it unsuited to fitting ^{14}C or O_2 -based PE data. To provide an example, Boatman, Geider and Oxborough (2019) used the procedure incorporated within RunSTAF to fit FLC-derived rPE data while the equations of Platt and Gallegos (1980) were used to fit data from PE curves generated from parallel O_2 measurements.

There are two phases to the rPE fitting process incorporated within RunSTAF: the alpha phase and the beta phase. The fitting process is based around minimisation of the sum of squares (SS) of the difference between actual and fit values. The mean of the actual values at each E level are used for the fit.

The alpha phase of the rPE fit uses the Webb model (Webb et al. 1974) to generate values for α and E_k . The value of F_q'/F_{mc}' used to generate each rPE value is calculated using Equation 10.10.

$$\frac{F_q'}{F_{mc}'} = \alpha \cdot E_k \cdot (1 - e^{-E/E_k}) \cdot E^{-1} \quad \text{Equation 10.10}$$

It follows that α is theoretically equal to F_v/F_{mc} and that E_k is the point on the rPE curve at which the value of F_q'/F_{mc}' is 63.2% of F_v/F_{mc} . For the alpha phase, the square of the difference between actual and fit values is multiplied by the square of the actual F_q'/F_{mc}' value at that point. This generates a fit that is heavily weighted towards low values of E and is the main reason why this approach is unsuitable for fitting ^{14}C or O_2 -based PE curve data.

The beta phase is generated using Equation 10.11. The beta phase is only applied to points after the E_k value generated by the alpha phase. This means that the values of α and E_k are the same for both Equation 10.10 and Equation 10.11.

$$\frac{F_q'}{F_{mc}'} = (\alpha \cdot E_k \cdot [1 - e^{-E/E_k}] - \beta \cdot E_{k\beta} \cdot [1 - e^{-E/E_{k\beta}}]) \cdot E^{-1} \quad \text{Equation 10.11}$$

The screenshot in Figure 10.9 shows the alpha phase fit to a complete rPE curve. The screenshot in Figure 10.10 shows the same fit with the beta phase added.

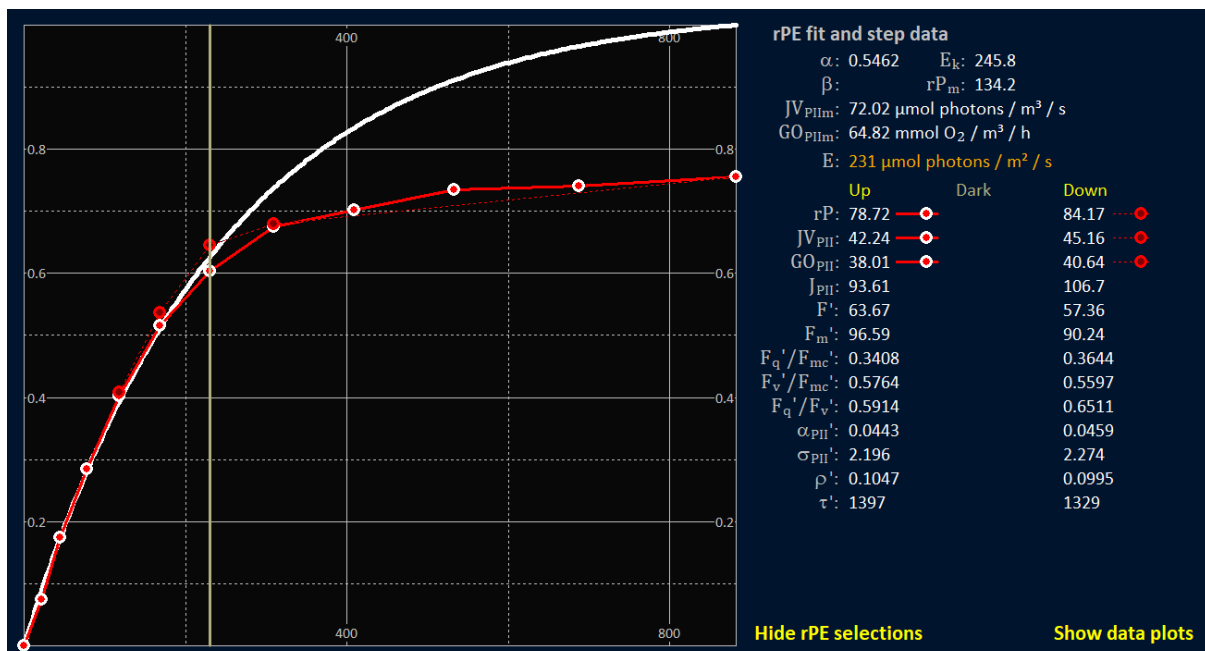


Figure 10.9: rPE curve fit with the beta phase blocked such that the (solid white) rPE fit line is defined by Equation 10.10.

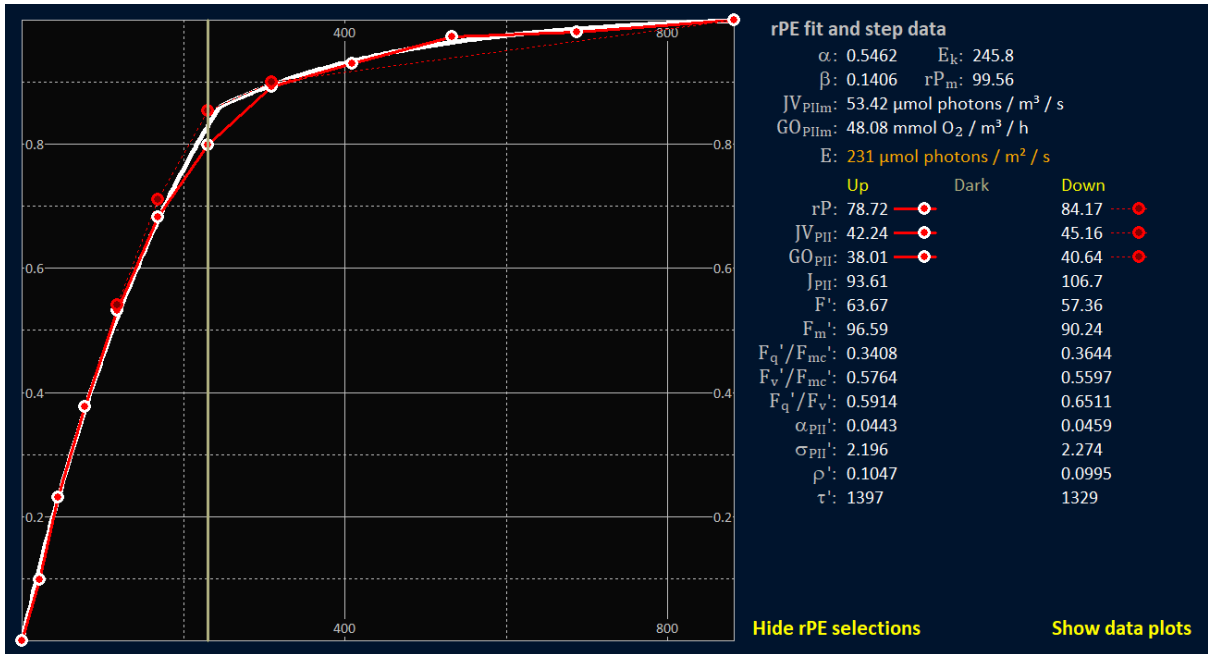


Figure 10.10: rPE curve fit with the beta phase applied such that the (solid white) rPE fit line is defined by Equation 10.11.

11 Generating values of J_{PII} , JV_{PII} and GO_{PII}

The combination of LabSTAF hardware and RunSTAF software allows for measurement of J_{PII} and JV_{PII} using the so-called sigma and absorption methods respectively. Because the spectral output of the LEDs used for ST measurements (MLEDs) is very different from the spectral output of the LED providing actinic illumination (ALED) a spectral correction step is required for both parameters. In the case of JV_{PII} , correction is also required for the package effect.

This section covers some basic concepts underlying the sigma and absorption algorithms. Application of the Photochemical Excitation Profile (PEP) for spectral correction and Package Effect Correction (PEC) are covered in Sections 13 and 14.

See: [Photochemical Excitation Profile \(PEP\)](#) and [Package Effect Correction \(PEC\)](#)

Under the assumption that every photon used to drive PSII photochemistry results in the transfer of an electron from water to the plastoquinone pool, JV_{PII} can be directly converted to Gross Oxygen release (GO_{PII}) with SI units of $\text{mol O}_2 \text{ m}^{-3} \text{ s}^{-1}$. While GO_{PII} can be derived from JV_{PII} with reasonable confidence, processes operating within phytoplankton can uncouple PhytoPP from JV_{PII} and GO_{PII} (Geider and MacIntyre, 2002; Behrenfeld et al., 2004; Halsey et al., 2010; Suggett et al., 2010; Lawrenz et al., 2013). It follows that while JV_{PII} can provide an upper limit for PhytoPP, the actual value may be significantly lower.

The value of JV_{PII} generated by STAF is the product of the rate at which photons are absorbed by the PSII light harvesting system per unit volume and the proportion of absorbed photons used to drive PSII photochemistry. This value is defined as the PSII photochemical flux per unit volume because it is directly proportional to the absorption cross section of PSII photochemistry provided by all PSII complexes within each unit volume of ocean or other medium.

11.1 Absorption cross section

As a term, absorption cross section describes the probability of an absorption process. There are two processes that are intrinsic to PSII photochemical flux and are driven by the absorption of photons: formation of an excited state within the PSII pigment matrix (PSII light harvesting, LHII) and PSII photochemistry (PII). Within this document, the absorption cross sections for these processes are defined by the terms σ_{LHII} and σ_{PII} , respectively, with SI units of $\text{m}^2 \text{ PSII}^{-1}$. Clearly, a photon can only drive PSII photochemistry after being absorbed. It follows that σ_{LHII} is always larger than σ_{PII} and that the relationship between σ_{LHII} and σ_{PII} is dependent on the proportion of absorbed photons absorbed used to drive PSII photochemistry. The absorption process is illustrated in Figure 11.1.

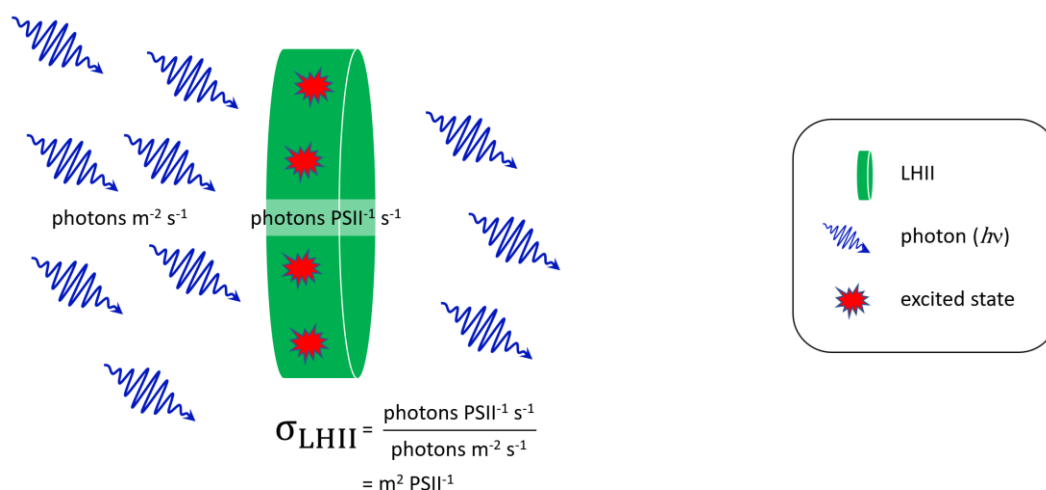


Figure 11.1: The absorption cross section of PSII light harvesting. A proportion of incident photons are absorbed and generate excited states within the pigment matrix.

At the simplest level, PSII photochemistry competes directly with two other absorption-dependent processes operating within the PSII complex: the loss of absorbed photons through thermal dissipation (DII) and the emission of photons as fluorescence (FII).

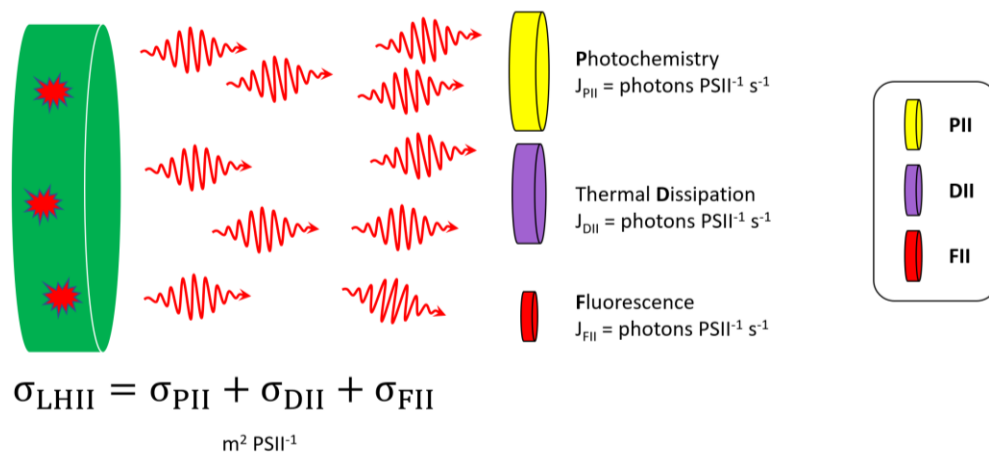


Figure 11.2: The excited states generated within the pigment matrix of the PSII light harvesting system through the absorption of incident photons are lost through photochemistry, thermal dissipation or re-emission as fluorescence.

The relationships between these processes can be defined by a series of simple equations. As a starting point, Equation 11.1 defines σ_{LHII} as the sum of the absorption cross sections for the three processes that are in direct competition with each other for absorbed photons.

$$\sigma_{LHII} = \sigma_{PII} + \sigma_{DII} + \sigma_{FII} \quad \text{Equation 11.1}$$

The probability that an absorbed photon will be lost through a particular process is defined by the yield for that process. In turn, the yield for each process can be defined by the rate constants for the three competing processes, as shown in Equations 11.2A, B and C.

$$\phi_{PII} = \frac{k_{PII}}{k_{PII} + k_{DII} + k_{FII}} \quad \text{Equation 11.2A}$$

$$\phi_{DII} = \frac{k_{DII}}{k_{PII} + k_{DII} + k_{FII}} \quad \text{Equation 11.2B}$$

$$\phi_{FII} = \frac{k_{FII}}{k_{PII} + k_{DII} + k_{FII}} \quad \text{Equation 11.2C}$$

Where ϕ_{PII} , ϕ_{DII} and ϕ_{FII} are all dimensionless. The sum of the yields for all three processes must be unity (Equation 11.3) since they collectively account for the fate of all absorbed photons.

$$\phi_{PII} + \phi_{DII} + \phi_{FII} = 1 \quad \text{Equation 11.3}$$

Equation 11.4 illustrates an important consequence of the relationships defined by Equations 11.1 and 11.3. This equation simply states that the absorption cross section of PSII photochemistry is equal to the product of the absorption cross section for PSII light harvesting and the probability that an absorbed photon will be used to drive PSII photochemistry.

$$\sigma_{PII} = \sigma_{LHII} \cdot \phi_{PII} \quad \text{Equation 11.4}$$

Values for two of the three parameters within Equation 11.4 can be generated directly from STAF data. A value for σ_{PII} can be generated using the equations provided by Kolber, Prášil and Falkowski (1998) and a value for ϕ_{PII} can be generated from F_{oc} and F_{mc} using Equation 11.5.

$$\Phi_{\text{PII}} = \frac{F_v}{F_{\text{mc}}} \quad \text{Equation 11.5}$$

Where $F_v = F_{\text{mc}} - F_{\text{oc}}$.

See: [The Rho ST curve fit](#) and [Glossary of parameter terms](#)

11.2 PSII photochemical flux (J_{PII} and JV_{PII})

As already noted, PSII photochemical flux is dependent on the absorption cross section for PSII photochemistry. This can be defined by a single PSII or all PSII complexes suspended within a unit volume of medium (m^3).

Equation 11.6 provides a simple expression for the relationship between J_{PII} and JV_{PII} . It should be noted that this equation is only valid for a theoretical situation where all RCIIIs within the sample are in the open state.

$$JV_{\text{PII}} = J_{\text{PII}} \cdot [\text{PSII}] \quad \text{Equation 11.6}$$

Where $[\text{PSII}]$ is the concentration of photochemically active PSII complexes, with units of PSII m^{-3} .

In the dark-adapted state, the absorption cross section of PSII photochemistry provided by a single PSII is defined by σ_{PII} (units of $\text{m}^2 \text{PSII}^{-1}$). In the case of all PSII complexes within a m^3 of medium, the absorption cross section of PSII photochemistry is defined as a_{PII} (units of $\text{m}^2 \text{m}^{-3} = \text{m}^{-1}$).

Within an illuminated sample containing multiple PSII complexes, some will be in the open state while others are in the closed state. The PSII photochemical flux for a single open PSII complex is given by Equation 11.7.

$$J_{\text{PII}} = \sigma_{\text{PII}} \cdot E \quad \text{Equation 11.7}$$

Where E is photon irradiance with units of photons $\text{m}^{-2} \text{s}^{-1}$.

Equation 11.8 generates an average photochemical flux through each PSII (open or closed) within an illuminated sample.

$$J_{\text{PII}} = \sigma_{\text{PII}}' \cdot \frac{F_q'}{F_v'} \cdot E \quad \text{Equation 11.8}$$

Where J_{PII} is PSII photochemical flux, $F_q' = F_m' - F'$ and $F_v' = F_m' - F_o'$.

Within this equation, σ_{PII}' denotes the absorption cross section of PSII photochemistry of each open PSII complex within the sample and F_q'/F_v' provides a baseline-independent estimate of the proportion of PSII complexes within the sample that are in the open state at the point of measurement.

An alternative approach is to use Equation 11.9 to generate a value for σ_{LHII} .

$$\sigma_{\text{LHII}} = \sigma_{\text{PII}} \cdot \frac{F_{\text{mc}}}{F_v} \quad \text{Equation 11.9}$$

The value of σ_{LHII} can then be incorporated within Equation 11.10.

$$J_{\text{PII}} = \sigma_{\text{LHII}} \cdot \frac{F_q'}{F_{\text{mc}}'} \cdot E \quad \text{Equation 11.10}$$

With this approach, we are using a STAF measurement from a dark-adapted sample to generate a value for σ_{LHII} and then using a STAF measurement from the same sample under illumination to generate a value for the efficiency at which harvested photons are used (F_q'/F_{mc}').

The PSII photochemical flux for all PSII complexes within a unit volume of water can be calculated using Equation 11.11.

$$JV_{PII} = a_{LHII} \cdot \frac{F_{q'}}{F_{mc'}} \cdot E \quad \text{Equation 11.11}$$

This approach is similar to Equation 11.10 in the sense that we are using a STAF measurement from a dark-adapted sample to quantify PSII light harvesting (in this case, for all PSII complexes within a unit volume of water) and the same measurement under illumination to define the average efficiency at which harvested photons are used.

We can define two routes for generating a value for a_{LHII} . The first route (Equation 11.12) incorporates the right hand side of Equation 11.9.

$$a_{LHII} = \sigma_{PII} \cdot \frac{F_{mc'}}{F_v} \cdot [PSII] \quad \text{Equation 11.12}$$

The second route for generating a value for a_{LHII} is illustrated by Equation 11.13 (Oxborough et al. 2012).

$$a_{LHII} = K_a \cdot \frac{F_{mc'} \cdot F_{oc}}{F_v} \quad \text{Equation 11.13}$$

Where K_a is an instrument-type specific constant, with units of m^{-1} .

See: [Derivation of \$K_a\$](#)

As an alternative to Equation 11.11, Equation 11.14 can be derived from the relationship defined by Equation 11.6 and the right hand side of Equation 11.8.

$$JV_{PII} = \sigma_{PII}' \cdot \frac{F_{q'}}{F_{v'}} \cdot [PSII] \cdot E \quad \text{Equation 11.14}$$

It follows that Equations 11.11 to 11.14 provide three routes to JV_{PII} :

- Equation 11.11 combined with Equation 11.12
- Equation 11.11 combined with Equation 11.13
- Equation 11.14

Equations 11.12 and 11.14 include $[PSII]$. A value for this parameter can be derived using Equation 11.15 (Oxborough et al. 2012).

$$[PSII] = K_a \cdot \frac{F_{oc}}{\sigma_{PII}} \quad \text{Equation 11.15}$$

Substituting the right hand side of Equation 11.15 for the $[PSII]$ in Equation 11.12 generates Equation 11.16, which simplifies to Equation 11.13.

$$a_{LHII} = \sigma_{PII} \cdot \frac{F_{mc'}}{F_v} \cdot K_a \cdot \frac{F_{oc}}{\sigma_{PII}} \quad \text{Equation 11.16}$$

Substituting the right hand side of Equation 11.15 for $[PSII]$ within Equation 11.14 generates Equation 11.17. This serves to emphasise the inclusion of both σ_{PII} and σ_{PII}' with this approach.

$$JV_{PII} = \sigma_{PII}' \cdot \frac{F_{q'}}{F_{v'}} \cdot K_a \cdot \frac{F_{oc}}{\sigma_{PII}} \cdot E \quad \text{Equation 11.17}$$

Consequently, we can now define two routes to JV_{PII} :

- **The absorption method:** which uses Equation 11.11
- **The sigma method:** which uses Equation 11.14

To select the best method for use in a particular situation, the following points should be considered:

1. Values of F_o , F_m , F' and F_m' can be measured at higher precision than values of σ_{PII} and σ_{PII}'
2. Values of F_o , F_m and σ_{PII} can be measured at higher precision than values of F' , F_m' and σ_{PII}'

3. F_o , F_m , F' and F_m' are all sensitive to baseline fluorescence
4. σ_{PII} and σ_{PII}' are insensitive to baseline fluorescence
5. F_{oc} , F_{mc} , F_c' and F_{mc}' are insensitive to heterogeneity within the sample
6. σ_{PII} and σ_{PII}' are sensitive to heterogeneity within the sample

The precision issue raised by Points 1 and 2 is most obvious when photon irradiance is increased to levels that saturate photosynthesis. This can decrease the amplitude of F_q' to the point where a reliable value of σ_{PII}' can no longer be generated.

With the absorption method, baseline fluorescence (Points 3 and 4) increases the value of a_{LHII} and decreases the value of F_q'/F_m' (Oxborough et al. 2012). With the sigma method, baseline fluorescence increases the value of [PSII] generated by Equation 11.14 in proportion to the increase in a_{LHII} .

Within Equation 11.14, the value of F_q'/F_v' is nominally independent of baseline fluorescence. However, if the required value of F_o' is generated using the method provided by Oxborough and Baker (1997), baseline fluorescence can decrease the calculated value of F_q'/F_v' . It should be noted that the baseline fluorescence-induced decrease in F_q'/F_v' is always lower than the baseline fluorescence-induced decrease in F_q'/F_m' and approaches zero with samples that exhibit low levels of downregulation.

An obvious potential form of heterogeneity within a sample (points 5 and 6) is the combining of phytoplankton species with differing σ_{PII} values within the waveband(s) used for the ST measurements. Providing the ST pulse is bright enough to ensure that F_m or F_m' is reached for all species within a sample, this type of heterogeneity does not generate errors with the absorption method (Equation 11.11). This is because the values of F_{oc} , F_{mc} , F_c' and F_{mc}' are additive and, as a result, both a_{LHII} and F_q'/F_{mc}' are unaffected. Conversely, this type of heterogeneity can generate an error with the sigma method (Equation 11.14) because the σ_{PII} value generated from adding multiple curves together and applying a single Rho fit is unlikely to generate the correct result. Errors generated are normally overestimates and, in theory, could reach tens of percent if the spectral profiles of phytoplankton species within the sample are very different. Combining phytoplankton species within a single sample can also impact on spectral correction.

See: [Photochemical Excitation Profile \(PEP\)](#)

11.3 Derivation of K_a

At the time of writing, an experimental programme to derive a LabSTAF-specific value for K_a is being conducted. The current default K_a value for LabSTAF is the same as used with FastOcean and the fluorescence values have been scaled to match with FastOcean through a small number of comparative measurements with natural samples. It is worth noting that K_a only impacts on the calculated values of JV_{PII} and GO_{PII} and that any change in the set value of K_a is immediately applied to existing data. A function has been incorporated within RunSTAF to allow for a folder-based update of K_a across files...

File → Run a folder-based K_a update

A derivation for K_a was originally provided by Oxborough et al. (2012). Within this manuscript, the term K_R was used in place of K_a . The only difference between K_R and K_a is that the former is only applicable to a single fluorometer while the latter can be used with any fluorometers built to the same design. This difference is illustrated by Equations 11.18 and 11.19.

$$K_R = [PSII] \cdot \frac{\sigma_{PII}}{F_{oc}} \cdot E_{ST} \quad \text{Equation 11.18}$$

$$K_a = [PSII] \cdot \frac{\sigma_{PII}}{F_{oc}} \quad \text{Equation 11.19}$$

The E_{ST} term incorporated within Equation 11.18 is required for systems where the primary fluorescence data are not scaled to MLED output. Equation 11.19, which omits the E_{ST} term, is applicable to LabSTAF because fluorescence values are automatically corrected for MLED output.

The accuracy of K_a derived using Equation 11.19 is dependent on σ_{PII} and F_{oc} scaling together. As already noted, the fluorescence signal and σ_{PII} have different sensitivities to baseline fluorescence and sample heterogeneity. It follows that the most accurate values for K_a from Equation 11.19 are likely to come from single species cultures with high values of F_v/F_m .

Within Equations 11.18 and 11.19, the value of [PSII] is derived using the flash- O_2 method described by Boatman, Geider and Oxborough (2019). Equation 11.20 provides an alternative for deriving K_a . Within this equation, JV_{PII} is derived from direct measurement of O_2 release.

$$K_a = JV_{PII} / \left(\frac{F_{mc} \cdot F_{oc}}{F_v} \cdot \frac{F_{q'}}{F_{mc'}} \cdot E \right) \quad \text{Equation 11.20}$$

From a purely practical point of view, it is much easier to derive K_a using Equation 11.20 than 11.19. One option is to derive the saturated rate of rP from an FLC (calculated as the product of $F_{q'}/F_{mc'}$ and E) and measure O_2 release at the same E using a spectrally matched actinic light source. Measuring at saturation is advantageous because although the value of $F_{q'}/F_{mc'}$ decreases with E, overall accuracy is improved through having the highest rate of O_2 evolution.

12 Deconstructing rho

This section has been included to provide a detailed overview of the rho (ρ) parameter that accounts for connectivity among PSII complexes.

See: [The Rho ST curve fit](#)

Equations 12.1 and 12.2 are valid for a dark-adapted sample and assume that all photochemically active RCII are in the open state at $t=0$. Equations 12.3 and 12.4 are valid for a light-adapted sample where a proportion of the photochemically active RCII within the sample are in the closed state.

$$C_t = C_{t-1} + C_{t-1} \cdot (1 - C_{t-1}) / (1 - C_{t-1} \cdot \rho) \quad \text{Equation 12.1}$$

$$F_t = F_0 + F_v \cdot C_t \cdot (1 - \rho) / (1 - C_t \cdot \rho) \quad \text{Equation 12.2}$$

$$C_t = C_{t-1} + C_{t-1} \cdot (1 - C_{t-1}) / (1 - C_{t-1} \cdot \rho') \quad \text{Equation 12.3}$$

$$F'_t = F' + F_q' \cdot C_t \cdot (1 - \rho') / (1 - C_t \cdot \rho') \quad \text{Equation 12.4}$$

Where t = time since the start of the ST pulse (μs) and C_t is the proportion of centres that were open at $t=0$ that are closed at t . As a consequence, C is 0 at $t=0$ in both the dark-adapted and light-adapted states, even though a proportion of the photochemically active RCII within the sample are in the closed state under ambient light.

Within a completely homogeneous population of perfectly or imperfectly connected PSII complexes, ρ can be defined as the probability of a photon absorbed by a PSII complex with a closed RCII being transferred to a PSII complex with an open RCII and then used to drive PSII photochemistry.

Figure 12.1 shows ST pulse data from dark-adapted cultured cells of *Chlorella vulgaris*. Both Rho and Dimer fits are also included.

See: [Fitting a dual ST pulse sequence](#)

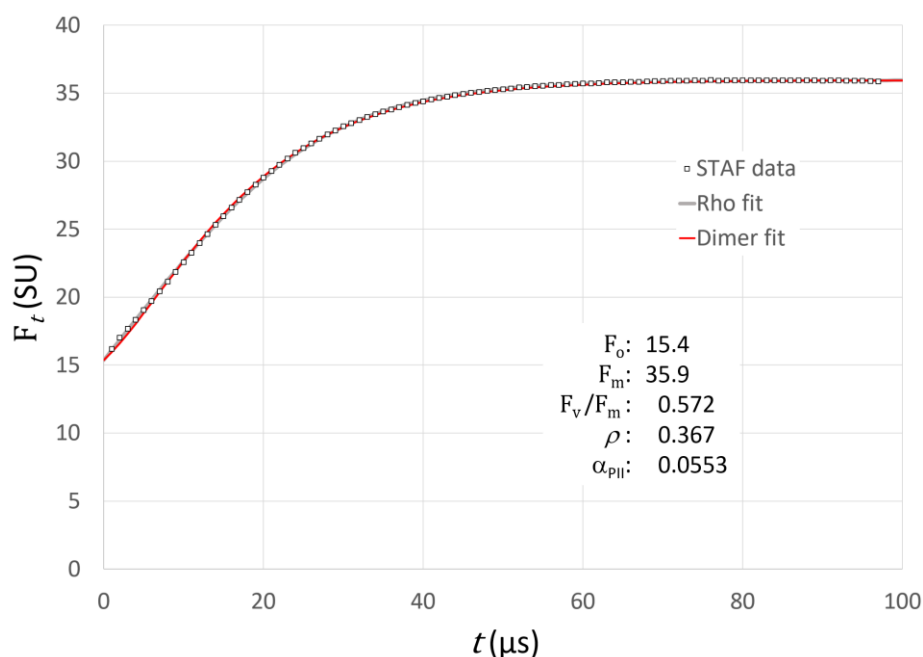


Figure 12.1: An example Saq ST curve recorded from cultured cells of *C. vulgaris*. The Rho fit was made using Equations 12.1 and 12.2. The Dimer fit was made using Equations 10.7 and 10.8. The first 76 points were incorporated within both fits ($t=1$ to $t=76$).

Although there is a close visual match between the ST data and either fit within Figure 12.1., the Rho fit provides a closer overall match than the Dimer fit. In this example, the closer match provided by the Rho fit is particularly evident over the first 10 μs or so. Because the value of F_v/F_m is high,

RunSTAF has limited the Rho ST fit to the first 76 points to limit the possible impact of electric field-dependent quenching. Within a theoretical model incorporating zero connectivity among RCII, the value of ρ in Equations 12.1 and 12.2 is zero and the values of α_{PII} and σ_{PII} derived from the fit are unchanged as C_t increases. At the other end of the scale, perfect connectivity among RCII (i.e. all RCII within the interrogated volume have equal access to a single light harvesting pigment matrix) generates a value of ρ equal to ϕ_{PII} and values of α_{PII} and σ_{PII} that increase with C_t . The curves in Figure 12.3 show the original ST curve and Rho fit from Figure 12.1 (A), the fit with zero connectivity among RCII (B) and the fit with perfect connectivity among RCII (C). For both B and C, the values of F_0 and F_m were fixed at the values generated by the Rho ST fit in A. The perfect connectivity in C was set by using the value of F_v/F_m from A as a proxy for ϕ_{PII} .

Setting the value of ρ to zero is equivalent to the 'separate package' or 'puddle' model while setting ρ as ϕ_{PII} is equivalent to the 'matrix' or 'lake' model of PSII connectivity (e.g. Butler et al. 1983; Kramer et al. 2004). Looking at the three fits within Figure 12.2, it is clear that a good fit to the entire ST curve is only achieved by allowing the value of ρ to assume an intermediate value during the iterative fitting process.

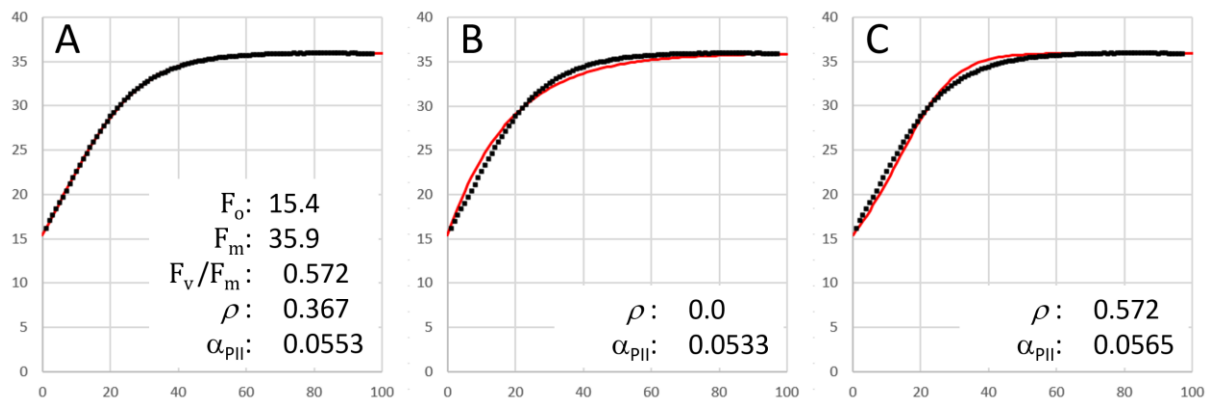


Figure 12.2: Rho ST curve fits to the same ST data as presented in Figure 12.1. The fit in A is identical to Figure 12.1 (F_0 , F_m , ρ and $C_{t=1}$ were all allowed to float in Equations 12.1 and 12.2). For the CT fits in B and C, only $C_{t=1}$ was allowed to float. The value of ρ was fixed as zero or 0.572 (the value of F_v/F_m from A). As with Figure 12.1, the x-axes values are t (μs) and the y-axes values are F_t (SU).

12.1 Estimating the proportion of PSII complexes in the open state

From Equations 12.2 and 12.4, it is clear that the relationship between F_t and C_t in the dark-adapted state and F'_t and C_t in the light-adapted state are dependent on the values of ρ and ρ' respectively. One situation where the impact of ρ' on the relationship between F'_t and C_t has practical relevance is when using fluorescence to estimate the proportion of the total pool of photochemically active PSII complexes in the open state at $t = 0$, defined here by the term $[Q_A]$. A value for $[Q_A]$ is required when using the sigma method to calculate J_{PII} (Equation 11.8) or JV_{PII} (Equation 11.14). Within both equations, this value is provided by F_q'/F_v' . It is worth noting that a value for $[Q_A]$ is not required when using the absorption method to calculate JV_{PII} (Equation 11.11).

Equations 12.5 and 12.6 can be used to calculate a value for $[Q_A]$ from a dark-adapted sample or a sample under actinic illumination, respectively, for any value of ρ or ρ' . Equation 12.5 can be used to quantify $[Q_A]$ at any point within an ST pulse applied to a dark-adapted sample. Equation 12.6 can be used to calculate $[Q_A]$ at the start of an ST pulse ($t = 0$) applied to a sample under actinic illumination.

$$[Q_A] = 1 - (F - F_0) / [(1 - \rho) \cdot (F_m - F_0) + \rho \cdot (F - F_0)] \quad \text{Equation 12.5}$$

$$[Q_A] = 1 - (F' - F_0') / [(1 - \rho') \cdot (F_m' - F_0') + \rho' \cdot (F' - F_0')] \quad \text{Equation 12.6}$$

Setting the value of ρ' in Equation 12.6 to zero makes the right hand side exactly equivalent to F_q'/F_v' . In other words, using F_q'/F_v' to estimate $[Q_A]$ is effectively assuming zero connectivity among PSII complexes and is consistent with the separate package or puddle model of connectivity (Baker and Oxborough, 2004). The parameter F_q'/F_v' is mathematically equivalent to the widely used parameter, qP. At the other end of the connectivity scale, the parameter qL provides an estimate of $[Q_A]$ assuming the matrix or lake model of connectivity (Kramer et al. 2004). Substituting $1 - F_o'/F_m'$ (as a proxy for ϕ_{PII}) for ρ' in Equation 12.6 makes the right hand side equivalent to qL. Equations 12.7A and 12.7B (Kramer et al. 2004) provide equivalent options for the calculation of qL.

$$qL = 1 - (1/F_o' - 1/F') / (1/F_o' - 1/F_m') \quad \text{Equation 12.7A}$$

$$qL = qP \cdot F_o' / F' \quad \text{Equation 12.7B}$$

The curves in Figure 12.3 were generated using three different values of ρ within Equation 12.7A. The F_q/F_v term on the x-axis is the dark-adapted equivalent of the F_q'/F_v' term within Equations 11.8 and 11.14. The values of F_o and F_m required to generate these curves were taken from the ST fit in Figure 12.1. Setting ρ as zero has generated a set of qP-based values while setting ρ as $1 - F_o/F_m$ (as a proxy for ϕ_{PII}) has generated a set of qL-based values. These two sets of values provide the theoretical extremes for the relationship between F_q/F_v and the value of $[Q_A]$. The third curve in Figure 12.3 uses the value of ρ from the ST fit in Figure 12.1 and, by definition, provides the most appropriate values of $[Q_A]$ for the homogeneous, imperfect level of connectivity that is intrinsic to the Rho ST model.

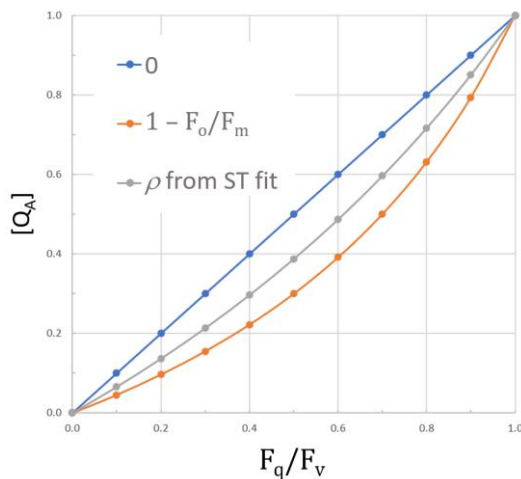


Figure 12.3: Data illustrating the relationship between F_q/F_m and values of ρ defined by qP, qL and the ST fit value. The ST curve in Figure 12.1 was used as the starting point for generating the theoretical values plotted. Data points were generated by initially setting F_q equal to F_o and then increasing the value in steps of 10% of F_v up to F_m .

12.2 The relationship between ρ and the yield of PSII photochemistry

The ST curves in Figure 12.4 are all derived from the single ST curve in Figure 12.1. Each curve within Figure 12.4 begins at the stated time within the original curve. The red fits are to the actual data points (Saq fits) and the green fits are to the Rho ST fit points (Rho fits). So, for example, the $t = 5 \mu s$ Saq curve in Figure 12.4 is a fit to the Saq ST curve points in Figure 12.1 between $t = 5 \mu s$ and $t = 76 \mu s$. These points are mapped to between $t = 0$ and $t = 71 \mu s$ for the new fit. The $t = 5 \mu s$ Rho curve in Figure 12.4 is a fit to the Rho ST fit points from Figure 12.1 between $t = 5 \mu s$ and $t = 76 \mu s$. As with the Saq fit, these points have been mapped to between $t = 0$ and $t = 71 \mu s$ for the fit.

As already noted, the value of C in Equations 12.1 and 12.2 is always zero at $t = 0$. This means that, for all curves in Figure 12.4, the value of C only tracks the closure of RCII that were in the open state at $t = 0$.

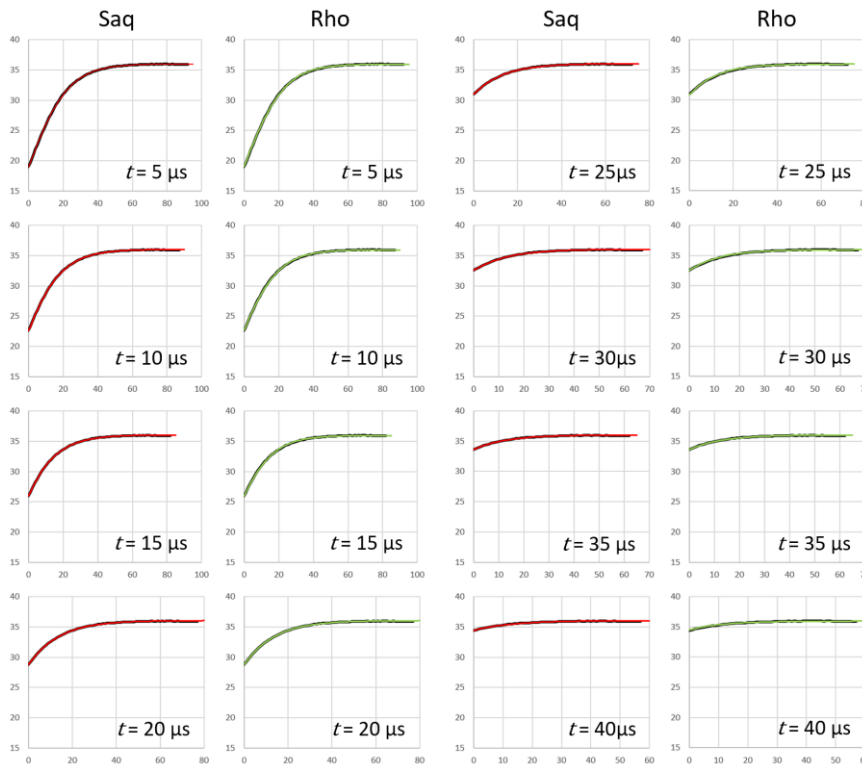


Figure 12.4: ST curve fits to subsets of the ST curve in Figure 12.1. The timestamps on each plot defines the points cropped from the initial ST curve. The red curves within the Saq columns are fits to the remaining raw data points. The green curves within the Rho column are fits to the equivalent section of the Rho ST curve fit from Figure 12.1. The x-axes are all t (μs). The y-axes are all F_t (SU).

The data presented within Figure 12.5 are derived from the Saq and Rho curve fits in Figure 12.4. The plots within **A** show how ρ changes as the starting point for the fit is increased from $t = 0$ to $t = 40 \mu\text{s}$. Within **B**, the same ρ values are plotted against F_q/F_m . The Rho plot shows a linear relationship between these values while the Saq plot deviates significantly from a linear relationship. The plots within **C** show how the differences in ρ derived from the Rho and Saq data impact on the derived values of σ_{PII} .

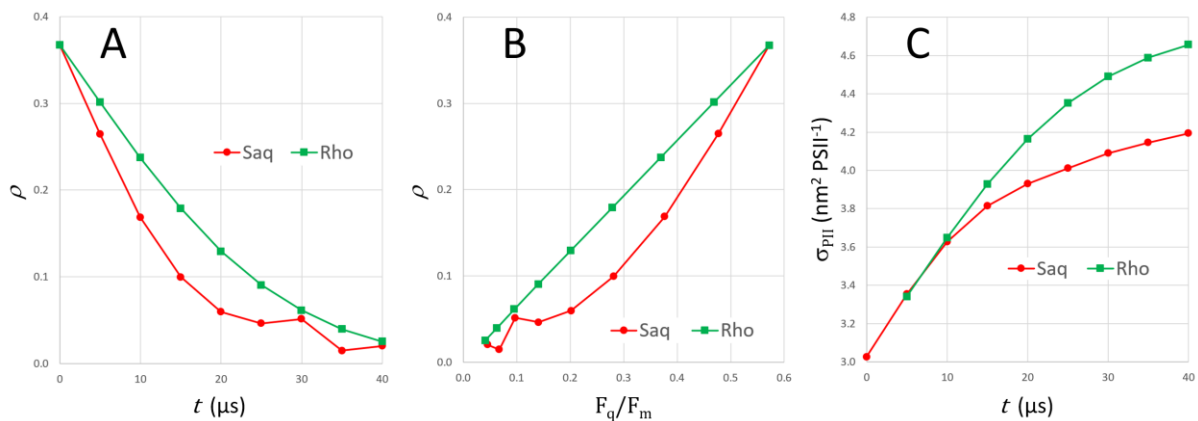


Figure 12.5: Data derived from the curve fits in Figures 12.1 and 12.2. Saq data and Rho fit data were derived for the entire curve with the starting point set between $t = 0$ and $t = 40 \mu\text{s}$. **A** shows ρ changing with t . **B** shows the relationship between ρ and F_q/F_m . **C** shows the change in σ_{PII} , derived from the curve fits.

Figure 12.6 provides additional examples of ρ plotted against F_q/F_m from Saq and Rho data fits. Example **A** is derived from a dark-adapted sample. As such, these values are directly comparable with those in Figure 12.5 **B**. Examples **B** and **C** within Figure 12.6 are from samples adapted to actinic light from the ALED at the values shown.

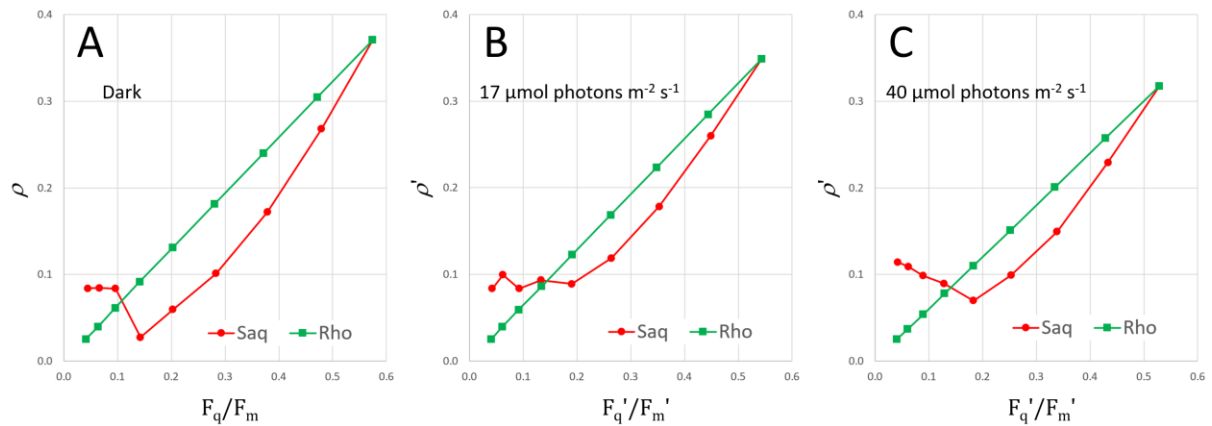


Figure 12.6: Data derived from fits to ST curves using the same fitting process as used for the example in Figure 12.4. Example **A** was dark adapted. Samples **B** and **C** were adapted to the actinic light levels shown.

When viewed in isolation, the non-linearity of the Saq plots in Figure 12.6 could perhaps be written off as a measurement artefact. However, the FLC-derived data presented within Figure 12.7 provide eight examples of a broadly similar relationship between ρ' and F_q'/F_m' with increasing incident photon irradiance. In all eight examples, the decrease in ρ' with increasing actinic light levels is faster than the concurrent decrease in F_q'/F_m' .

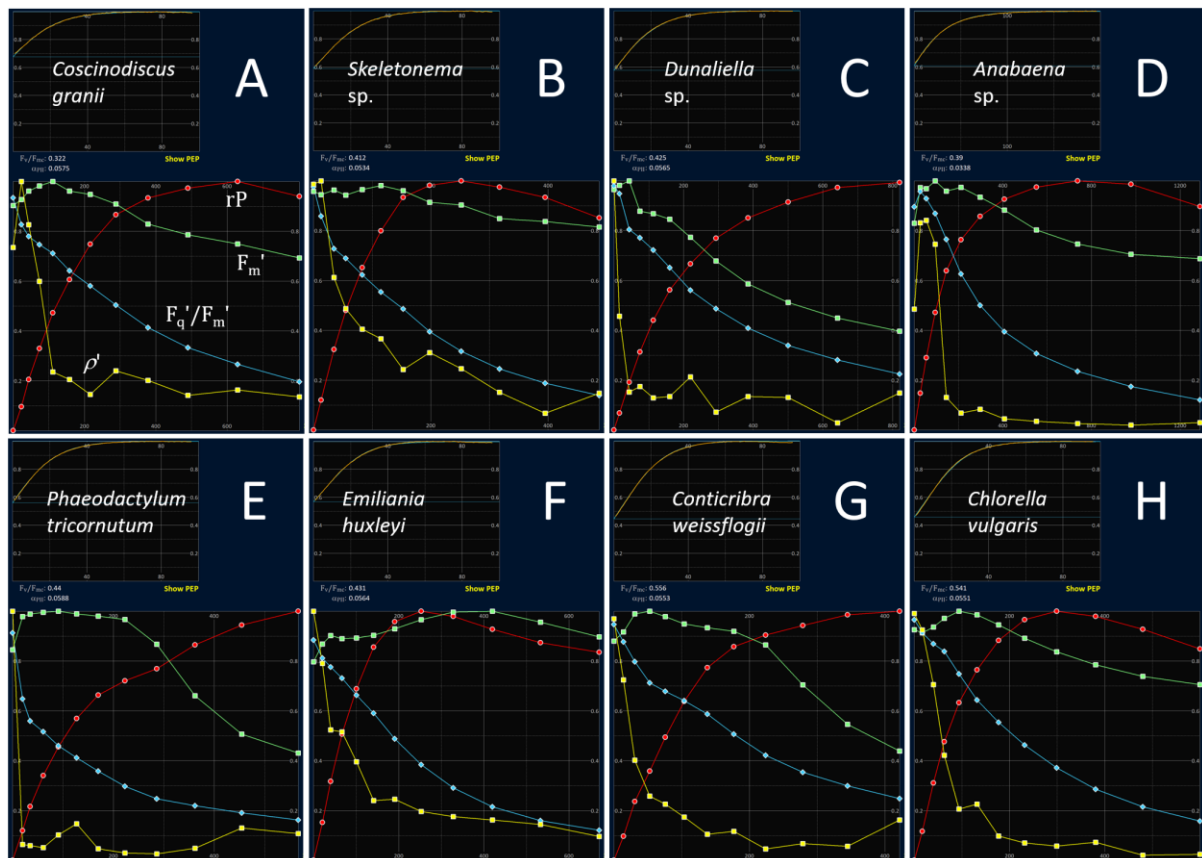


Figure 12.7: Screen shot crops of FLC-derived sample data from cultured cells of the species shown within each crop. The x-axis is incident photon irradiance with units of $\mu\text{mol photons m}^{-2} \text{s}^{-1}$. The ST curve shown within each crop is the first dark-adapted Saq within each dataset. The plot colours code the same parameters within each crop: Red = rP , Green = F_m' , Teal = F_q'/F_m' and Yellow = ρ' , as labelled in **A**.

The plots of F_m' within the examples in Figure 12.7 track non-photochemical quenching due to downregulation. In some examples, most notably **B** and **F**, there is very little change in F_m' during the

FLC. At the other end of the scale, the plots in **C**, **E** and **G** show very significant quenching of F_m' , starting at around E_k .

The homogeneous model defined by Equations 12.1 to 12.4 doesn't distinguish between changes in ρ' and F_q'/F_m' driven by the accumulation of closed RCII or by downregulation. It follows that the model defined by 12.1 to 12.4, while generally providing a convincing fit, can only represent a good approximation of the underlying mechanism.

12.3 Heterogeneity induced by dimerization of PSII

As already noted, it seems likely that dimerization of PSII could be responsible for a high proportion of the connectivity defined by ρ .

See: **The Dimer ST curve fit**

While the Rho fit assumes a homogeneous, imperfect level of connectivity among PSII complexes, the Dimer fit makes three basic assumptions: that the two RCII within the dimer are perfectly connected, that there is no connectivity among dimers and that all dimers are in the oo state (both RCII in the open state) at $t = 0$. Another difference between the Rho and Dimer fits is that while the Rho fit does not include a value for $[Q_A]$ at $t = 0$ in the light-adapted state, the relative proportions of oo, oc and cc dimers at $t = 0$ is fixed through extrapolation from the dark-adapted fit.

Because of the additional constraints imposed by the Dimer fit, SE values for the Dimer fit tend to be higher than for the Rho fit. One feature that is commonly observed is a higher level of sigmoidicity in the early part of a Dimer fit to a dark-adapted sample, compared to either the Rho fit or the actual ST data points (e.g. Figure 12.1). Given the constraints incorporated within the Dimer fit, it is not too surprising that some deviation is observed between the fit and the actual trace. For example, heterogeneity introduced by the combination of PSII α and PSII β (discussed in the next section) is not incorporated within the algorithm.

Figure 12.8 provides an example of how dimerization changes the relationship between F_q/F_v and ρ .

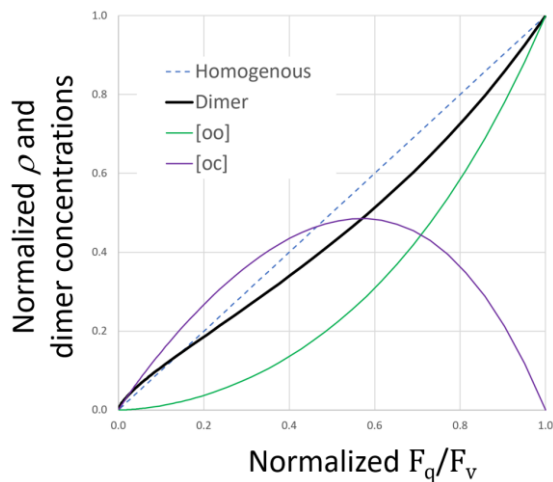


Figure 12.8: Normalized values of F_q/F_v and ρ generated from the dark-adapted ST curve example shown in Figure 12.1. **Homogeneous** shows the linear relationship between F_q/F_v and ρ that is intrinsic to the Rho fit. **Dimer** show the overall level of ρ generated as **[oo]** and **[oc]** change with F_q/F_v . Data have been normalized to the $t = 0$ value for each parameter.

Because the Dimer fit assumes perfect connectivity within each dimer and zero connectivity among dimers, the normalized value of ρ at any point within Figure 12.8 is provided by Equation 12.8.

$$\text{Normalized } \rho = \frac{[\text{oo}]}{[\text{oo}] + [\text{oc}] \cdot 0.5 / (1 - 0.5 \cdot \rho)} \quad \text{Equation 12.8}$$

Tracking the change in normalized Dimer ρ values through the ST curve (from right to left along the x-axis), the shape is defined by a first order decay in **[oo]** accompanied by an increase in **[oc]** driven by closure of one of the two open RCII within an **[oo]** dimer and a decrease in **[oc]** driven by closure of the remaining open RCII. This biphasic change in **[oc]** generates the 'S' shape of the Dimer

curve and may at least partly explain the S_{aq} relationships between F_q/F_v and ρ in B of Figure 12.5 and A of Figure 12.6 and between F_q'/F_v' and ρ' in B and C of Figure 12.6.

12.4 The impact of connectivity on quantification of $[Q_A]$

The data presented within this section show that the value of $[Q_A]$ derived from fluorescence analysis is dependent on the assumed level and type of connectivity among PSII complexes. Assuming either of the two extreme levels of connectivity (the separate package model or lake model) often provides a poor fit to ST data (see Figure 12.2 for examples). If it is assumed that the fit value of ρ or ρ' within Equation 12.5 or 12.6 generates the correct value of $[Q_A]$ then the separate package and lake models generate values for $[Q_A]$ that may be significantly too high or too low respectively.

The examples presented in Figure 12.7 show a more rapid drop in ρ' than F_q'/F_m' with increasing actinic photon irradiance. As discussed above, this difference strongly implies a heterogeneous model of connectivity which can be at least partly explained in terms of dimerization of PSII. Because ρ' generally decreases more rapidly than F_q'/F_m' , the estimate of $[Q_A]$ generated using the measured ρ' value within Equation 12.6 will approach the separate package value generated by F_q'/F_v' with increasing actinic photon irradiance. As a consequence, it seems reasonable to suggest that use of F_q'/F_v' within Equations 11.8 and 11.14 is likely to generate an overestimate of $[Q_A]$ at low actinic photon irradiance but reasonably accurate values at E_k and above. In contrast, the lake model values of $[Q_A]$ generated by qL are likely to underestimate values of $[Q_A]$ through the entire curve with the largest errors being generated at around E_k .

13 Photochemical Excitation Profile (PEP)

The main value of PEP data is to facilitate spectral correction of J_{PII} , JV_{PII} and GO_{PII} . The two PEPs incorporate values of F_V and σ_{PII} generated by different combinations of MLED channels. For the F_V PEP, the reported values are relative photon yield (relative values of fluorescence generated per incident photon). The reported σ_{PII} PEP values have nominal standard units of $\text{nm}^2 \text{PSII}^{-1}$. As discussed within this section, correction of a spectrally heterogeneous sample using the σ_{PII} PEP can generate large errors. In contrast, correction using the F_V PEP is highly tolerant of spectral heterogeneity within the sample.

13.1 Excitation wavebands for the PEP

STAF setup

Auto LED: Active

Target α_{PII} : 0.056

416 nm: 0

452 nm: 0.72

452 nm: 0.72

473 nm: 0

495 nm: 0

534 nm: 0

594 nm: 0

622 nm: 0

Total E_{ST} : 1.44

The labelling of the eight LabSTAF MLED channels within LabSTAF is as shown in this screenshot crop from the RunSTAF home screen. As part of the LabSTAF calibration, the emission spectra for all eight MLED channels and the ALED channel are recorded from within the sample chamber and stored at 1 nm resolution within the scs calibration file for the attached LabSTAF. The two 452 nm channels are combined into a single waveband. PEP data are processed using the wavelength of the measured emission peak for each MLED waveband in preference to the channel name values.

See: [LabSTAF calibration](#)

Figures 13.1 and 13.2 show a completed PEP, cropped from the home screen, with the option to show the Spectral Correction Spectra (**Show SCS**) option inactive and active respectively.

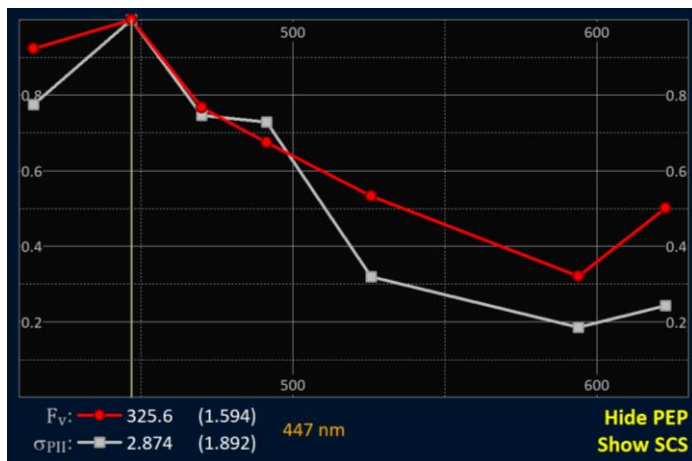


Figure 13.1: A completed PEP recorded from cultured cells of *Conticribra weissflogii* with the **Show SCS** option inactive. The 447 nm label in orange text defines the central wavelength for this waveband as measured during calibration.

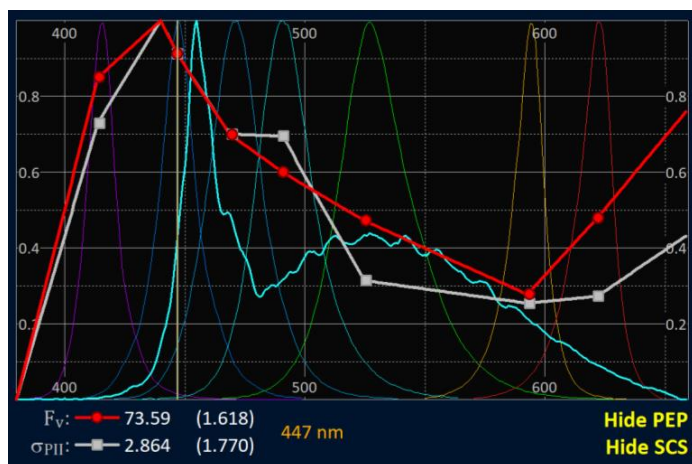


Figure 13.2: A completed PEP recorded from cultured cells of *Conticribra weissflogii* with the **Show SCS** option active. The extrapolations to virtual points (at 380 nm, 440 nm and 660 nm) within these plots are discussed within this section.

13.2 The PEP protocols

The PEP function generates three reps of seven waveband combinations. With the default settings, RunSTAF cycles through all seven waveband combinations at approximately 1 Hz. A user-defined number of Seqs are averaged within each rep. The number of Seqs averaged per PEP rep (Seq_{PEP}) is defined by Equation 13.1.

$$Seq_{PEP} = (Seq / Acq) \times (Acq / Saq) \times 2 \quad \text{Equation 13.1}$$

Where (Seq / Acq) and (Acq / Saq) are as set under **STAF setup** on the home screen.

There are currently two protocol options for generating a PEP. The default option is run if the two 452 nm MLED channels are the only ones with a non-zero value under **STAF setup**. This option (PEP-bc) is optimised for samples that are dominated by phytoplankton incorporating chlorophylls *b* or *c* as the main light harvesting pigments.

The second option (PEP-cy) is run for any other combination of MLED channels (other than just the two 452 nm channels) and is primarily intended for samples that are dominated by cyanobacteria incorporating phycobilins as the main light harvesting pigments. Table 12.1 shows the LED combinations at each step of the PEP within the PEP-bc and PEP-cy protocols. For mixed samples, PEP-bc is usually the best option.

Step	PEP-bc active channels (nm)	PEP-cy active channels (nm)
1	1 st 452 nm + 416 nm	534 nm + 622 nm + 416 nm
2	1 st 452 nm + 2 nd 452 nm	534 nm + 622 nm + 2 nd 452 nm
3	1 st 452 nm + 473 nm	534 nm + 622 nm + 473 nm
4	1 st 452 nm + 495 nm	534 nm + 622 nm + 495 nm
5	1 st 452 nm + 2 nd 452 nm + 534 nm	534 nm + 622 nm
6	1 st 452 nm + 2 nd 452 nm + 594 nm	534 nm + 622 nm + 594 nm
7	1 st 452 nm + 2 nd 452 nm + 622 nm	622 nm

Table 13.1: The waveband combinations used for the PEP-bc and PEP-cy functions implemented through RunSTAF. The system cycles through all seven steps repeatedly until the programmed level of signal averaging has been reached. Typically, each loop through all seven steps takes approximately one second.

For PEP-bc, the 1st 452 nm channel is as set by the Auto LED function while the 2nd 452 nm channel is attenuated to 72% of the optimum value generated during the Auto LED function. The 416 nm and 473 nm channels are both set as close as possible to the E_{ST} output for the 1st 452 nm channel. The remaining channels (534 nm, 594 nm and 622 nm) are set to maximum output.

For PEP-cy, all seven MLED channels used are set to maximum output.

Gorbunov et al. (2020) recently described a method for physiological and taxonomic analysis of phytoplankton communities. Within this study, a mini-FIRE fluorometer was used to provide ST pulses from six independent measuring LED wavebands centred at 435, 450, 470, 500, 530 and 590 nm. Most of the experimental work was focussed on species within four major eukaryotic phytoplankton groups: diatoms, dinoflagellates, green algae and haptophytes. All four of these groups incorporate chlorophyll *b* or *c* as a PSII light harvesting pigment.

To generate reliable spectral data from ST measurements, three parameters are required from each individual measurement: F_o , F_m and σ_{PII} . The accuracy of F_m and σ_{PII} is dependent on a high proportion of the photochemically active RCII in the open state at the start of the ST pulse being closed by the end of the pulse. The σ_{PII} values for diatoms, dinoflagellates, green algae and haptophytes tend to be much lower between 500 and 590 nm than they are between 435 and 470

nm. For example, σ_{PII} values at 590 nm are approximately 25% of values at 435 and 450 nm. It follows that you need to deliver approximately four times as many photons from measuring LEDs at 590 nm, compared to 450 nm, in order to close the same proportion of RCIs within the same timeframe.

Within the study conducted by Gorbunov et al. (2020) the required level of saturation at 530 and 590 nm was achieved through a combination of higher photon irradiances and longer ST pulses than were used with the shorter wavebands (150 μ s for the 530 and 590 nm wavebands, compared with 80 μ s for the 435 and 450 nm wavebands). With the PEP function incorporated within RunSTAF, the ST pulse duration is the same for all wavebands and the required level of saturation is reached by combining wavebands (Table 13.1).

Table 13.2 provides a comparison of the maximum measuring LED output for the seven wavebands incorporated within LabSTAF and the nearest equivalent wavebands used within Gorbunov et al. (2020).

Waveband central λ (nm)	Maximum photon irradiance (typical) μ mol photons $m^{-2} s^{-1}$ [photons $nm^{-2} (100 \mu s)^{-1}$]	Gorbunov et al. (2020) μ mol photons $m^{-2} s^{-1}$
416	13,851 [0.834]	20,000 – 25,000 for each waveband between 435 and 505 nm
452 x 2	34,047 [2.051]	
473	16,574 [0.998]	
495	10,142 [0.611]	
534	9267 [0.558]	40,000 – 60,000 for the 530 and 590 nm wavebands
594	2500 [0.151]	
622	8206 [0.494]	NA

Table 13.2: The maximum photon irradiance provided by the measuring LED wavebands incorporated within LabSTAF and those used by Gorbunov et al. (2020). The 452 nm photon irradiance is the sum of both channels.

A central feature of the PEP method is determination of waveband-specific photon yield of F_v , and σ_{PII} values by combining different wavebands to reach saturation. For the PEP-bc option, the 452 nm waveband is incorporated within all seven waveband combinations. Because σ_{PII} is high at 452 nm for the four major eukaryotic phytoplankton groups, its incorporation provides saturation with all waveband combinations within PEP-bc. Step 2 of PEP-bc in Table 13.1 provides direct 452 nm-specific values of the photon yield of F_v , and σ_{PII} . Values of these parameters for the other wavebands are then calculated as the difference between the 452 nm-specific values and the values measured using the waveband combinations listed in the PEP-bc column of Table 12.1.

Automated optimisation of MLED intensity is incorporated within the PEP procedure. With PEP-cy, achieving saturation is more challenging than with PEP-bc and often requires increasing the duration of the ST pulse from the default of 100 μ s.

13.3 Checking PEP saturation

Figure 13.3 provides two example PEP plots from a freshwater chlorophyte (*Chlorella vulgaris*) and a freshwater cyanobacterium (*Anabaena* sp.). Although there is a reasonable match between the F_v and σ_{PII} traces within each example, there are also some highly reproducible differences.

Also included within this figure are the ST traces generated by the PEP protocol. These data are not shown within RunSTAF but can be accessed through the **Clipboard → PEP data** option on the RunSTAF menu. The ST traces all show good saturation for all waveband combinations. For

Anabaena sp., the ST pulse duration has been increased from the default of 100 μ s to 200 μ s to ensure good saturation.

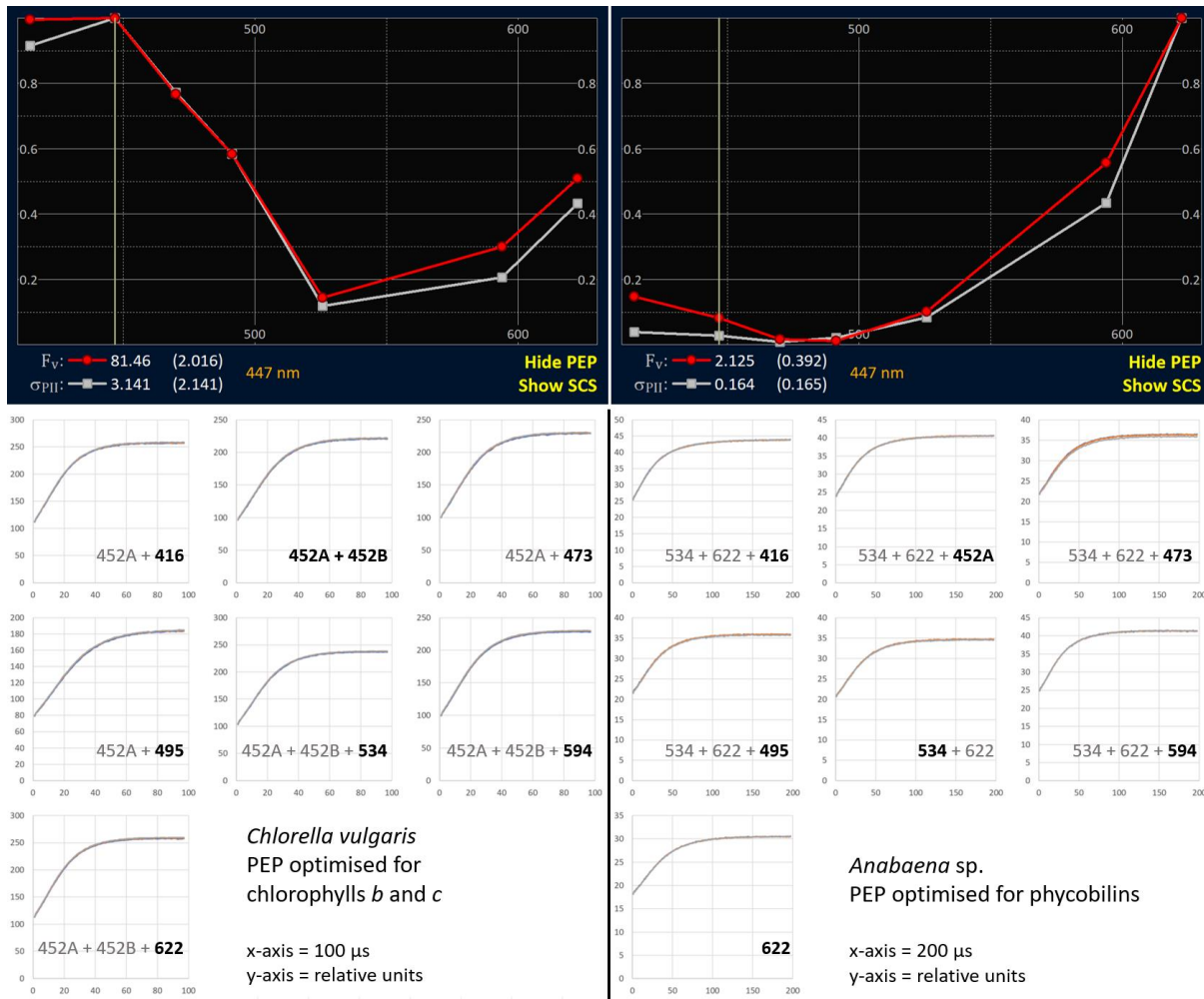


Figure 13.3: Sample PEPs optimised for chlorophylls *b* and *c* (PEP-bc) or for phycobilins (PEP-cy). The waveband evaluated by each ST pulse is shown in bold.

13.4 The impact of heterogeneity on PEP data

Figure 13.4 shows five PEP screen crops from each of three different phytoplankton cultures. The F_v and σ_{PII} values are both plotted on a scale that goes from zero to one. For spectra with all values greater than zero, points are normalized to the highest value. For plots with one or more negative values, the entire range is rescaled to between zero and one.

The PEPs in the first set (Figure 13.4, **A1 – A5**) were recorded from samples of *C. vulgaris* (CCAP 211/11B), using the PEP-bc protocol. In all cases, all points shown within the F_v and σ_{PII} PEPs are greater than zero and the highest values are at the 452 nm waveband. This is because all points within each PEP have been normalized to the value at this waveband. Although the F_v and σ_{PII} PEPs are closely matched overall, it is worth noting that the normalised σ_{PII} values are consistently lower than normalised values for F_v at 416 nm and 622 nm.

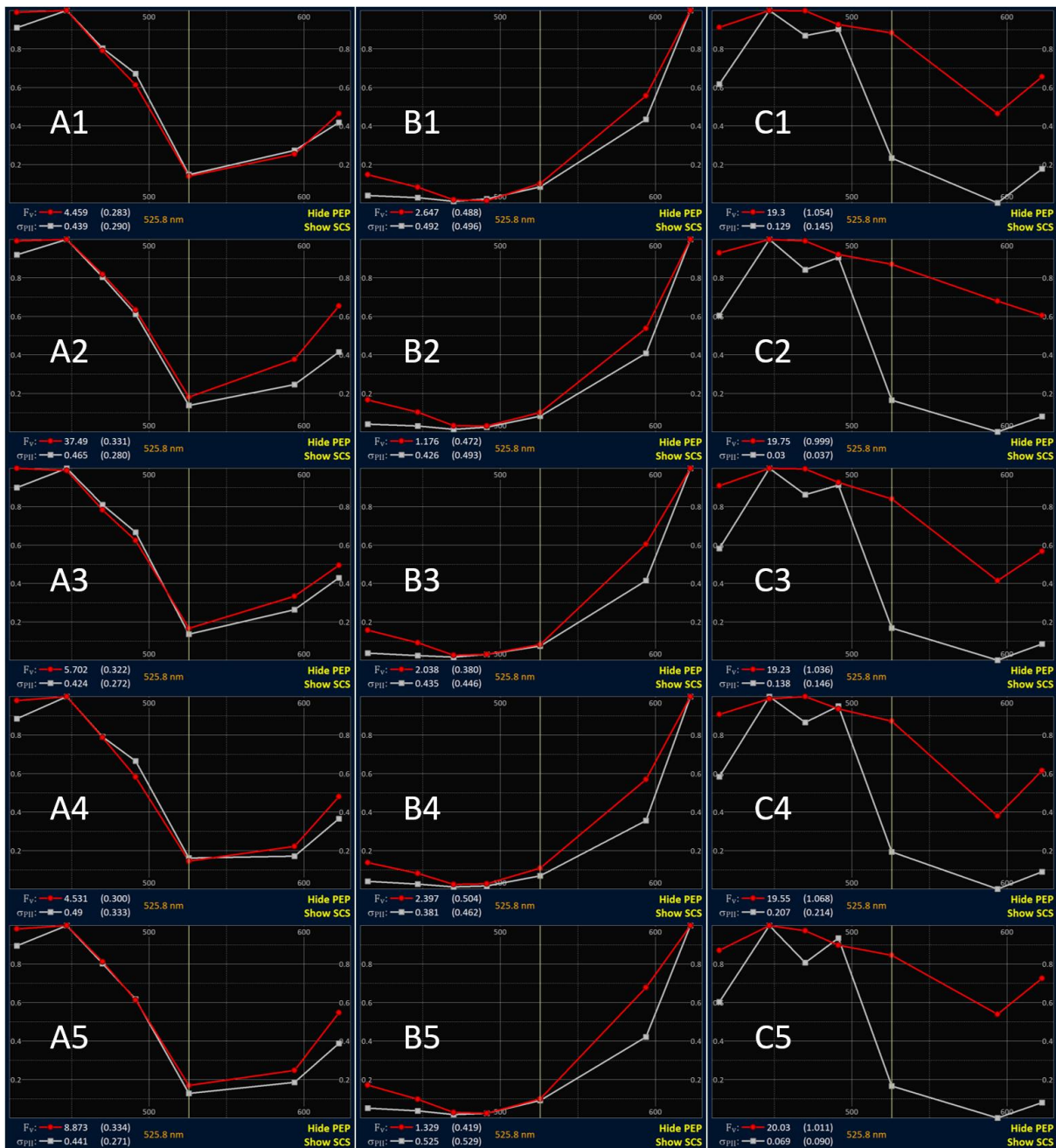


Figure 13.4: Sets of five PEPs from three phytoplankton species. **A1 – A5** are from *Chlorella vulgaris*. **B1 – B5** are from *Anabaena* sp. **C1 – C5** are from *Alexandrium catenella*.

For a completely homogeneous population of PSII_s, $F_v \cdot \sigma_{PII}$ should be constant across all wavebands. However, there is scope for F_v and σ_{PII} to diverge where some form of heterogeneity exists within the sample at the level of PSII light harvesting. One documented heterogeneity of this type within chlorophytes is the division between PSII α and PSII β (Andr e, Weis and Krieger, 1998; Black, Brearley and Horton, 1986; Guenther and Melis, 1990; de Marchin et al. 2014). PSII β are less numerous than PSII α , have a much smaller light harvesting complex and a higher ratio of chlorophyll *a* to chlorophyll *b*. In combination, these characteristics have the potential to account for the divergence between F_v and σ_{PII} at the 416 nm and 622 nm wavebands. Within the proposed model, the reported F_v at each waveband is the sum of the signals from PSII α and PSII β . In contrast, σ_{PII} is much lower for PSII β than PSII α , because the PSII β light harvesting complex is much smaller than the PSII α light harvesting complex. As a consequence, the measured values of σ_{PII} for PSII α plus PSII β are lower than for PSII α alone. Because PSII β have a higher chlorophyll *a* to chlorophyll *b* ratio than

PSII α , the PSII β -dependent decrease in σ_{PII} is more evident at the 416 nm and 622 nm wavebands because absorption by chlorophyll *a* relative to chlorophyll *b* is highest at these points.

The PEPs in the second set (Figure 13.4, **B1 – B5**) were recorded from samples of *Anabaena* sp. (CCAP 1403/13A), using PEP-cy. As with the *C. vulgaris* set, all points within the F_v and σ_{PII} PEPs are greater than zero. The F_v and σ_{PII} PEPs are both normalized to the 622 nm waveband.

Within all of the *Anabaena* sp. plots, the normalized values of F_v are consistently higher than the normalized values of σ_{PII} values at the 416 nm, 452 nm, 534 nm and 594 nm wavebands. The PSII light harvesting system within *Anabaena* sp. comprises a relatively small compliment of chlorophylls *a* within each PSII core complex plus phycocyanin and allophycocyanin within phycobilisomes. It follows that the heterogeneity causing divergence between F_v and σ_{PII} values at 416 nm and 452 nm may simply be between PSII complexes that are energetically connected to phycobilisomes and PSII complexes that are not. Within this model the phycobilisome-connected PSII complexes would generate much higher σ_{PII} and F_v in the red (594 nm and 622 nm) than in the blue (416 nm and 452 nm). For the disconnected PSII complexes, σ_{PII} and F_v would both be higher in the blue than in the red. Because F_v is additive, the disconnected PSII complexes increase the overall signal within the blue but do not contribute significantly in the red. In contrast, the phycobilisome-connected and disconnected PSII complexes would have very similar σ_{PII} values in the blue while σ_{PII} values in the red would be almost entirely attributable to the phycobilisome-connected PSII complexes. As a consequence, the σ_{PII} PEP is likely to be representative of the phycobilisome-connected PSII complexes while the F_v PEP provides a more accurate assessment of the complete PSII population within the sample.

The PEPs in the third set (Figure 12.4, **C1 – C5**) were recorded from samples of a marine dinoflagellate, *Alexandrium catenella* (CCAP 1119/17), using the PEP-bc protocol. Of the three examples, this one shows the greatest divergence between the normalized F_v and σ_{PII} values. As with *C. vulgaris*, the highest values for F_v and σ_{PII} are at the 452 nm waveband and both PEPs are normalised to this point. As with both *C. vulgaris* and *Anabaena* sp., the normalized σ_{PII} value is lower than F_v at the 416 nm waveband. The PEP-bc protocol was used for this set because *A. catenella* incorporates chlorophyll *c* as a PSII light harvesting pigment. Because the PEP-bc protocol was used, any PSII complexes within the sample that rely on longer wavelength light harvesting pigments, such as phycocyanin and allophycocyanin, are unlikely to have been saturated. This could be an issue here because the greatest divergence between F_v and σ_{PII} occurs at the three longest wavebands. This divergence at the three longest wavebands may indicate that the samples used were contaminated with cryptophytes and/or cyanobacteria or that the cells of *A. catenella* incorporate cyanobacteria cells as symbionts (e.g. Nakayama et al. 2019).

13.5 Scaling PEP data

The data presented within Figure 13.5 are derived from the same datasets as presented in Figure 13.4. The left columns show the standard F_v PEP and σ_{PII} PEP values. The values in the right columns are normalized to the ALED F_v and σ_{PII} values.

Normalizing F_v PEP data to the ALED F_v values neutralizes the impact of differences in cell density between reps. Although the expectation is for σ_{PII} to be independent of cell density, normalizing to ALED values of σ_{PII} has brought rep values closer together for all three species.

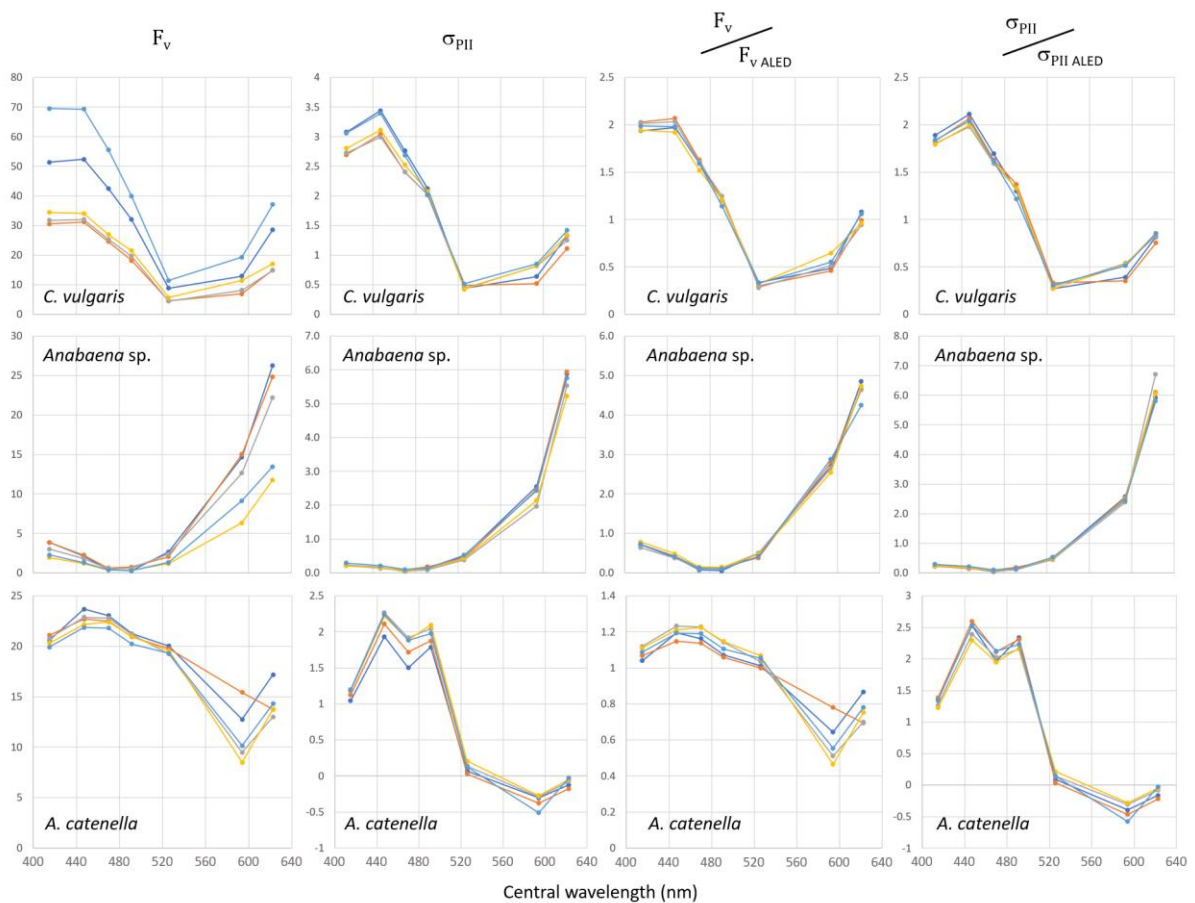


Figure 13.5: Data derived from the PEPs shown in Figure 13.4. The leftmost column shows F_v PEP values on the SU scale. The next column from the left shows σ_{PII} PEP values with units of $\text{nm}^2 \text{PSII}^{-1}$. The two remaining columns show the F_v PEP and σ_{PII} PEP values normalized to the ALED F_v and σ_{PII} values.

Figure 13.6 shows a representative single PEP plus dark ST pulse combination from each of ten species of phytoplankton, including the three species represented in Figures 13.4 and 13.5. Multiple reps (minimum of three) from each culture exhibited the same relationship between the F_v PEP and σ_{PII} PEP as shown within these examples.

Examples **A** to **E** within Figure 13.6 are all diatoms. Both the F_v and σ_{PII} PEPs for **A**, **B** and **C** are very similar to each other in shape and significantly different from the non-diatom examples provided by **F** to **J**. The σ_{PII} PEPs for **D** and **E** show a slightly different shape to **A**, **B** and **C** in that the 495 nm channel is relatively high and the 534 nm channel is relatively low. The 416 nm channel is also noticeably lower for **E**. Within **D** and **E**, there are clearer gaps between the F_v and σ_{PII} PEPs than are evident within **A**, **B** and **C**. This may indicate the presence of one or more additional phytoplankton species within these cultures. It is noticeable that the relative shapes of the F_v and σ_{PII} PEPs in the example for the large diatom, *C. granii* (**E**) is similar to the dinoflagellate, *A. catenella* (**J**).

Most of the σ_{PII} PEP data within Figure 13.6 are consistent with the spectra presented by Gorbunov et al. (2020). The two notable differences are with *C. granii* and *A. catenella*. In both cases, it seems reasonable to suggest that the cultures may be contaminated by at least one additional species with a significantly different spectral profile.

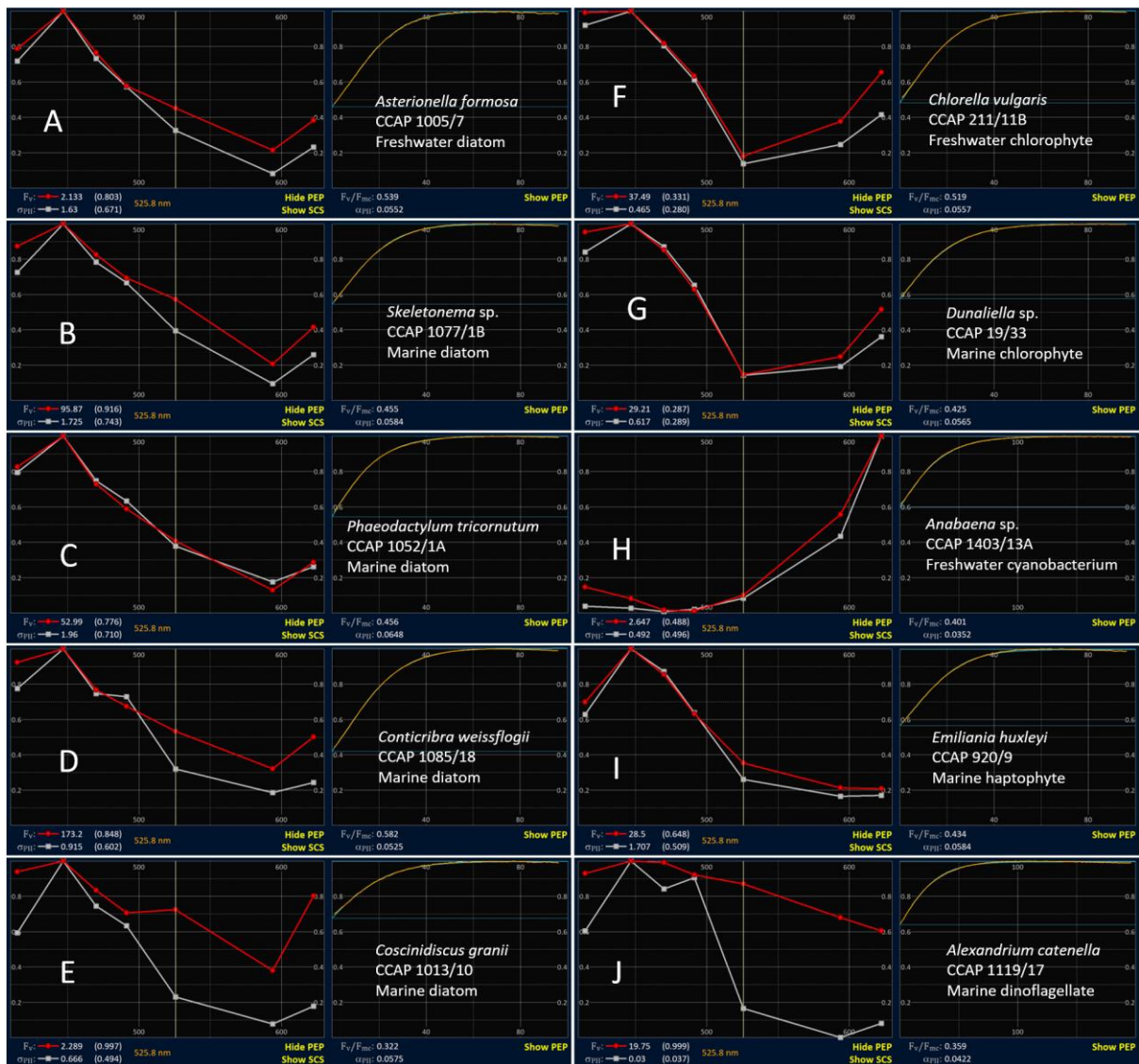


Figure 13.6: Representative PEP plus ST pulse for each of ten phytoplankton species. All samples are from cultures grown at 15 °C on a 16h/8h day/night cycle. Incident photon irradiance (white light) was 50 $\mu\text{mol photons m}^{-2} \text{s}^{-1}$ for A to E and I, 120 $\mu\text{mol photons m}^{-2} \text{s}^{-1}$ for F and G and 80 $\mu\text{mol photons m}^{-2} \text{s}^{-1}$ for H and J.

Although the examples presented within Figures 13.6 provide a very limited dataset, it seems reasonable to conclude that combining F_v PEP data and σ_{PII} PEP data is likely to add significantly to the information provided by either data set alone.

13.6 Using PEP data to apply a Spectral Profile Correction (SPC)

The target range for application of a SPC is between 380 nm and 660 nm which requires extrapolation beyond the spectral range of the PEP at each end. Figure 13.7 shows the extrapolations made to generate the SPCs from PEP data for the ten species shown in Figure 13.6.

To complete the PEP spectral range, the following extrapolations are implemented:

1. A straight line is applied between the 416 nm waveband point and zero at 380 nm
2. The slope of the line between the 473 nm waveband point and the 452 nm waveband point is extrapolated to 440 nm (the absorption peak of chlorophyll *a* within this region)
3. A straight line connection is drawn between the derived 440 nm point and the measured 416 nm point

- The slope of the line between the 594 nm waveband point and the 622 nm waveband point is used to extrapolate to 660 nm

Extrapolation 1 has minimal impact on the SPC, simply because the actinic light emits very little between 380 and 416 nm. The other three extrapolations do have a small impact on the SPC.

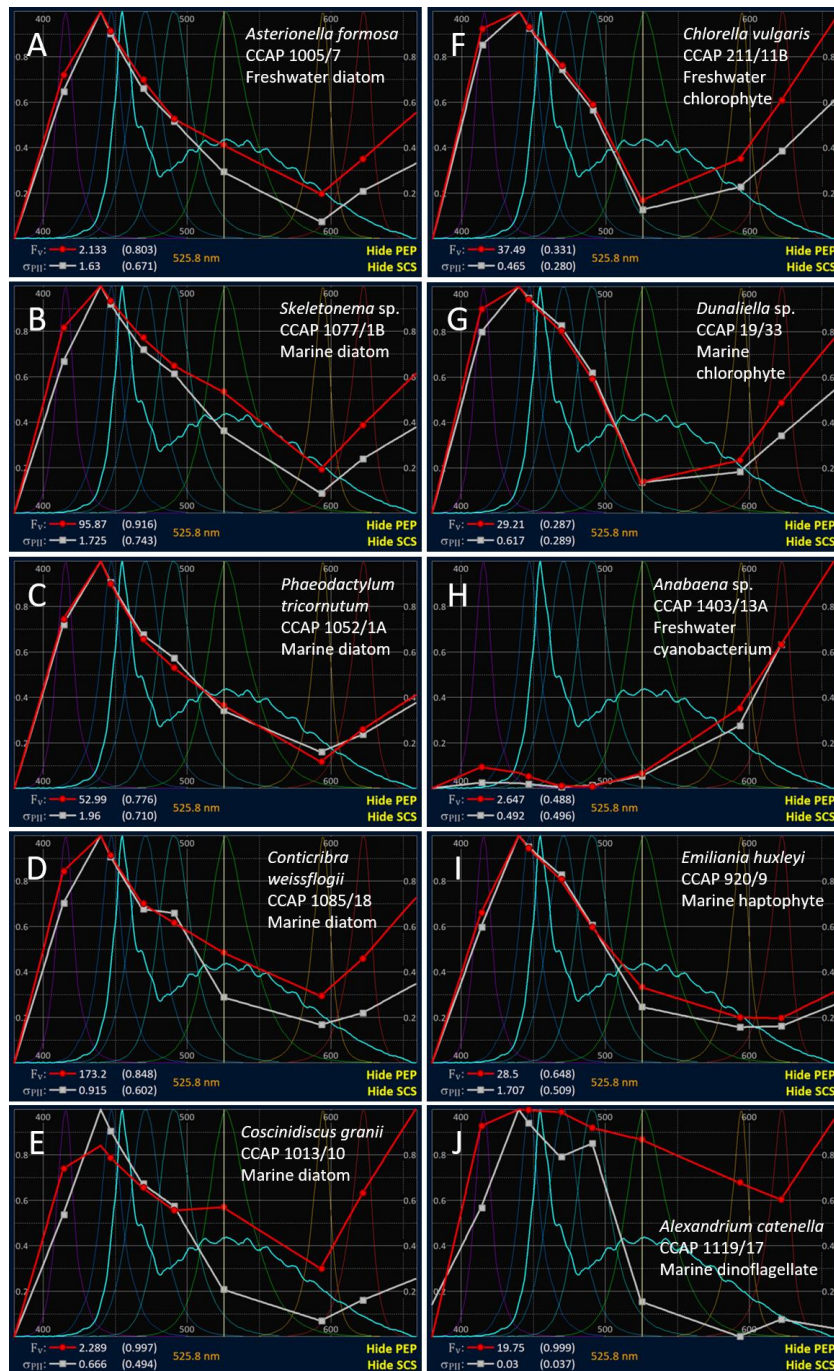


Figure 13.7: Representative PEP data plots with Spectral Correction Spectra (SCS) activated. All examples are the same as presented within Figure 13.6.

These extrapolations are based on comparisons made between PEP data and high resolution Fluorescence Excitation Spectra (FES). Figure 13.8 provides some comparisons between FES data generated from four phytoplankton species during the study by Silsbe et al. (2015) and RunSTAF-generated SPC data. The paired species within each plot have been selected to provide the best

available match of light harvesting pigments. In examples **A**, **B** and **C**, the main PSII light harvesting pigments are chlorophylls *a* and *c*. In example **D**, both species incorporate chlorophylls *a* and *b*.

In assessing the differences between the spectra within each plot, it is important to note that while the F_v data used to generate the SPC plot are exclusively from functional PSII complexes, the F_m data used to generate the FES plots potentially include fluorescence from photoinactivated PSII and other sources. One clear objective for future work is to generate FES and SPC data from the same samples.

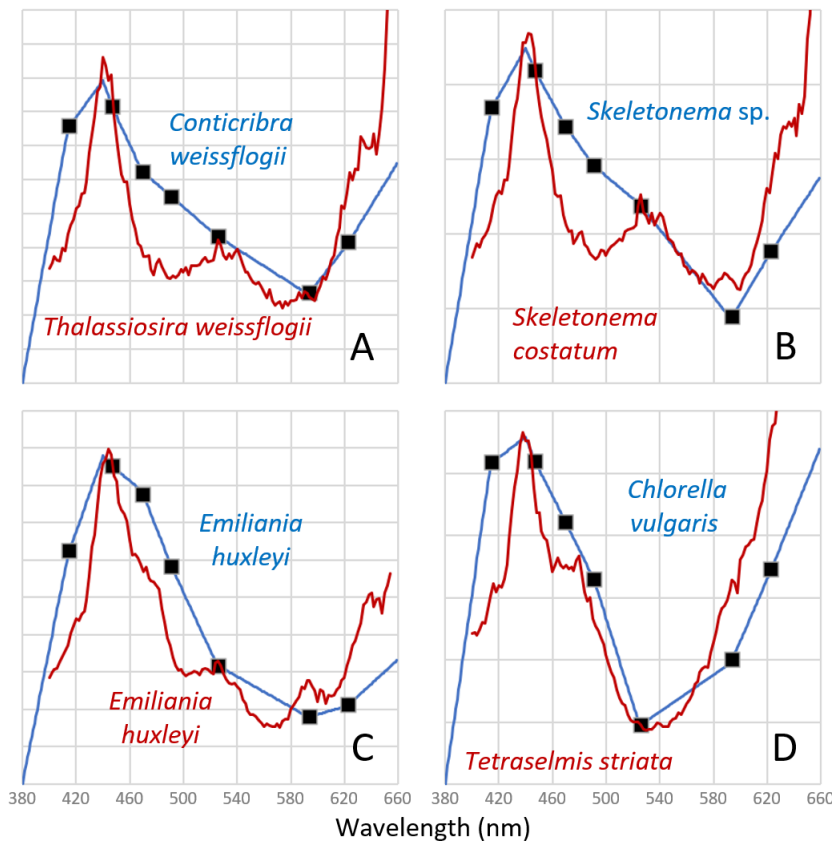


Figure 13.8: The Fluorescence Excitation Spectra (FES) traces are from Silsbe et al. (2015). The SPC traces were extracted from recent LabSTAF data.

It is possible that implementation of the SPC will undergo modifications in future, as more data become available. The logging of primary STAF data within RunSTAF files makes it possible to rapidly apply updates of this kind across large datasets.

13.7 Derivation of PEP values

As already noted, the values of F_v and σ_{PII} for each waveband within each PEP are calculated through simple subtraction. For the PEP-bc values, Step 2 (the 452 nm only waveband) provides the subtracted value for the other six wavebands. An intensity correction is applied to the subtracted 452 nm value for Steps 1, 3 and 4 (the 416 nm, 473 and 495 nm wavebands, respectively) to account for the use of only one of the two 452 nm channels. For the PEP-cy values, Step 5 (the 534 nm plus 622 nm wavebands) provide the subtracted value for Steps 1, 2, 3, 4 and 6 (wavebands 416 nm, 452 nm, 473 nm, 495 nm and 594 nm, respectively). Step 7 then provides the subtracted value for the 534 waveband.

As an alternative to the simple subtraction of F_v and σ_{PII} values derived from the ST curve fits, it is feasible to subtract one curve from another and apply a fit to the difference. The data in Figure 13.9 provide an example of this approach.

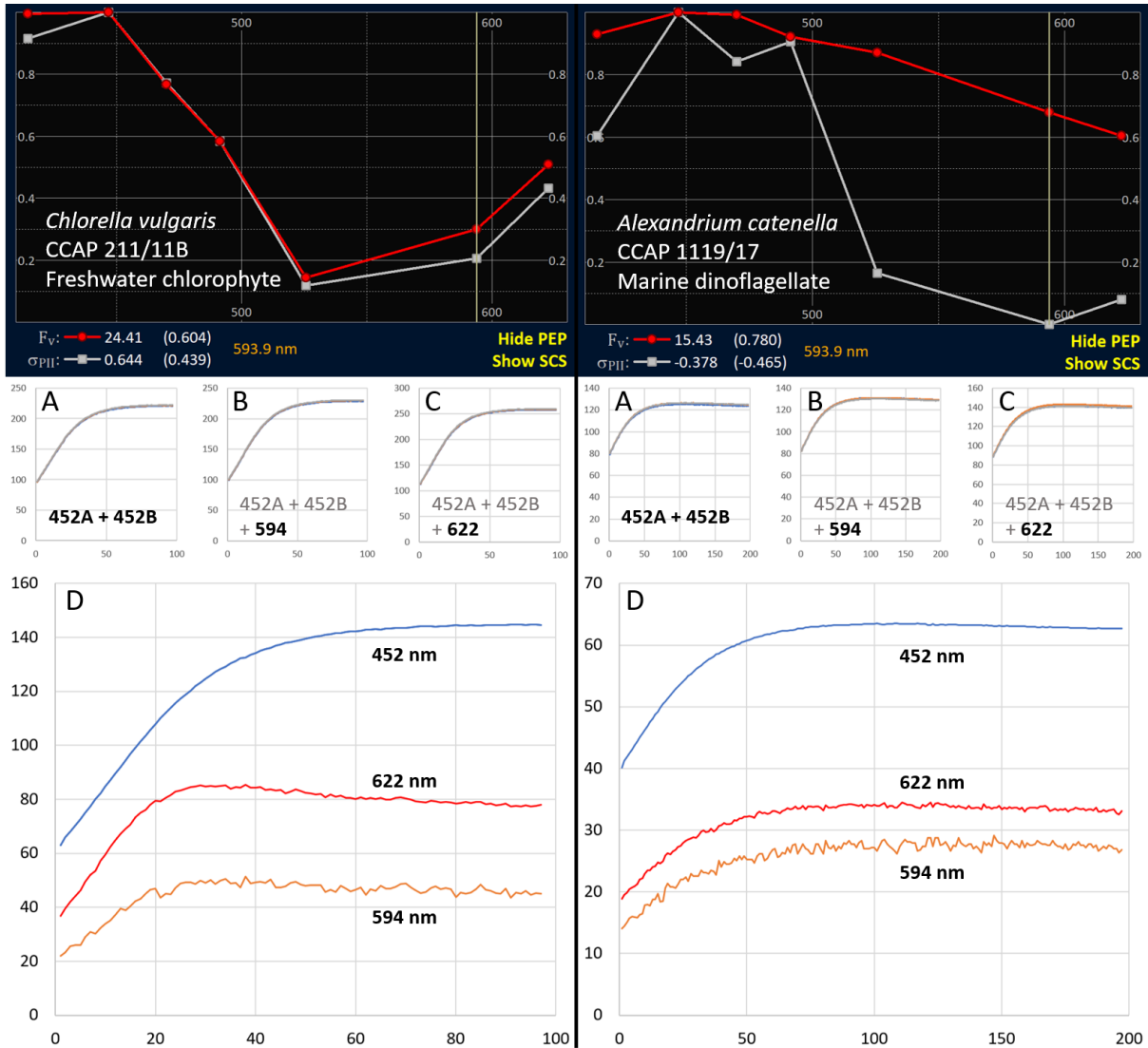


Figure 13.9: PEP data from cultured cells of *C. vulgaris* (left) and *A. catenella* (right) acquired using PEP-bc. The ST traces within **A**, **B** and **C** for each culture are the three reps used for evaluation of the 452 nm, 594 nm and 622 nm wavebands. The ST traces within **D** for each culture show average traces for **A** (452 nm), **B** minus **A** (594 nm) and **C** minus **A** (622 nm) normalized to the appropriate E_{ST} value.

Plots **A**, **B** and **C** of Figure 12.8 show the three ST trace reps for the 452 nm, 594 nm and 622 nm waveband evaluations for the two cultures. Note that these are the primary data incorporated within the Clipboard output and are not normalized to E_{ST} values. In all cases, the noise level is low enough and the degree of saturation high enough to be confident of the σ_{PII} , F_o and F_m values derived from the fits.

The traces in the **D** plots of Figure 13.8 are derived from the average of the three reps in each of **A**, **B** and **C** and are all normalized to the appropriate E_{ST} values. The **452 nm** trace is simply the average of the three reps in **A** normalized to E_{ST} values from the 452A plus 452B channels. The **594 nm** and **622 nm** traces are the average of the traces in **B** or **C** respectively minus the average of **A**, normalized to E_{ST} values for the 594 or 622 channel respectively.

For *C. vulgaris*, the highest fluorescence values within the normalized 594 nm and 622 nm traces are at around 30 μ s. In both cases, these values are approximately 8% higher than the end point of each trace. If these high point values were taken as F_m , the values of F_v would be assessed as 10 to 20% higher than the values calculated in the normal way. In contrast to the normalized 594 nm and 622

nm traces within **D** of *C. vulgaris*, the equivalent traces for *A. catenella* show a similar 'shape' to the 452 nm trace.

The simplest interpretation of the 594 nm and 622 nm traces within plots **D** for both cultures is that they quantify the increase in fluorescence induced by addition of the 594 or 622 channel respectively to the 452A and 452B channels. In the case of *C. vulgaris*, this is almost certainly not the case. A more likely explanation is that the rise to the 30 μ s peak seen in both traces is due to connectivity between PSII complexes such that addition of the 594 nm or 622 nm waveband increases the rate at which the 452 nm waveband closes RCII during the early part of the curve.

In contrast to the example of *C. vulgaris*, where the F_v and σ_{PII} PEPs are closely matched through the entire range, the F_v and σ_{PII} PEPs from *A. catenella* diverge widely within the spectral range that incorporates the 594 nm and 622 nm traces. Earlier in this section, this divergence was attributed to the presence of two populations of PSII complexes within the sample that are spectrally very different from each other: the assumption being that one population is intrinsic to *A. catenella* and the other to a separate symbiotic or contaminating species. This explanation is supported by the similarity of the shape of all three ST traces in the **D** plot for *A. catenella* which is most easily understood in the context of a lack of connectivity between one population of PSII complexes dominating absorption at 452 nm and the other population of PSII complexes dominating absorption at 594 nm and 622 nm.

13.8 Which PEP should be used for SPC?

From the data presented within this section, it seems reasonable to conclude that the F_v PEP provides a more reliable spectral correction than the σ_{PII} PEP. A potential limitation to the accuracy of the F_v PEP is that the value for each waveband is dependent on the F_m asymptote being determined correctly by the fitting process. For samples with closely matched F_v and σ_{PII} PEPs, visual inspection of the ST data is likely to provide a reliable check on the asymptote being reached. For samples exhibiting significant differences between the F_v and σ_{PII} PEPs, it is conceivable that a small error could be introduced by one sub population of PSII complexes with high σ_{PII} at a specific combination of wavebands masking the presence of a second sub population with a low σ_{PII} at the same combination of wavebands.

The main value of extracting both F_v and σ_{PII} PEPs is for qualitative assessment of heterogeneity within a sample. In addition to providing a basic assessment of community structure within natural samples and contamination of cultures, comparison of F_v and σ_{PII} PEPs also have potential for monitoring dynamic changes in community structure, as might occur during bloom development.

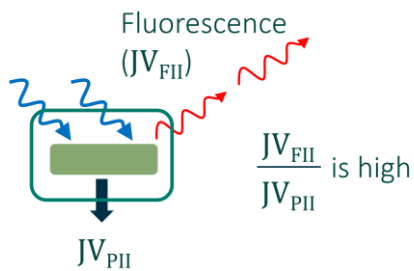
14 Package Effect Correction (PEC)

When using the absorption method to derive values for JV_{PII} , measurement accuracy is highly dependent on there being a consistent ratio between photons used to drive photochemistry and photons emitted as fluorescence (i.e. the ratio between JV_{PII} and JV_{FII} must be consistent). The package effect can have a very significant impact on this ratio.

The package effect is largely a consequence of the high concentration of chlorophyll *a* and other light-absorbing pigments within phytoplankton cells. To put this in context, while the concentration of chlorophyll *a* within the open ocean is often below 0.1 mg m⁻³, the concentration within phytoplankton cells is approximately a million times higher than this, at 0.1 kg m⁻³ (calculated from data within Montagnes et al., 1994). It follows that while sea water with phytoplankton cells suspended within it can be considered optically thin, the localized volume within each phytoplankton cell is optically very thick (see Boatman, Geider and Oxborough, 2019 and references therein).

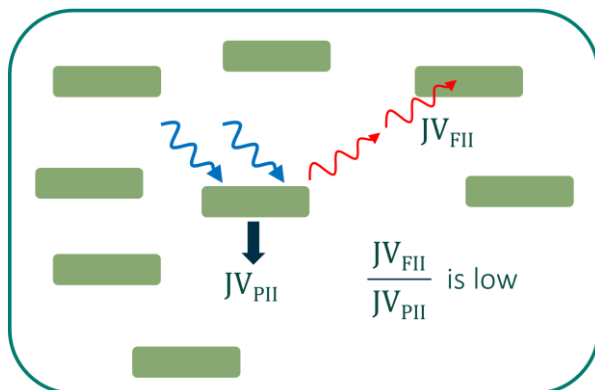
With LabSTAF, fluorescence emission is normally defined by a 685 nm bandpass filter in front of the PMT. Because this is very close to the emission peak from PSII within phytoplankton cells (around 683 nm) the proportion of the fluorescence signal coming from PSII is maximised. On the downside, the red absorption peak of chlorophyll *a* is Stokes shifted by only 2-3 nm from the emission peak and, consequently, reabsorption of fluorescence is also maximised. The probability of reabsorption is dependent on the size and optical characteristics of the cell plus the concentration of chlorophyll within the cell. At one end of the scale, it is likely that reabsorption within a small cell with a simple cell wall will be low (low package effect) while reabsorption within, for example, a large haptophyte surrounded by coccoliths will be much higher (high package effect). The images below illustrate this phenomenon.

Package effect (small cells)



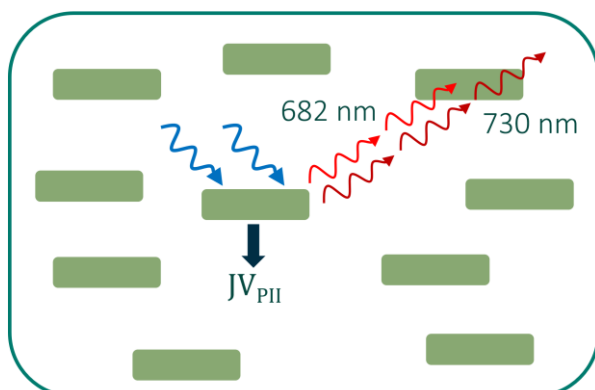
With a simple small cell, a high proportion of the photons emitted as fluorescence make it out of the cell. Consequently, the measured ratio of JV_{FII} to JV_{PII} is at the higher end of possible values.

Package effect (large cells)



With increasing size and changes in optical characteristics, the proportion of photons emitted as fluorescence that make it out of the cell decreases due to reabsorption. Consequently, the measured ratio of JV_{FII} to JV_{PII} becomes lower.

Package effect correction



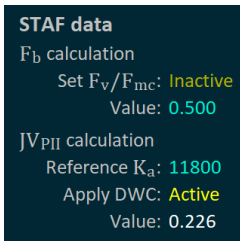
Fluorescence emission is much higher at 682 nm than at 730 nm. However, reabsorption of fluorescence at 682 nm, relative to 730 nm, is orders of magnitude higher still. It follows that the 730 nm : 682 nm emission ratio has the potential to provide a correction for the package effect.

In addition to the 685 nm bandpass filter that is normally used to define fluorescence emission, LabSTAF incorporates a 730 nm bandpass filter. Both filters are ± 10 nm Full Width-Half Max FWHM. A linear actuator is used to switch between these two filters as the DWC is run. Three reps of 685 and 730 nm measurements are made and stored within the RunSTAF data file. These primary data are available through **Clipboard** \rightarrow **DWC data**.

The number of sequences averaged within each rep ($n\text{Seq}_{\text{DWC}}$) is defined by Equation 14.1.

$$n\text{Seq}_{\text{DWC}} = (\text{Seq} / \text{Acq}) \times (\text{Acq} / \text{Saq}) \times 2 \quad \text{Equation 14.1}$$

Where **Seq / Acq** and **Acq / Saq** are as set under **STAF setup** on the home screen. The **Seq interval** set under STAF setup is applied when the DWC is run. The **2nd pulse** is always set to zero length while a DWC is running.



If the **Apply DWC** option is active, the **Value** is applied and values of JV_{PII} and GO_{PII} are immediately updated.

For reference, the transmission spectra for the 685 nm and 730 nm bandpass filters incorporated within each LabSTAF unit are provided on the **Spectra** tab within the Excel calibration workbook. This workbook can be found on the Surface Go2 computer provided as part of the LabSTAF delivery pack.

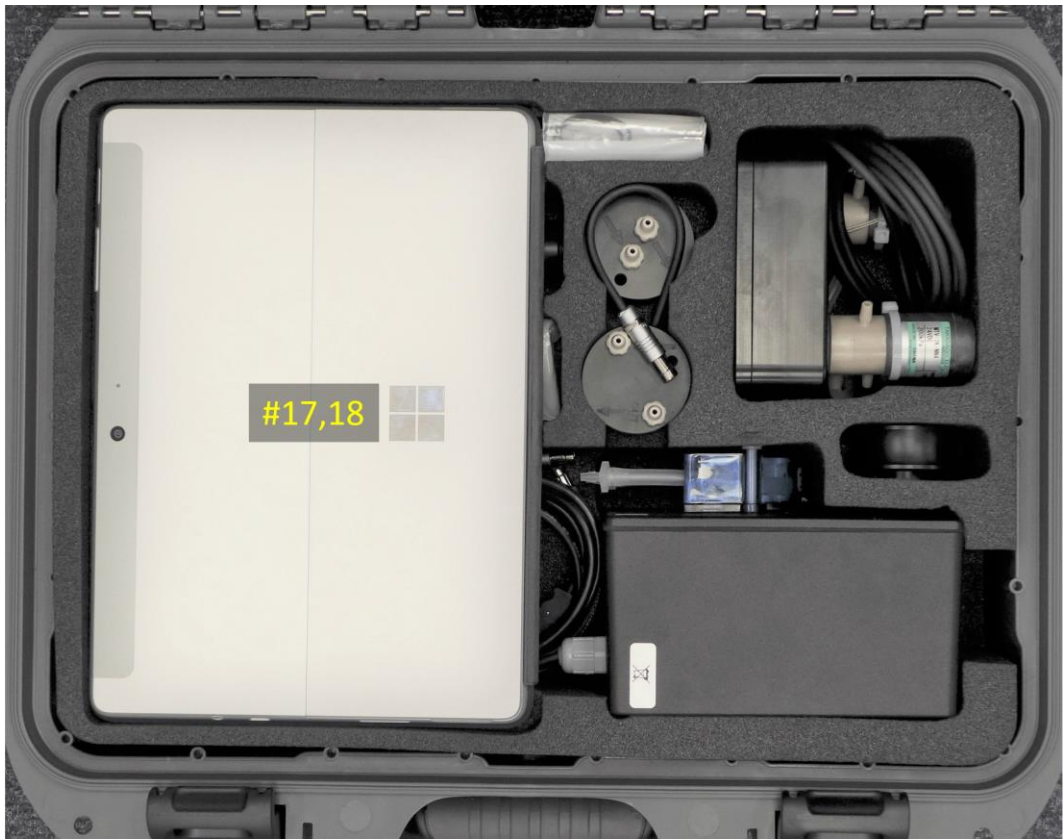
15 Delivery pack

In addition to the LabSTAF unit and the contents of Table 15.1, the delivery pack includes 3 m of 3 mm ID silicon tubing and mains cables.

#	CTL reference	Item	Quantity
1	2408-099-AS	24 V DC Power supply for LabSTAF	1
2	113607	USB-A to LabSTAF cable	1
3	105244	USB-C to USB-A adapter	1
4	2408-024-AS	Peristaltic pump unit	1
5	2408-169-AS	Solenoid unit	1
6	113604	Solenoid unit to LabSTAF cable	1
7	2408-160-AS	Flow-through stirrer unit	1
8	2408-070-AS	Flow-through unit	1
9	2408-157-MD	Calibration plug	1
10	2408-158-MD	Sample chamber lid	1
11	925791278	Connectors: 7 – 11 mm + 11 – 16 mm	2
12	117250	8 mm ID silicon tubing	2 x 80 mm
13	118054	4 mm ID tubing	80 mm
14	114126	O-rings (spare)	4
15	113639	7 mL sachet of silicon grease	1
16	118842	Fischer 102 blanking plug (spare)	2
17	105243	Surface Go 2 Intel Core M3 and power supply	1
18	12052	Surface Go Keyboard	1

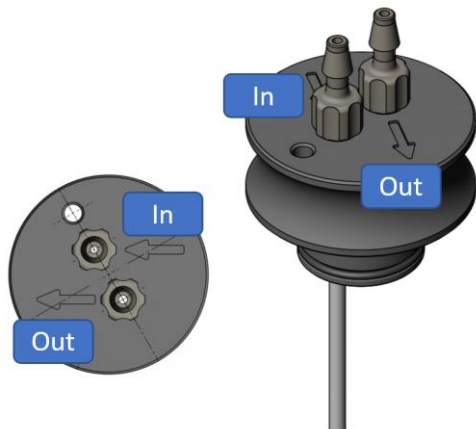
Table 15.1: Items stored within the LabSTAF accessory case.

The images on the next page show the contents of the accessory case. The Surface Go 2 and Surface Go Keyboard (#17 and #18) are absent in the top image, to show the underlying parts, and in place in the lower image.



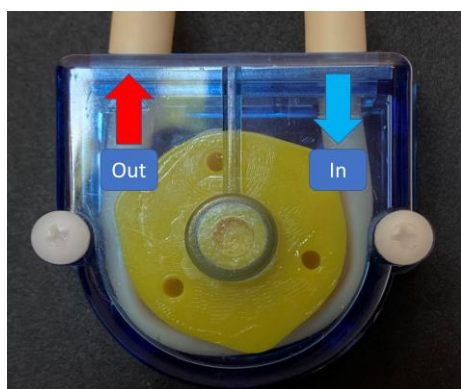
16 LabSTAF hardware setup

16.1 Plumbing the flow-through unit, peristaltic pump and solenoid unit



The LabSTAF flow-through unit with **In** and **Out** ports labelled. Make sure the connectors are screwed in tightly before using.

If the Auto FLC mode is being used without the solenoid unit, the **In** on the flow-through unit can be connected directly to the **Out** connector on the peristaltic pump unit. Otherwise, the **Out** on the flow-through unit should be connected to the **In** on the peristaltic pump unit.



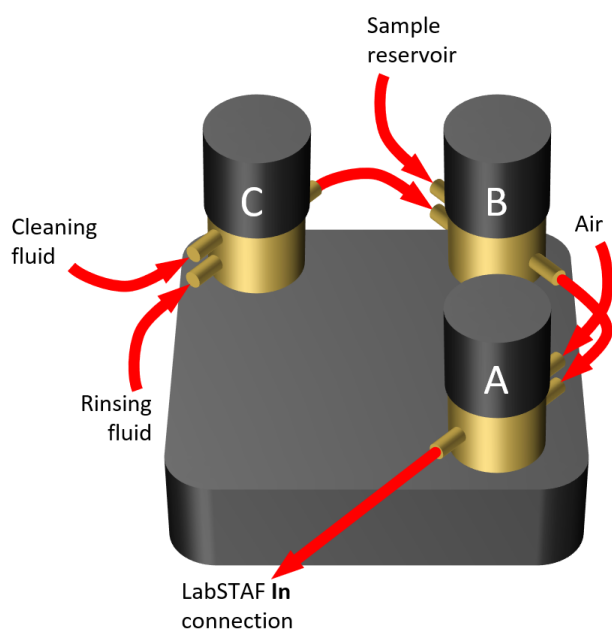
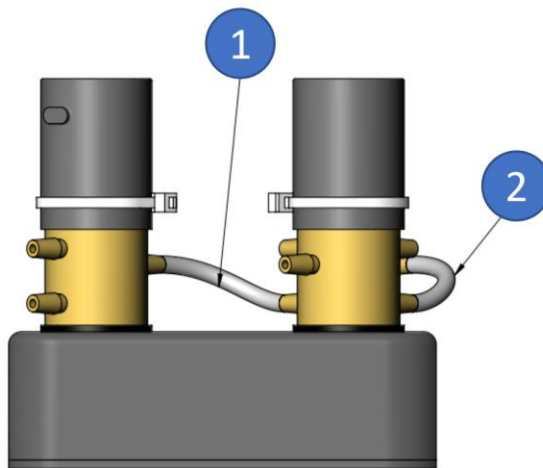
Detail of the peristaltic pump head with **In** and **Out** ports labelled.

When running the system in Auto FLC mode, the plumbing shown below must be adhered to.



This image shows a valve of the type used within the LabSTAF solenoid unit. The single port on the left is the Common port (**COM**). This is the output for each of the three valves (A, B and C) when the unit is plumbed in correctly. The upper port on the right is Normally Open (**NO**) and the lower port is Normally Closed (**NC**). Table 14.1 shows the status of each valve for each Auto FLC function.

The switch from NO to NC requires 24 V delivered from the LabSTAF unit through the **SOLENOID VALVE UNIT** connector located on the top panel.



The images above show the solenoid unit as supplied from the factory. On the left, the unit is viewed from above to show the labelling of Solenoids **A**, **B** and **C**. On the right, the unit is oriented to show Solenoids **A** and **C** from the side. Tube **1** connects the common from Solenoid **C** to the Normally Closed (NC) on Solenoid **B**. Tube **2** connects the common from Solenoid **B** to the NC of Solenoid **A**. Both tubes are 60 mm lengths of 3 mm ID silicon.

The image left shows the inlets and outlets for the standard configuration, as detailed within the table below.

Solenoid connection	Connects to...
Solenoid A, COM	In connector on the LabSTAF flow through unit
Solenoid A, NO	No connection (air input)
Solenoid A, NC	Solenoid B, COM (sample exchange and/or cleaning)
Solenoid B, COM	Solenoid A, NC
Solenoid B, NO	Sample exchange reservoir
Solenoid B, NC	Solenoid C, COM (cleaning)
Solenoid C, COM	Solenoid B, NC
Solenoid C, NO	Cleaning fluid (first step of cleaning cycle)
Solenoid C, NC	Rinsing fluid (second step of cleaning cycle)

17 LabSTAF calibration

The calibration values used to process data are always saved within the RunSTAF file and are easily accessible. This approach maximises the options for reprocessing of primary data.

17.1 Calibration data stored within the LabSTAF unit

To view the calibration values, select...

Settings → Factory → View calibration data

From the menu bar. The screenshot crops within Figure 18.1 provide an example of the calibration values automatically loaded from an attached LabSTAF unit.

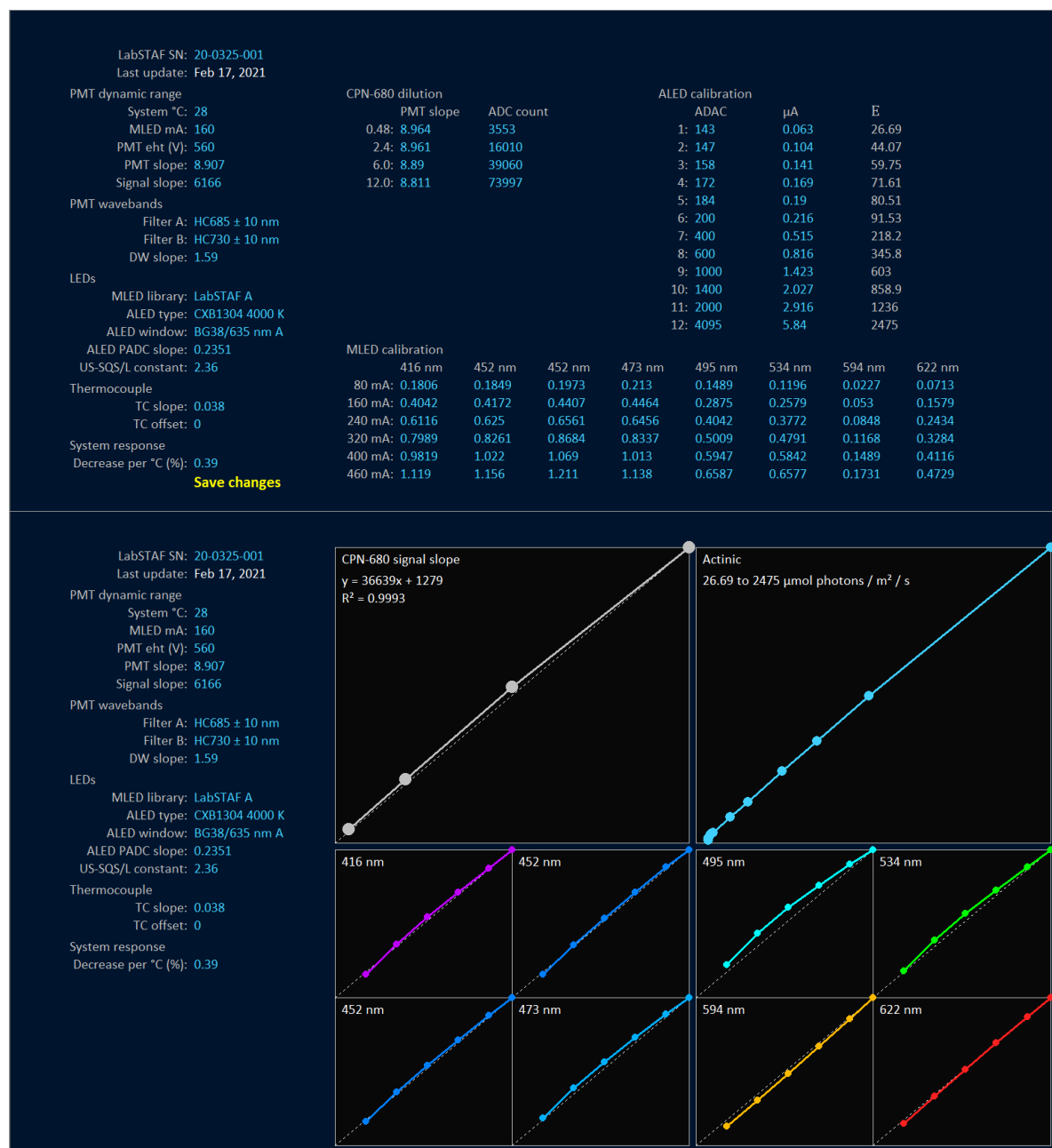


Figure 17.1: Screenshot crops from the RunSTAF calibration screen with a LabSTAF unit attached. The **Show plots** and **Hide plots** buttons (not shown here but located at bottom right of the full calibration screen) switch between the two screens. The **Save changes** button included within the upper screenshot is only shown after one or more values have been changed.

17.2 The spectral calibration spectra (scs) data file

In addition to the calibration data loaded from the attached LabSTAF, the spectral output of all seven MLED wavebands and the actinic LED within the LabSTAF unit are loaded from a spectral correction spectra (scs) file installed on the controlling computer. The scs filename is matched to a specific LabSTAF unit through the serial number without the dashes. For example, the LabSTAF unit attached in the above screenshots has the serial number 20-0325-001. The matching scs file is 200325001.scs. This file must be located within this folder:

Documents → LabSTAF → Calibration files

The **Calibration files** folder is created by RunSTAF. The scs files for multiple LabSTAF units can be stored within this folder. RunSTAF will select the correct file based on the filename (matched to the serial number of the attached LabSTAF unit).

17.3 Create a local backup of the calibration data stored within LabSTAF

All calibration data for all LabSTAF units are stored by CTL and are available on request. A local backup of the calibration data stored within an attached LabSTAF unit can be made by selecting...

Settings → Factory → Save calibration data

From the menu bar. This generates a file within this folder:

Documents → LabSTAF → Calibration files

The filename for the calibration backup is matched to a specific LabSTAF unit through the serial number without the dashes. The file extension is stc. For example, the LabSTAF unit attached in the above screenshots has the serial number 20-0325-001. The matching stc file is 200325001.stc. This file can be used to overwrite any changes made to the calibration data. The file can be recovered by first selecting...

Settings → Factory → View calibration data

end then selecting...

Settings → Factory → Load calibration data

The **Save changes** button must be pressed to update the changes within the attached LabSTAF unit.

17.4 Post-processing with the scs data file

The scs data are used to apply a spectral correction to RunSTAF data. This correction is required to generate values for J_{PII} , JV_{PII} and GO_{PII} . If the scs file is absent during data acquisition, values for these parameters will not be generated in real time. However, it is possible to post-process the data to apply the spectral correction and generate values for J_{PII} , JV_{PII} and GO_{PII} .

To apply post-processing, the required scs file must be copied to the **Calibration files** folder. Now, when RunSTAF data files are opened, the scs file will be used to automatically apply spectral correction and generate values for J_{PII} , JV_{PII} and GO_{PII} . When the updated data file is saved, the scs data are incorporated within it. This means it can be opened on another computer without the scs data file being present.

17.5 On-site calibration of sample chamber temperature

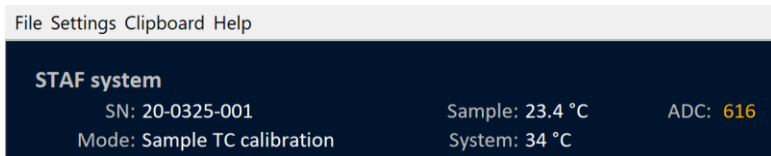
The temperature within the sample chamber is monitored by an internal thermocouple. If there is a large difference between the ambient temperature and the temperature within the sample chamber, the reported value may be significantly higher than the actual sample chamber temperature. The steps below can be used to generate a more accurate value.

In most cases, a single point calibration can be run to generate a new TC slope. To activate the calibration mode, start RunSTAF and select...

Settings → Acquisition mode → Manual

...from the menu bar. Then select...

Settings → Factory → Manual calibration modes → Sample TC



This will activate an ADC field next to the Sample temperature, as shown here.

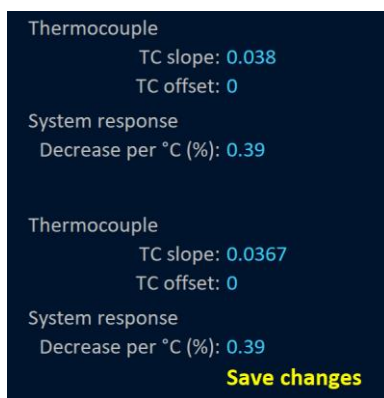
The formula for using the ADC value to set the reported temperature is provided by Equation 18.1.

$$\text{Sample } ^\circ\text{C} = \text{ADC} \times \text{TC slope} + \text{TC offset} \quad \text{Equation 18.1}$$

In this example, the actual temperature within the sample chamber was 22.6 °C. The reported temperature (**Sample**) is **23.4 °C** and the reported **ADC** value is **616**.

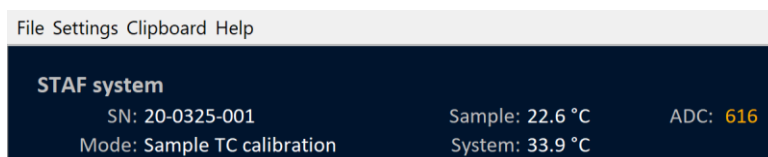
To change the calibration values for the sample thermocouple, select...

Settings → Factory → View calibration data



The current **TC slope TC offset** is **0.038**. Dividing the actual temperature by the reported ADC value of **616** gives a new TC slope of **0.0367**.

Changing the **TC slope** value activates the **Save changes** button. Pressing this button saves the changes to the attached LabSTAF unit.



The reported value is now correct.

17.6 Updating calibration values across existing data files

This function has been incorporated within RunSTAF to allow for the updating of calibration data across data files when one or more incorrect values have been found. Although the most likely mismatch is the TC slope used to define the recorded sample temperature, all calibration values are assessed for changes and any required re-calculation of data is applied.

The function can be accessed through...

Settings → Factory → Update across files

18 Technical information

Basic specifications of the LabSTAF unit	
Power requirements	Between 140 and 400 mA at 24 V (3.4 and 9.7 W)
Dimensions	235 x 320 x 420 mm
Mass (approximate)	8.1 kg
Sample chamber	20 mL maximum sample volume
Excitation wavebands	Central wavelengths at: 416, 452 x 2, 473, 495, 534, 594, 622 nm
Actinic light source	Collimated output from 10 to 2000 $\mu\text{mol photons m}^{-2} \text{s}^{-1}$
Detection limit (approximate)	Can resolve F_v with an amplitude equivalent to the fluorescence signal generated under 452 nm excitation by 0.001 mg m^{-3} of chlorophyll
IP rating	IP64 (protected from water spray from any direction)

Table 18.1: Basic specification of the production LabSTAF unit (2408-040-AS).

18.1 The measurement LEDs and PMT

The measurement LEDs (MLEDs) provide the ST pulses. There are eight channels with five LEDs in each, distributed between two four channel arrays. Each array is connected to a four channel drive circuit which allows the drive current to be set independently for each channel.

The maximum drive current rating for the LEDs used within LabSTAF is between 700 mA (594 nm and 624 nm) and 1000 mA (all other wavebands). The maximum drive current settable through RunSTAF is 460 mA. This limitation is imposed to ensure that the intensity of each ST pulse remains constant for the entire duration.

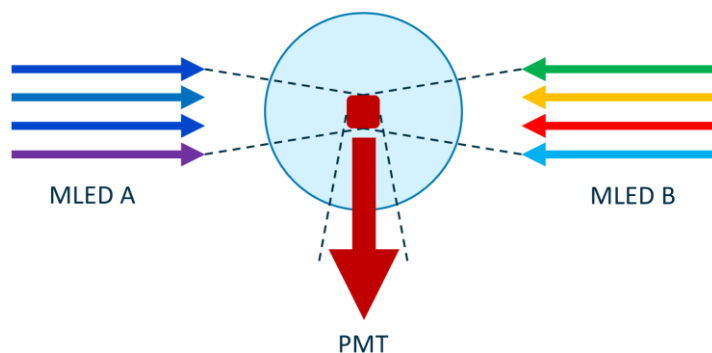


Figure 18.1: Two-stage MLED optics provide homogeneous illumination throughout an interrogated volume of approximately 0.5 mL.

The collimated MLED light from each array is passed through a cutoff filter (625 nm shortpass for MLED A, 650 nm shortpass for MLED B) before being directed through the interrogated volume. The fluorescence emission from the interrogated volume is Lambertian (uniformly spherically radiative). The first stage of the MLED and PMT optics collects a proportion of the emitted photons which are directed through a bandpass filter, centred at 685 nm or 730 nm, and a 630 nm longpass filter before being focussed onto the active area of the PMT.

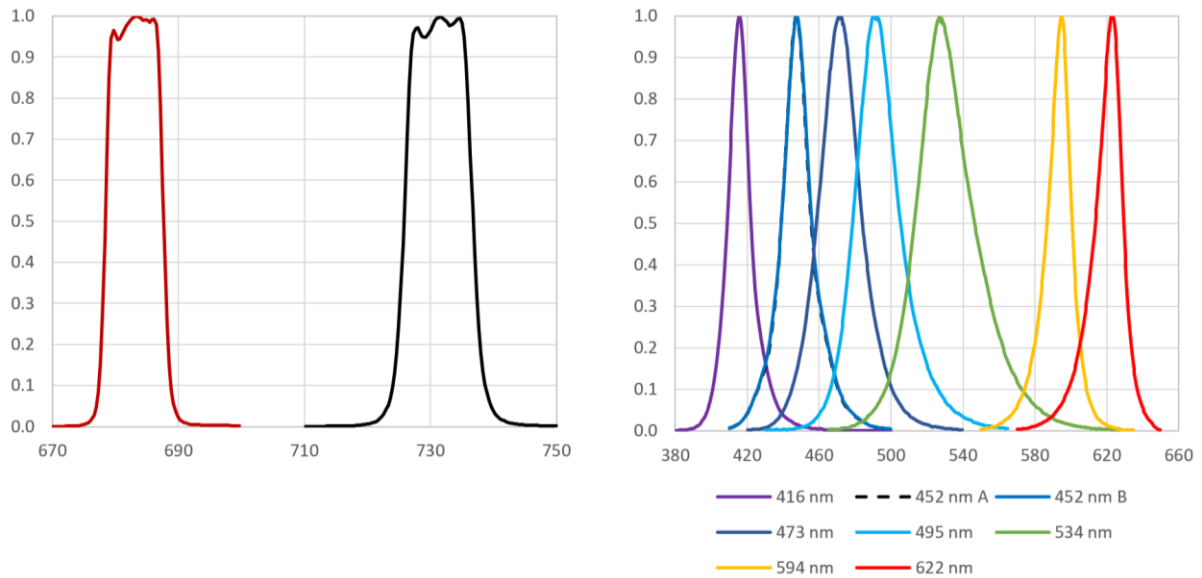


Figure 18.2: Transmission spectra from the bandpass filters in front of the PMT (left) and emission spectra from the MLEDs. These spectra are recorded for all production units and incorporated within the calibration certificate at 0.1 nm resolution.

18.2 The actinic light source

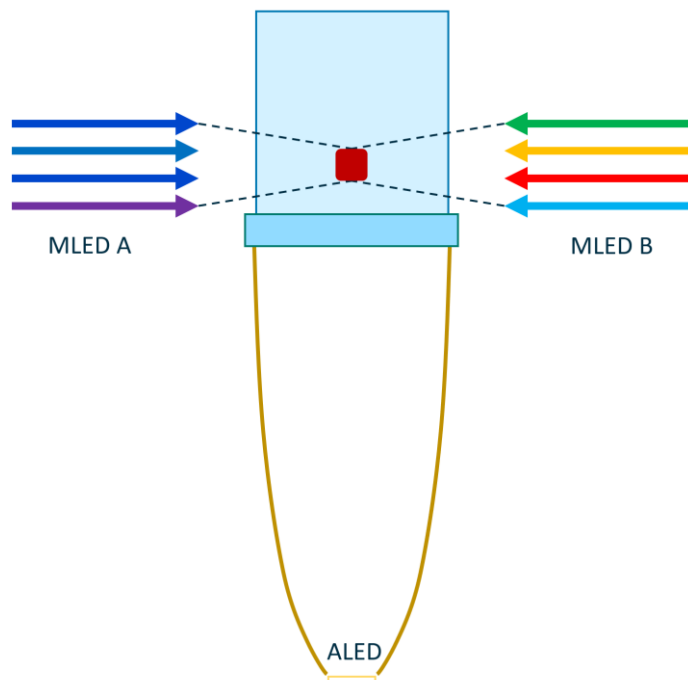


Figure 18.3: Actinic light is delivered to the entire sample from a single Actinic LED (ALED) via a collimating Compound Parabolic Collector (CPC). The base of the sample chamber is a 3 mm BG38 glass filter, sandwiched between two 0.5 mm layers of BK7 glass. A multi-layer coating on the BK7 surface facing the ALED provides a 635 nm shortpass filter.

The output range of 10 to 2000 $\mu\text{mol photons m}^{-2} \text{s}^{-1}$ is provided by a single LED using a 12-bit constant current DC drive circuit. At very low current, where output is temperature sensitive, a photodiode integrated within the CPC monitors the actual output and adjusts the drive current to get as close as possible to the requested value. The actual value is logged.

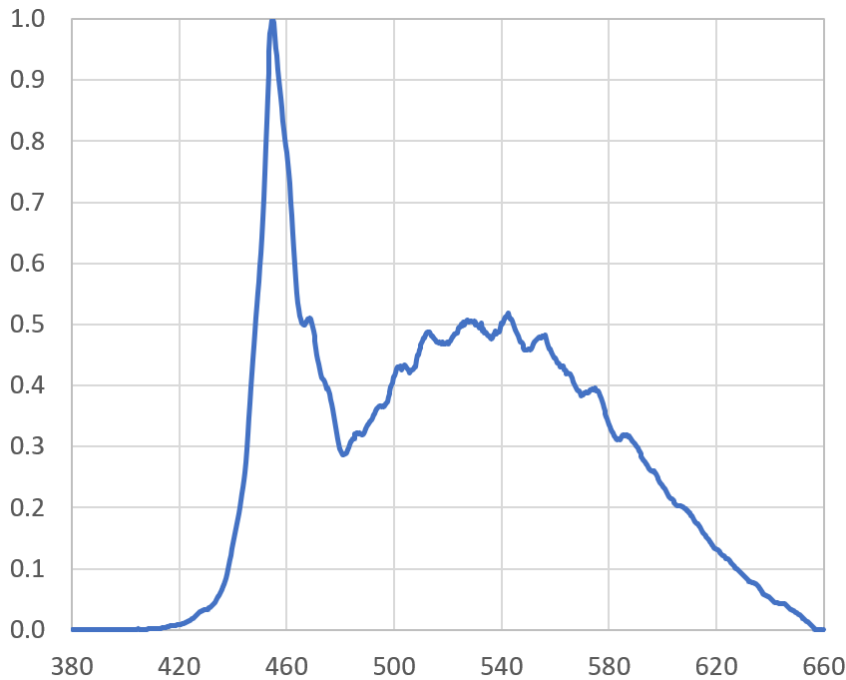


Figure 18.4: Emission spectrum recorded from an ALED. The ALED spectrum is recorded for each production unit and incorporated within the calibration certificate at 0.1 nm resolution.

18.3 Sample temperature control

The sample chamber thermal block is insulated from the main internal volume. However, this thermal block has a much better thermal connection to the internal optics than the internal electronics. Consequently, running the sample at very low temperature can result in the internal optics being cooled to the point where there is a significant temperature differential between the optics and the internal electronics. A humidity sensor has been incorporated within the main internal volume (the space occupied by the internal electronics) to check for the possibility of condensation forming on the optics. Table 18.2 provides a guide to the dew point on a mirror surface at different **System RH** values when the **System** temperature (inside the unit) is 32 °C.

Relative Humidity (RH) at 32 °C	Dew point
10%	-3.4 °C
12%	-1.0 °C
14%	1.1 °C
18%	4.7 °C
24%	8.9 °C
30%	12.2 °C
36%	15.0 °C
42%	17.5 °C

Table 18.2: Dew point values at different **System RH** values when the **System** temperature is 32 °C.

18.4 PMT temperature coefficient

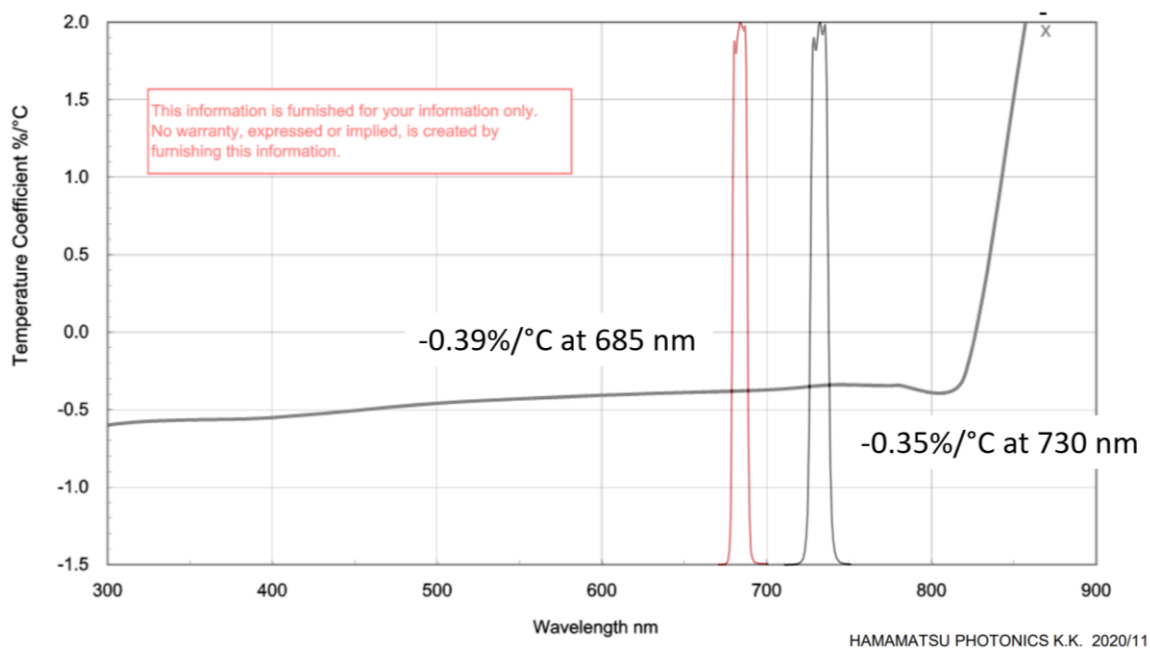


Figure 18.5: Continuous recording of the system temperature allows RunSTAF to apply an appropriate correction to the PMT output. The temperature coefficient applied is the 685 nm value from data provided by Hamamatsu.

18.5 Events log

A range of operational events are logged within a text file stored at the following location...

Documents → CT-RunSTAF → Events

A new file is created each day. As an example, an events file created on 14th May 2021 will be named...

210514 events.txt

The events recorded are:

AB reset

ST reset

Auto MLED failed

DWM failed

PEP failed

The **AB reset** and **ST reset** events are triggered together after a successfully reset. The reset is usually triggered by after being subjected to a high voltage spike through the mains supply.

The **Auto MLED failed**, **DWM failed** and **PEP failed** events can be triggered by low signal to noise. Increasing the **Seq / Acq** value under **STAF setup** will often help with this.

In addition to the events listed above, a series of diagnostic codes are recorded within the events file if the Log commands function is active...

Settings → Factory → Calibration and test modes → Log commands

These codes are for factory use only.

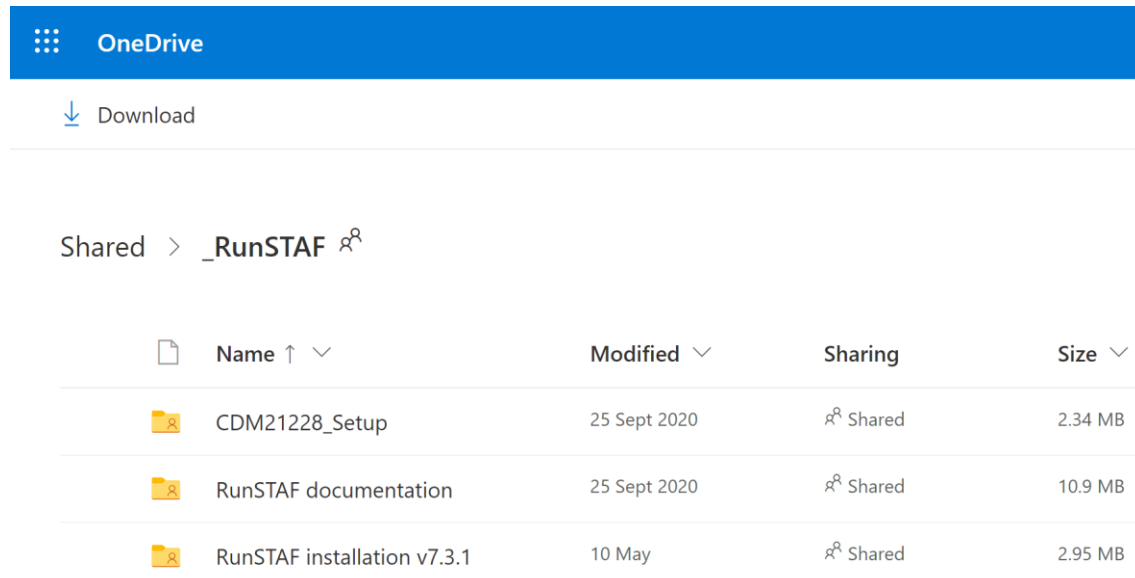
19 RunSTAF installation and setup

19.1 Updating an existing RunSTAF installation

To access the most recent version of RunSTAF, use this link...

<https://1drv.ms/u/s!AkUtV8PHZSmVsME08Sk09MUnV1O4vg?e=iSldaA>

This provides access to the three folders shown here:



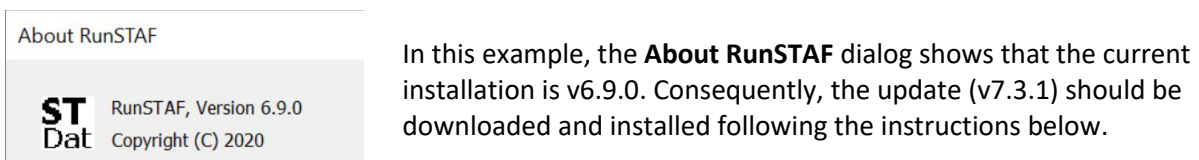
The screenshot shows a OneDrive interface for a shared folder named '_RunSTAF'. At the top, there is a blue header with the OneDrive logo and a 'Download' button. Below the header, the breadcrumb path is 'Shared > _RunSTAF'. A table lists the contents of the folder:

Name	Modified	Sharing	Size
CDM21228_Setup	25 Sept 2020	Shared	2.34 MB
RunSTAF documentation	25 Sept 2020	Shared	10.9 MB
RunSTAF installation v7.3.1	10 May	Shared	2.95 MB

The **CDM21228_Setup** folder contains a single file which is also named **CDM21228_Setup**. This is an application file that will install essential drivers. This file is not required when updating RunSTAF as the required drivers will already be installed.

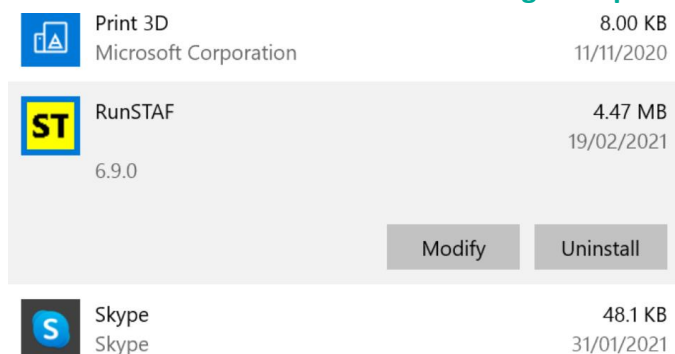
The **RunSTAF documentation** folder includes the most up-to-date version of this handbook plus other relevant documentation.

The **RunSTAF installation v7.3.1** folder includes two files named **RunSTAF setup** and **setup**. The first step is to compare the version number of this installation with the existing installation. To do this select **Help** → **About RunSTAF** from the RunSTAF menu bar.



The screenshot shows the 'About RunSTAF' dialog box. On the left, there is a logo with 'ST' and 'Dat' and text: 'RunSTAF, Version 6.9.0 Copyright (C) 2020'. On the right, there is a text area that reads: 'In this example, the **About RunSTAF** dialog shows that the current installation is v6.9.0. Consequently, the update (v7.3.1) should be downloaded and installed following the instructions below.'

19.2 Uninstall RunSTAF before installing the update



The screenshot shows the 'Apps & features' section in Windows Settings. It lists several installed applications:

App Name	Size	Installation Date
Print 3D (Microsoft Corporation)	8.00 KB	11/11/2020
RunSTAF (6.9.0)	4.47 MB	19/02/2021
Skype	48.1 KB	31/01/2021

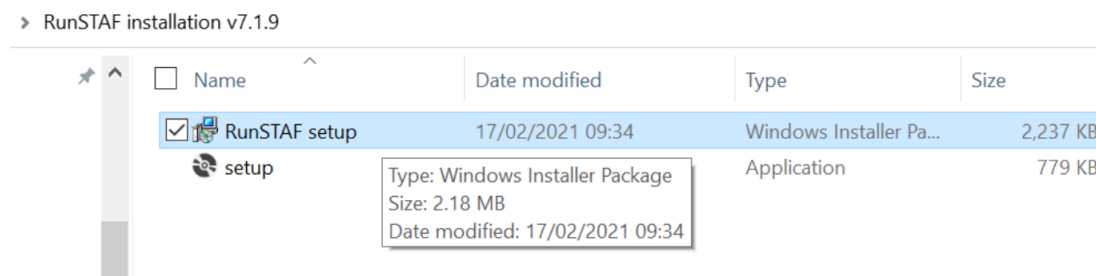
Below the RunSTAF entry, there are 'Modify' and 'Uninstall' buttons.

Go to **Add or remove programs** within Windows **System settings**. Under Apps & features, find the **RunSTAF** tab and select **Uninstall**.

Accept all the default options to complete the uninstall.

19.3 Install the new version of RunSTAF

Double click the **RunSTAF setup** Windows Installer Package.



Accept all the default options to complete the installation.

19.4 First RunSTAF installation

When installing RunSTAF for the first time on a computer, drivers related to the LabSTAF hardware need to be installed and the computer needs to be connected to a LabSTAF unit.

- Run the CDM21228_Setup application supplied with the download
- Install RunSTAF
- Connect the computer to the LabSTAF unit and power it up
- Start RunSTAF

Uninstalling RunSTAF in preparation for installation of an update (see above) does not uninstall the required drivers.

19.5 Run LabSTAF on power up

To run the LabSTAF system on power up, you will need to bypass the Windows 10 login and install RunSTAF as a start-up program (see below).

You will also need to ensure that the **Look for STAF system** function is activated through **Settings** on the menu bar.

19.5.1 Bypass the Windows 10 login

You will need to be logged on as an administrator to set this up.

- Go to Windows Start Menu and type **Run**
- Hit **Enter**
- In the Open field, type **netplwiz**
- Hit **Enter**
- Uncheck the box next to **Users must enter a username and password to use this computer**
- Press the **Apply** button
- Type the password for the account in the **Password:** and **Confirm password:** boxes
- Press **OK** and **OK** again

19.5.2 Run as a start-up program

You will need to be logged on as an administrator to set this up.

- Go to start menu and type **Run**

- Hit **Enter**
- In the Open field, type **shell:common startup**
- Hit **Enter**

This should open File Explorer at the following location...

C:\ProgramData\Microsoft\Windows\Start Menu\Programs\StartUp

If you already have a shortcut to RunSTAF on your desktop, drag it to the **StartUp** folder. If you don't have a shortcut on your desktop, open a second instance of File Explorer at the following location...

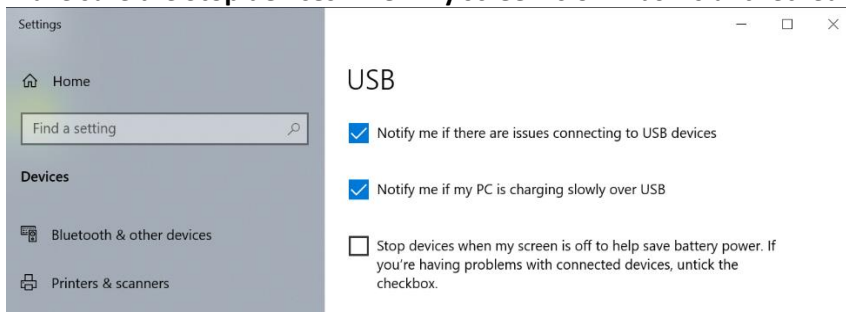
C:\Program Files\Chelsea Technologies Ltd\RunSTAF

Right click on the **RunSTAF** exe file and select **Create shortcut** from the popup menu. This will give you the option of creating a shortcut on your desktop which you can then drag to the **StartUp** folder.

19.6 Prevent the USB port going to sleep

One power saving option with Windows 10 is to turn the screen off after a set period of inactivity. With some systems, this can lead to the USB port being powered down and data transfer from the attached LabSTAF unit being blocked. The safest option is to set the Screen to never turn off under **Settings → Power & sleep**. If this is not an option, the following steps will usually keep the USB port active.

- Go to **Settings → Devices → USB**
- Make sure the **Stop devices when my screen is off...** box is unchecked



- Go to Windows Start Menu and type **device manager**
- Hit enter to start the Device Manager application and go to **Universal Serial Bus controllers...**



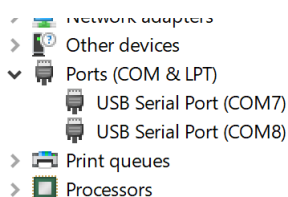
- For each device that include **USB Root Hub** in the description, double click to open the **Properties** and, under the **Power Management** tab, ensure that the **Allow the computer to turn off this device to save power** option is unchecked



19.7 Block the Serial Enumerator

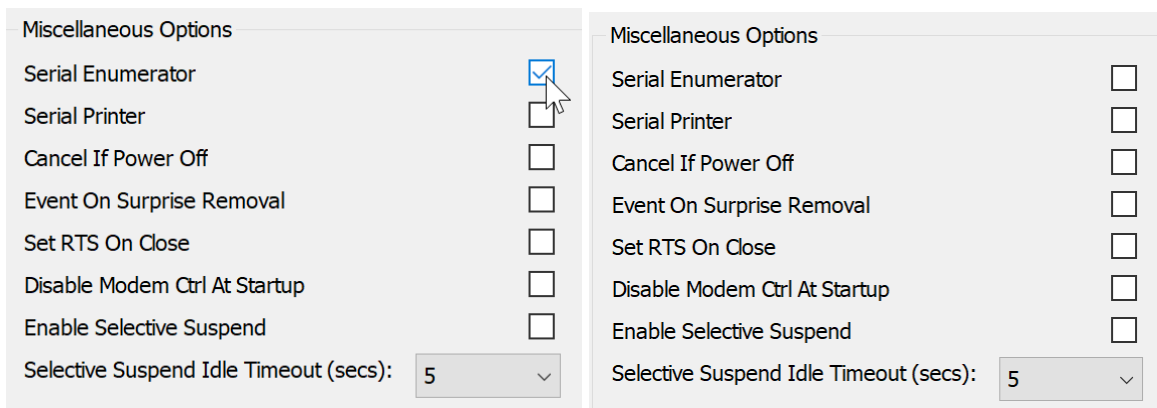
Ideally, the **Serial Enumerator** option for each of the COM ports provided by the LabSTAF unit should be blocked.

- Go to Windows Start Menu and type **device manager**
- Hit enter to start the Device Manager application...



When LabSTAF is connected and powered up, you should find two instances of USB Serial Port (COM) under Ports (COM & LPT). In this example, the LabSTAF ports are **COM7** and **COM8**.

- Double click on **COM7** to open its **Properties** window
- Select the **Port Settings** tab and press the **Advanced...** button
- Within **Advanced Settings for COM7**, under **Miscellaneous Options**, uncheck the **Serial Enumerator** box

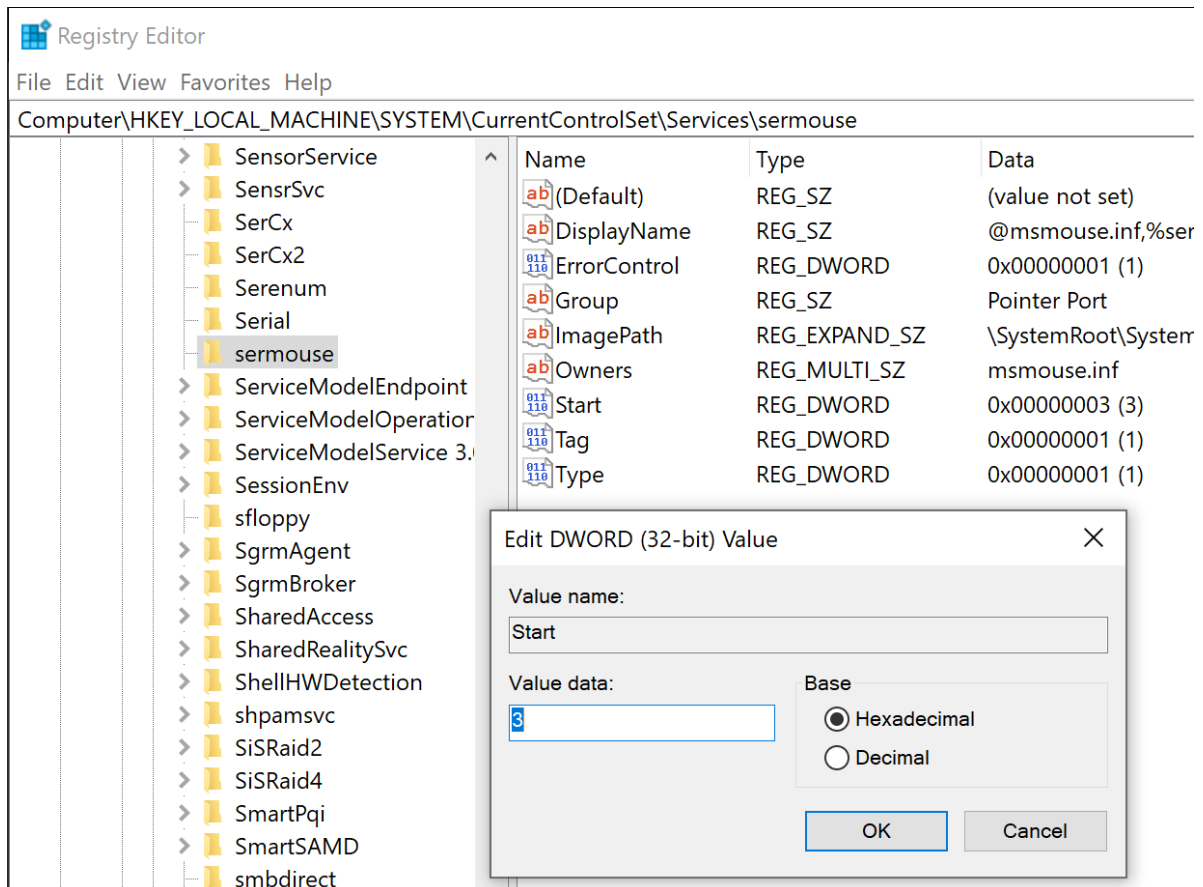


- Click the **OK** button to closed Advanced Settings for COM7
- Click **OK** again to close the Properties window
- Repeat for COM8
- Restart the computer

19.8 Block serial mouse detection on Startup

In some situations, the data stream from LabSTAF can be interpreted as output from a serial mouse. The steps below can be used to prevent this.

- Go to Windows Start Menu and type **regedit**
- Hit **Enter** to open the **Registry Editor** application
- Navigate to: **HKEY_LOCAL_MACHINE\SYSTEM\CurrentControlSet\Services\sermouse**
- Double click on the **Start** tag and change the **Value data** field from **3** to **4**
- Hit the **OK** button
- Exit Registry Editor and restart the computer



20 Glossary of terms

This section provides a summary of the terms used within this handbook. A more extensive list of terms used within the relevant literature has been compiled by Schuback et al. (2021).

20.1 Acronyms

20.1.1 CCAP

Culture Collection of Algae and Protozoa (<https://www.sams.ac.uk/facilities/ccap/>). Many of the examples provided within this handbook use cultures from CCAP.

20.2 Term modifiers

The base (unmodified) terms used within RunSTAF are valid for ST pulse measurements from a dark-adapted sample. There are four modifiers used to define terms that don't fit with this description.

20.2.1 The light-adapted state prime modifier (')

Within the relevant scientific literature, the prime symbol is widely used to signify that a parameter is from a light-adapted sample. Within LabSTAF, a prime is always used when the integrated actinic light source is turned on. It should be noted that no minimum exposure time is defined for inclusion of the prime symbol. Consequently, the prime symbol should not be taken as indicating a steady-state condition.

Example: F_m in the dark becomes F_m' in the light

20.2.2 The baseline corrected modifier (c)

Baseline fluorescence (from any source other than photochemically active PSII complexes) contributes to the measured value of some fluorescence terms. Where a correction has been applied to subtract baseline fluorescence from the total signal, a lowercase c is added to the subscript of the fluorescence term.

Example: F_m becomes F_{mc} after baseline fluorescence has been subtracted

20.2.3 The second ST pulse modifier (s)

The dual pulse method incorporated within LabSTAF generates a number of additional parameters. A non-subscripted lower case s is used to define a second ST pulse parameter. This is added to the left of the main term.

Example: F_m for the first ST pulse becomes sF_m for the second ST pulse

20.2.4 The dimer modifier (d)

RunSTAF incorporates two fitting algorithms for ST curves: the widely used Rho ST fit and the Dimer ST fit. For a relevant parameter, a lower case d is used to indicate it was generated from the Dimer ST fit. This modifier is added to the left of the main term. When combined with a second ST pulse modifier, the dimer modifier is closest to the term.

Example: $s\sigma_{PII}$ for the Rho ST fit becomes $sd\sigma_{PII}$ for the Dimer ST fit

20.3 Basic STAF terms

Term	Meaning	SI units (reported units, if different)
ϕ_{xII}	Yield	dimensionless
k_{xII}	Rate constant	s^{-1}
τ_{xII}	Time constant	s
σ_{xII}	Absorption cross-section	$m^2 PSII^{-1}$ ($nm^2 PSII^{-1}$)
α_{xII}	Absorption coefficient	m^{-1}
J_{xII}	Photon flux	photons $PSII^{-1} s^{-1}$
JV_{xII}	Photon flux per unit volume	photons $m^{-3} s^{-1}$ ($\mu mol photons m^{-3} s^{-1}$)

Table 20.1: STAF terms for PSII process 'x', where x is a placeholder for the terms in Table 19.2 (Boatman, Geider and Oxborough, 2019).

Term	Meaning
LH	Light harvesting
P	Photochemistry
F	Fluorescence
D	Thermal Dissipation or non-radiative Decay

Table 20.2: Subscripts for use with STAF terms for each PSII process (Boatman, Geider and Oxborough, 2019).

20.4 Additional STAF terms

Term	Meaning	SI units (reported units)
α_{PII}	The initial rate at which photons are used to drive PSII photochemistry during a ST pulse	photons $PSII^{-1} s^{-1}$ (photons $PSII^{-1} \mu s^{-1}$)
ρ	Apparent connectivity among PSII complexes	dimensionless
E_{ST}	Photon irradiance provided to the interrogated volume by the MLEDs during a ST pulse	photons $m^{-2} s^{-1}$ (photons $nm^{-2} [100 \mu s]^{-1}$)
$[Q_A]$	Proportion of photochemically active PSII complexes in the open state	dimensionless

Table 20.3: Additional STAF terms. The parameter ρ can also be defined as the probability of a photon absorbed at a closed PSII that was in the open state at $t=0$ during a ST pulse being used to drive PSII photochemistry. Clearly, this requires that the photon is first transferred to an open PSII.

20.5 Dimer-specific STAF terms

Term	Definition
[oo]	The proportion of PSII dimers in the oo state (both centres open)
[oc]	The proportion of PSII dimers in the oc state (one centre open, the other closed)
[cc]	The proportion of PSII dimers in the cc state (both centres closed)

Table 20.4: Dimer-specific STAF terms

20.6 Basic fluorescence terms

Term	Definition
F_o	Extrapolation to $t = 0$ at the first ST pulse (origin of variable fluorescence) <ul style="list-style-type: none"> All photochemically active RCII are in the open state A pre-ST dark pulse of approximately 1 s is required for measurement of F_o'
F_m	At the asymptote of the first ST pulse (maximum fluorescence)
F_v	$F_m - F_o$ (variable fluorescence)
F	Any point between F_o and F_m
F_q	$F_m - F$ (fluorescence quenched by photochemistry)
F_b	Fluorescence signal not attributable to functional PSII centres
F_{oc}	The baseline subtracted value of F_o such that $F_{oc} = F_o - F_b$
F_{mc}	The baseline subtracted value of F_m such that $F_{mc} = F_m - F_b$
F_c	The baseline subtracted value of F such that $F_c = F - F_b$

Table 20.5: Basic fluorescence terms. Only dark terms are shown. The light-equivalent terms all carry a prime. For example, F_m in the dark becomes F_m' in the light.

20.7 Additional fluorescence terms for the second ST pulse

Term	Definition
sF	Extrapolation to $t = 0$ at the second ST pulse
sF_m	At the asymptote of the second ST pulse
sF_q	$sF_m - sF$
sF_{mc}	The baseline subtracted value of sF_m such that $sF_{mc} = sF_m - F_b$
sF_c	The baseline subtracted value of sF such that $sF_c = sF - F_b$

Table 20.6: Additional fluorescence terms required for the second ST pulse in a dual pulse sequence. Only dark terms are shown. The light-equivalent terms all carry a prime. For example, sF_m in the dark becomes sF_m' in the light.

20.8 Derived fluorescence parameters

Parameter	Definition
F_v/F_m	Theoretically equivalent to ϕ_{PII} when all PSII centres are in the open state and $F_b = 0$
F_v/F_{mc}	As above when non-zero F_b has been subtracted
F_q/F_m	Theoretically equivalent to ϕ_{PII} when some centres are closed and $F_b = 0$
F_q/F_{mc}	As above when non-zero F_b has been subtracted
F_q/F_v	The so-called 'photochemical factor' (Baker and Oxborough, 2004)
F_o/F_v	Normalized Stern-Volmer equation when $F_b = 0$
F_{oc}/F_v	As above when non-zero F_b has been subtracted

Table 20.7: Derived fluorescence parameters. Only dark parameters are shown. The light-equivalent parameters all carry primes on each term. For example, F_q/F_m in the dark becomes F_q'/F_m' in the light.

21 Answers to FAQs and background material

21.1 Deriving your own values of a_{LHII} and/or PSII concentration

As noted within RunSTAF terminology, the fluorescence values reported are on a defined STAF Unit scale. When incorporating fluorescence values within the derivation of a_{LHII} or PSII concentration, the reported fluorescence values should be divided by 10^6 to bring them onto the same scale as K_a (default value of $11,800 \text{ m}^{-1}$). Similarly, reported values for σ_{PII} and σ_{LHII} should be converted from $\text{nm}^2 \text{ PSII}^{-1}$ to $\text{m}^2 \text{ PSII}^{-1}$ to bring them onto the same scale as K_a .

21.2 Units for measuring LED photon irradiance (E_{ST})

The reported units for E_{ST} are photons nm^{-2} ($100 \mu\text{s}$) $^{-1}$.

A value of $1.0 \text{ photons nm}^{-2} (100 \mu\text{s})^{-1}$ is equivalent to $16,603 \mu\text{mol photons m}^{-2} \text{ s}^{-1}$.

21.3 Dark FLC step F_v/F_m and F_v'/F_m' values

When running a FLC, it is common practice to include a dark step after the highest **Up** step and before the **Down** steps. In the example shown below-left, a 120 s Dark step has been included after the 60 s $917 \mu\text{mol photons m}^{-2} \text{ s}^{-1}$ **Up Step 12** and before the 120 s $318 \mu\text{mol photons m}^{-2} \text{ s}^{-1}$ **Down Step 8** (as indicated by the red arrows). The data values for the $917 \mu\text{mol photons m}^{-2} \text{ s}^{-1}$ **Up** step and **Dark** step are shown below-right. For the **Dark** step, the values are the dark equivalent of the light-adapted terms shown. For example, the **Dark** value in the F' line is F_0 and the F_m' value is F_m .

Step	E	Up	Dark	Down	E: $917 \mu\text{mol photons / m}^2 / \text{s}$		
1:	0	60	0	60	Up	Dark	Down
2:	32	180	0	0	rP: 80.67	—	—
3:	46	60	0	0	JV _{PII} : 5.291	—	—
4:	79	60	0	0	GO _{PII} : 4.762	—	—
5:	120	60	0	60	F': 3.22	2.76	—
6:	172	60	0	60	F _m ': 3.53	5.35	—
7:	237	60	0	60	F _q '/F _{mc} ': 0.088	0.484	—
8:	318	60	0	120	F _v '/F _{mc} ': 0.3885	0.4905	—
9:	421	60	0	0	F _q '/F _v ': 0.2265	—	—
10:	550	60	0	0	α_{PII} ': 0.0378	0.0586	—
11:	713	60	0	0	ρ ': 0.039	0.4226	—
12:	917	60	120	0	τ_{ES} ': 3953	1548	—

In the case of F_q'/F_{mc}' , the **Dark** value is F_v/F_{mc} . The values of F_0 and F_m required to generate the Dark F_v/F_{mc} are from the ST data acquired during the **Dark** step.

In the case of F_v'/F_{mc}' , the **Dark** value is also defined as F_v'/F_{mc}' . The value of F_{oc}' required for the **Dark** F_v'/F_{mc}' is generated using Equation 20.1 (Oxborough and Baker, 1997).

$$F_{oc}' = F_{oc} / \left(\frac{F_v}{F_{mc}} + \frac{F_{oc}}{F_{mc}'} \right) \quad \text{Equation 20.1}$$

Within Equation 20.1, the only value measured from **Dark Step 12** is F_{mc}' . All the remaining values on the right-hand side are from **Up Step 1**.

By allowing for comparison between the F_v/F_{mc} measured directly in the dark and the calculated value, this process provides a check for the validity of F_v'/F_{mc}' and F_q'/F_v' parameters calculated from the same sample under illumination, which both require F_{oc}' from Equation 20.1.

21.4 The Stern-Volmer relationship, NPQ and NSV

The Stern-Volmer relationship provides a theoretical basis for the decrease in F_m to F_m' that is commonly observed under actinic illumination: so-called non-photochemical quenching. The basic

concept of Stern-Volmer quenching within PSII is that quenching is induced by the accumulation of a class of molecules within the PSII light harvesting system with the capacity to accelerate the deactivation of excited light harvesting molecules. Under the Stern-Volmer relationship, this intermolecular quenching is in direct proportion to the concentration of quencher.

It is important to note that Stern-Volmer quenching is not the only mechanism that can potentially change the value of F_m' . For example, so-called state-transitions can increase or decrease F_m' by modifying the physical cross section of the PSII light harvesting system. Within some setups, a simple change in biomass within the interrogated volume could also be responsible for an increase or decrease in F_m' .

Non-photochemical quenching attributed to Stern-Volmer quenching is widely assumed to be at least partly regulated through the xanthophyll cycle in chlorophytes and brown algae and diadinoxanthin cycle in diatoms, dinoflagellates and haptophytes (See Goss and Latowski, 2020 for a recent review). Typically, the xanthophyll cycle is stimulated as incident light is increased beyond E_k . Within the chlorophytes and brown algae, violaxanthin is converted to zeaxanthin via the intermediate antheraxanthin. Within diatoms and dinoflagellates, diadinoxanthin is transformed into diatoxanthin (diatoms) or dinoxanthin (dinoflagellates). The conversion (de-epoxidation) of violaxanthin to zeaxanthin is reversed over tens of second to minutes in the dark. In contrast, de-epoxidation of diadinoxanthin may not reverse in the dark. If, for example, diatoms are rapidly taken from high light to darkness, downregulation can remain locked in. A routine method for reversing this is to apply low light treatment for several minutes. An incident photon irradiance of 10 – 20 $\mu\text{mol photons m}^{-2} \text{s}^{-1}$ for 10 to 20 minutes at ambient temperature is a reasonable starting point for establishing the optimum pre-FLC treatment conditions (Schuback et al. 2021).

Equation 22.2 provides a general equation for the Stern-Volmer relationship.

$$\frac{I_f^0}{I_f} = 1 + k_q \tau_0 \cdot [Q] \quad \text{Equation 20.2}$$

Where I_f^0 is the fluorescence intensity in the absence of the quencher, I_f is the fluorescence intensity in the presence of the quencher, k_q is the quencher rate constant and τ_0 is the lifetime of the excited state of the fluorescent molecule in the absence of quencher. For PSII fluorescence, we can substitute the terms on the left-hand side of Equation 20.2 to form Equation 20.3.

$$\frac{F_m}{F_m'} = 1 + k_q \tau_0 \cdot [Q] \quad \text{Equation 20.3}$$

Although routine measurement of k_q and τ_0 is not practical, we can simplify Equation 20.3 to provide Equation 20.4.

$$[Q] \propto \frac{F_m}{F_m'} - 1 \quad \text{Equation 20.4}$$

To generate a value for NPQ, we simply replace the proportionality sign with an equal sign.

$$\text{NPQ} = \frac{F_m}{F_m'} - 1 \quad \text{Equation 20.5}$$

From Equations 20.3, 20.4 and 20.5 it should be clear that values for NPQ can only be compared if k_q and τ_0 are constant and $[Q]$ is zero at F_m . A significant problem with Equation 20.5 is that the calculated value of NPQ is sensitive to baseline fluorescence as well as $[Q]$. It follows that that NPQ values cannot reliably be compared between samples with different values of F_v/F_m .

NSV was used as an alternative to NPQ within McKew et al. (2013) to allow for comparison of downregulation between high light-grown and low light-grown cells of *Emiliania huxleyi* (clone CCMP 1516). Within this study, it was assumed that differences in F_v/F_m between high and low light-grown cells were due to differences in pigment composition, rather than differences in baseline

fluorescence. This assumption was supported through HPLC analysis of pigments. Values for NSV can be generated using Equation 20.5.

$$\text{NSV} = \frac{F_o'}{F_v'} \quad \text{Equation 20.5}$$

While both NPQ and NSV can be used to track changes in downregulation with increasing incident photon irradiance within a single sample, NSV also allows for comparison between samples with different values of F_v/F_m . In the study of McKew et al. (2013) there were no significant differences in NPQ values for the high light-grown and low light-grown cells between zero and 300 $\mu\text{mol photons m}^{-2} \text{s}^{-1}$. In contrast, the high light-grown cells had higher values of NSV at all points between zero and 1200 $\mu\text{mol photons m}^{-2} \text{s}^{-1}$.

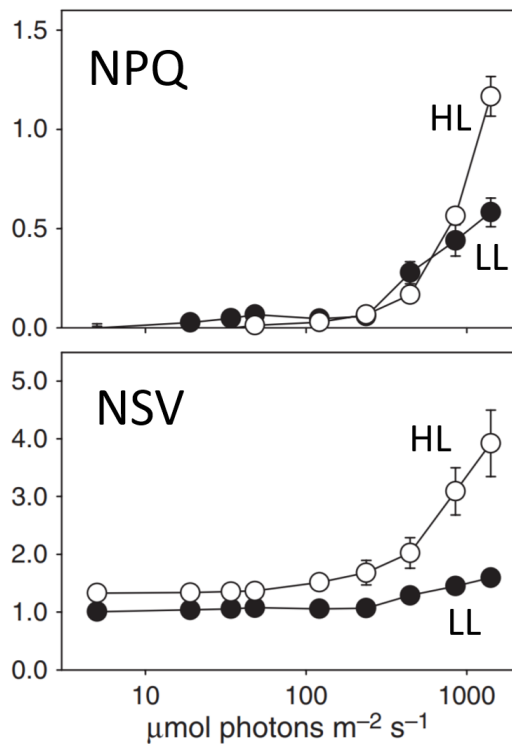


Figure 20.1: Comparison of NPQ and NSV data for High Light (HL) and Low Light (LL) grown cells of *Emiliana huxleyi* (clone CCMP 1516). The F_v/F_m values were 0.4 for the HL-grown cells and 0.5 for the LL-grown cells.

These data are from parts **d** and **e** of Figure 2 within McKew et al. (2013).

21.5 Alternative terminology

As noted in Section 2, a structured approach has been taken to the terminology used within this document. As far as possible, terms are derived from core elements that have been in use for several decades. The aim has been to employ terminology that is both self-consistent and unambiguous. Inevitably, this has led to alternatives to some established terms being generated. This section compares the terminology used within this document with terminology used more widely.

21.5.1 Absorption cross sections

The most widely used equations for fitting ST curves to generate a value for the absorption cross section of PSII photochemistry were originally published by Kolber, Prášil and Falkowski (1998). Table 20.1 provides a comparison of the terminology used within this original publication and the terminology used here.

KPF term (reported units)	RunSTAF term (reported units)	KPF description	RunSTAF description
$\sigma_{\text{PS II}} (\text{\AA}^2 \text{ photon}^{-1})$	$\sigma_{\text{PII}} (\text{nm}^2 \text{ PSII}^{-1})$	Functional absorption cross section	Absorption cross section of PSII photochemistry
$a_{\text{PS II}} (\text{\AA}^2 \text{ photon}^{-1})$	$\sigma_{\text{LHII}} (\text{nm}^2 \text{ PSII}^{-1})$	Optical absorption cross section	Absorption cross section of PSII light harvesting
p (dimensionless)	ρ (dimensionless)	Extent of energy transfer	Apparent connectivity among PSII complexes

Table 20.8: KPF references Kolber, Prášil and Falkowski (1998).

Units of nm^2 are used in preference to \AA^2 because the Angstrom is not part of the SI system. Within the relevant scientific literature, the Greek letter Rho is now more widely used than an italicised p to define connectivity or energy transfer. Although 'functional absorption cross section' and 'effective absorption cross section' are widely used within the literature, they are inconsistent with the overall terminology used within this document. The units for σ_{PII} within the literature are now more likely to be reported as unit area per PSII rather than unit area per photon.

22 References

- Andrée, S. Weis, E. and Krieger, A. (1998) Heterogeneity and Photoinhibition of Photosystem II Studied with Thermoluminescence. *Plant Physiol.* 116: 1053–1061.
- Dau, H. and Sauer, K (1991) Electric field effect on chlorophyll fluorescence and its relation to Photosystem II charge separation reactions studied by a salt-jump technique. *Biochim. Biophys. Acta* 1098: 49-60.
[https://doi.org/10.1016/0005-2728\(91\)90008-C](https://doi.org/10.1016/0005-2728(91)90008-C)
- Baker, N.R. and Oxborough, K. (2004) Chlorophyll Fluorescence as a Probe of Photosynthetic Productivity. In: Chlorophyll *a* fluorescence. A signature of photosynthesis. pp. 65-82. George Papageorgiou and Govindjee Eds. Springer, Dordrecht, The Netherlands. ISBN 1-4020-3217-X
- Behrenfeld, M. J., Prášil, O., Babin, M., and Bruyant, F. (2004). In search of a physiological basis for covariations in light-saturated photosynthesis. *J. Phycol.* 40: 4–25.
<https://doi.org/10.1046/j.1529-8817.2004.03083.x>
- Björn, L.O. (2015) Photobiology : The Science of Light and Life, 3rd Edition. *Elsevier*. ISBN13 9781493914678
- Black, M.T., Brearley, T.H. and Horton P. (1986) Heterogeneity in chloroplast photosystem II. *Photosynth. Res.* 8: 193–207.
<https://doi.org/10.1007/BF00037128>
- Boatman, T.G., Geider R.J. and Oxborough, K. (2019) Improving the accuracy of single turnover active fluorometry (STAF) for the estimation of phytoplankton primary productivity (PhytoPP). *Front. Mar. Sci.*
<https://doi.org/10.3389/fmars.2019.00319>
- Geider, R. J., and MacIntyre, H. L. (2002). “Physiology and biochemistry of photosynthesis and algal carbon acquisition,” in *Phytoplankton Productivity: Carbon Assimilation in Marine and Freshwater Ecosystems*, eds P. J. L. B. Williams, D. N. Thomas, and C. S. Reynolds (Oxford: Blackwell), 44–77.
<https://doi.org/10.1002/9780470995204.ch3>
- Geider, R. J. and Osborne, B.A. (1992) *Algal Photosynthesis*: Prentice Hall. ISBN 978-1-4757-2155-3
- Gorbunov, M.Y., Shirsin, E., Nikonova, E., Fadeev, V.V., and Falkowski, P.G. (2020) A multi-spectral fluorescence induction and relaxation (FIRE) technique for physiological and taxonomic analysis of phytoplankton communities. *MEPS* 644: 1-13
<https://doi.org/10.3354/meps13358>
- Goss, R. and Latowski, D. (2020) Lipid dependence of xanthophyll cycling in higher plants and algae. *Front. Plant. Sci.*
<https://doi.org/10.3389/fpls.2020.00455>
- Guenther, J.E., Melis, A. (1990) The physiological significance of photosystem II heterogeneity in chloroplasts. *Photosynth. Res.* 23: 105–109
<https://doi.org/10.1007/BF00030070>
- Halsey, K. H., Milligan, A. J., and Behrenfeld, M. J. (2010). Physiological optimization underlies growth rate-independent chlorophyll-specific gross and net primary production. *Photosynth. Res.* 103: 125–137.
<https://doi.org/10.1007/s11120-009-9526-z>
- Johnson, M.P. and Ruban, A.V. (2014) Rethinking the existence of a steady-state $\Delta\psi$ component of the proton motive force across plant thylakoid membranes. *Photosynth. Res.* 119: 233 – 242.
<https://doi.org/10.1007/s11120-013-9817-2>
- Kolber, Z. S., Prášil, O., and Falkowski, P. G. (1998). Measurements of variable chlorophyll fluorescence using fast repetition rate techniques: defining methodology and experimental protocols. *Biochim. Biophys. Acta* 1367: 88–106.
[https://doi.org/10.1016/s0005-2728\(98\)00135-2](https://doi.org/10.1016/s0005-2728(98)00135-2)
- Lacour, T., Larivière, J., Ferland, J., Bruyant, F., Lavaud, J., and Babin, M. (2018). The role of sustained photoprotective non-photochemical quenching in low temperature and high light acclimation in the bloom-forming arctic diatom *Thalassiosira gravida*. *Front. Mar. Sci.* 5, 1–16.
<https://doi.org/10.3389/fmars.2018.00354>

- Lavaud, J., and Goss, R. (2014). The Peculiar Features of Non-Photochemical Fluorescence Quenching in Diatoms and Brown Algae. In: *Advances in Photosynthesis and Respiration* (Springer, Dordrecht), 421–443. https://link.springer.com/chapter/10.1007/978-94-017-9032-1_20
- Lawrenz, E., Silsbe, G., Capuzzo, E., Ylöstalo, P., Forster, R. M., and Simis, S. G. (2013) Predicting the electron requirement for carbon fixation in seas and oceans. *PLoS One* 8:e58137. <https://doi.org/10.1371/journal.pone.0058137>
- Lee, Z., Marra, J. Perry, M.J. and kahru M. (2015) Estimating oceanic primary productivity from ocean color remote sensing: A strategic assessment. *J. Mar. Sys.* 149: 50-59. <http://dx.doi.org/10.1016/j.jmarsys.2014.11.015>
- MacIntyre, H.L., Kana, T.M., Anning, T. and Geider, R.J. (2002). Photoacclimation of photosynthesis irradiance response curves and photosynthetic pigments in microalgae and cyanobacteria. *J. Phycol.* 38:17-38.
- Marchin, T. de, Ghysels, B., Nicolay, S. and Franck F (2014). Analysis of PSII antenna size heterogeneity of *Chlamydomonas reinhardtii* during state transitions. *Biochim. Biophys. Acta* 1837: 121-130. <https://doi.org/10.1016/j.bbabi.2013.07.009>
- McKew, B.A., Davey, P., Finch, S.J., Hopkins, J., Lefebvre, S.C., Metodiev, M.V., Oxborough, K., Raines, C.A., Lawson, T. and Geider, R.J. (2013). The trade-off between the light-harvesting and photoprotective functions of fucoxanthin-chlorophyll proteins dominates light acclimation in *Emiliania huxleyi* (clone CCMP 1516). *New Phytol.* 200:74-85. <https://doi.org/10.1111/nph.12373>
- Montagnes, D. J. S., Berges, J. A., Harrison, P. J., and Taylor, F. J. R. (1994). Estimating carbon, nitrogen, protein, and chlorophyll *a* from volume in marine phytoplankton. *Limnol. Oceanogr.* 39: 1044–1060. <https://doi.org/10.4319/lo.1994.39.5.1044>
- Nakayama, T., Nomura, M., Takano, Y., Tanifuji, G., Shiba, K., Inaba, K., Inagaki, Y., and Kawata, M. (2019) Single-cell genomics unveiled a cryptic cyanobacterial lineage with a worldwide distribution hidden by a dinoflagellate host. *Proc. Natl. Acad. Sci. USA.* 116(32):15973-15978 <https://doi.org/10.1073/pnas.1902538116>
- Nield, J. and Barber, J. (2006) Refinement of the structural model for the photosystem II supercomplex of higher plants., *Biochim. Biophys. Acta* 1757: 353-361
- Quick, W.P. and Horton, P. (1984) Studies on the induction of chlorophyll fluorescence quenching by redox state and transthylakoid pH gradient. *Proc. R. Soc. Lond. B* 220: 371–382 <https://royalsocietypublishing.org/doi/10.1098/rspb.1984.0006>
- Sakshaug, E., Bricaud, A., Dandonneau, Y., Falkowski, P. G., Kiefer, D. A., Legendre, L., Morel, A. Parslow, J. and Takahashi, M. (1997) Parameters of photosynthesis: definitions, theory and interpretation of results *J. Plank. Res.* 19: 1637-1670 <https://doi.org/10.1093/plankt/19.11.1637>
- Schuback, N., Tortell P.D. and 22 others (2021) Single-turnover variable chlorophyll fluorescence as a tool for assessing phytoplankton photosynthesis and primary productivity: Opportunities, caveats and recommendations. *Front. Mar. Sci.* <https://doi.org/10.3389/fmars.2021.690607>
- Silsbe, G.M., Oxborough, K., Suggett, D.J., Forster R.M., Ihnken, S. Komárek, O. Lawrenz, E., Prášil, O., Röttgers, R., Sicner, M., Simis, S., Van Dijk, M.A. and Kromkamp, J.C. (2015). Toward autonomous measurements of photosynthetic electron transport rates: An evaluation of active fluorescence-based measurements of photochemistry. *Limnol. Oceanogr.: Methods.* 13: 138-155 <https://doi.org/10.1002/lom3.10014>
- Suggett, D.J., MacIntyre, H.L. and Geider, R.J. (2004). Evaluation of biophysical and optical determinations of light absorption by photosystem II in phytoplankton. *Limnol. Oceanogr.: Methods.* (2) 316-332.
- Suggett, D. J., Moore, C. M., and Geider, R. J. (2010). “Estimating aquatic productivity from active fluorescence measurements,” in *Chlorophyll a Fluorescence in Aquatic Sciences: Methods and Applications*, eds D. Suggett, O. Prášil, and M. Borowitzka (Dordrecht: Springer), 103–127. https://doi.org/10.1007/978-90-481-9268-7_6

- Oxborough, K., Moore, C.M., Suggett, D.J., Lawson, T., Chan, H.G and Geider, R.J. (2012) Direct estimation of functional PSII reaction centre concentration and PSII electron flux on a volume basis: a new approach to the analysis of Fast Repetition Rate fluorometry (FRRf) data. *Limnol. Oceanogr.: Methods*. (10) 142-154
<https://doi.org/10.4319/lom.2012.10.142>
- Oxborough, K. and Baker, N.R. (1997) Resolving chlorophyll *a* fluorescence images of photosynthetic efficiency into photochemical and non-photochemical components - calculation of q_p and F_v'/F_m' without measuring F_o' . *Photosynth. Res.* 54: 135-142
<https://link.springer.com/article/10.1023/A:1005936823310>
- Platt, T., and Gallegos, C. L. (1980). "Modelling primary production," in Primary productivity in the Sea, ed. P. G. Falkowski (Boston, MA: Springer), 339–362
https://doi.org/10.1007/978-1-4684-3890-1_19
- Umena, Y., Kawakami, K., Shen, JR. et al. Crystal structure of oxygen-evolving photosystem II at a resolution of 1.9 Å. *Nature* 473, 55–60 (2011).
<https://doi.org/10.1038/nature09913>
- Vernotte, C. Etienne, A.L. and Briantais, J.M. (1979) Quenching of the system II chlorophyll fluorescence by the plastoquinone pool. *Biochim. Biophys. Acta* 545: 519-527
- Watanabe, M., Iwai, M., Narikawa, R. and Ikeuchi, M. (2009) Is the Photosystem II complex a monomer or a dimer? *Plant Cell Physiol.* 50: 1674-1680
<https://doi.org/10.1093/pcp/pcp112>
- Webb, W. L., Newton, M., and Starr, D. (1974). Carbon dioxide exchange of *Alnus rubra*. *Oecologia* 17, 281–291
<https://doi.org/10.1007/BF00345747>
- Witt, H.T. (1971) Coupling of quanta, electrons, fields, ions and phosphorylation in the functional membrane of photosynthesis. *Quart. Rev. Biophys.* 4:365-477



55 Central Avenue
West Molesey
Surrey KT8 2QZ
United Kingdom

T +44 (0)20 8481 9000
E sales@chelsea.co.uk

chelsea.co.uk